SHAKE TABLE SEISMIC PERFORMANCE ASSESSMENT AND FRAGILITY ANALYSIS OF LIGHTLY REINFOCED CONCRTE BLOCK SHEAR WALLS

SHAKE TABLE SEISMIC PERFORMANCE ASSESSMENT AND FRAGILITY ANALYSIS OF LIGHTLY REINFOCED CONCRTE BLOCK SHEAR WALLS

By

SAEID MOJIRI, M. A. Sc.

B. Sc., Isfahan University of Technology
M. A. Sc., Universitat Politècnica de Catalunya – Ecole Centrale de Nantes

A Thesis Submitted to the School of Graduate Studies in Partial Fulfillment of the Requirements for the Degree of Master of Applied Science

McMaster University

MASTER OF APPLIED SCIENCE (2013) McMaster University

(CIVIL ENGINEERING) Hamilton, Ontario

Title: Shake table Seismic Performance Assessment and Fragility Analysis of Lightly Reinforced Concrete Block Shear Walls

Author: Saeid Mojiri, M. A. Sc.
B. Sc., Isfahan University of Technology
M. A. Sc., Universitat Politècnica de Catalunya – Ecole Centrale de Nantes

Advisors: Dr. W.W. El-Dakhakhni, Dr. M. J. Tait

Number of Pages: xviii, 223

ABSTRACT

There is an urgent need to develop a reinforced masonry (RM) seismic performance database (SPD) of experimental results in order to facilitate adoption of RM seismic force resisting systems (SFRS) in the next generation performance-based seismic design (PBSD) codes. To respond to this need, this thesis reports on shake table tests on fully-grouted RM shear walls. The test walls covered a range of design parameters to facilitate benchmarking, a thorough performance investigation, and calibration of numerical models as well as development of fragility curves within the context of PBSD. The intent was to evaluate the seismic performance of RM shear walls conforming or not conforming to the minimum seismic design requirements of the Canadian masonry design code. The details of the experimental program undertaken, including general observations in terms of cracking patterns and failure modes of the tested walls and the results on the lateral strength, hysteretic response, dynamic properties, and the contribution of different displacement components to the response of the walls, are presented. More detailed analyses include seismic performance quantification of the walls in terms of inelastic behaviour characteristics, various energy components, and the effective dynamic properties of the tested walls. The analysis is concluded with development of simplified nonlinear response history analytical models and seismic fragility assessment tools for the tested walls. In general, the study results indicated that the displacement ductility capacity of the RM walls and their capability to dissipate energy through plastic hinging are higher than what is currently recognized by the National Building Code of Canada (NBCC). The fragility assessment study further indicated that similar walls are expected to conform to the current drift limits of the NBCC even at high seismic regions in Canada. The results of this study are expected to contribute to the growing SPD of RM SFRS, and to the understanding of the lightly reinforced masonry wall system behaviour.

To my lovely wife, Parisa

and to my father and mother

ACKNOWLEDGMENTS

The financial support for this project was provided by the McMaster University Centre for Effective Design of Structures (CEDS) funded through the Ontario Research and Development Challenge Fund (ORDCF) as well as an Early Researcher Award (ERA) grant, both are programs of the Ministry of Research and Innovation (MRI). Support was also provided through the Natural Sciences and Engineering Research Council (NSERC) of Canada. The above financial supports are greatly appreciated. Provision of mason time by the Ontario Masonry Contractors Association (OMCA) and the Canada Masonry Design Centre (CMDC) is also appreciated. The provision of the scaled blocks through a grant from the Canadian Concrete Masonry Producers Association (CCMPA) is gratefully acknowledged.

I would like to thank my advisers, Dr. El-Dakhakhni and Dr. Tait for their insightful advices and continuous support during the course of this research study, without which this work would have not been possible. Special thanks go to the Applied Dynamics Laboratory (ADL) technicians especially Mr. Kent Wheeler for his instructions and thoughtful advices during the experimental phase of the research. His input greatly improved my engineering vision and creativity that will definitely help me throughout my future professions. I would also like to thank all my colleagues who devoted their time for helping me in the ADL.

Finally, I am very grateful to my wife, Parisa. I would have definitely not finished this work successfully without her continuous sacrifice, love, and support.

CONTENTS

LIST OF FIGURES

LIST OF TABLES

LIST OF ABBREVIATIONS AND ACRONYMS

CMU	Concrete Masonry Unit
DBSD	Displacement-Based Seismic Design
NBCC	National Building Code of Canada
NRHA	Nonlinear Response History Analysis
PBSD	Performance-Based Seismic Design
PSDA	Probabilistic Seismic Demand analysis
RC	Reinforced Concrete
RM	Reinforced Masonry
SFRS	Seismic Force Resisting System
SPD	Seismic Performance Database
URM	Unreinforced Masonry

DECLARATION OF ACADEMIC ACHIEVEMENT

This thesis presents experimental and analytical work carried out by Saeid Mojiri, herein referred to as “the author” with advice and guidance provided by the academic supervisors Dr. Wael W. El-Dakhakhni and Dr. M. J. Tait.. Information used from outside sources towards analysis or discussion is cited appropriately in the report.

CHAPTER 1: INTRODUCTION

1.1 Introduction

Most of the current modern seismic codes in the world are essentially prescriptive, which means they are based on a set of prescribed requirements for design of buildings that are expected to result in structures that can attain certain performance levels, mostly life safety, during an earthquake event. The exact performance of such structures under an actual earthquake is unknown because of the inherent uncertainties in the level of ground shaking and material and structural behaviour. As such, performance can vary between structures designed based on the same prescriptive requirements and under the same seismic hazard levels. This uncertainty also leads to a non-uniform risk of failure for different structures, which is philosophically in contrast to current uniform-seismic-hazard-based codes.

Following the provisions of modern seismic design codes, structures are allowed to undergo inelastic deformations during moderate and strong earthquake events. This allows damage to occur in specific regions of the structure in which part of the seismic energy is dissipated. This approach has many economical implications on seismic design as it reduces the force demand on structural components of the seismic force resisting system. However, for the life safety performance level, which is one of the key target levels in most modern seismic codes, such damage is to be expected and often considered to be acceptable, under the maximum considered seismic event.

The life safety performance level targeted in most current codes has been considered to be non-reflective of the needs of modern societies where the economical losses during downtime of the business due to damage to structures or the damage to the contents of the structures can be far more than the construction costs of the structure itself. Moreover, the uncertainties regarding the real performance of structures designed based on prescriptive codes as stated above makes it impossible to estimate the probable performance of structures and thereby providing probabilistic estimation of economical losses and casualties in a actual future earthquake. These issues have been reaffirmed after major seismic events like Northridge, California (1994) and Kobe, Japan (1995) where the life safety was well preserved by the structures, but there was a disproportionate economical loss due to structural damage and business interruptions.

These facts emphasized the importance of redefining the meaning of *seismic performance* of structures and lead to the development of the performance-based seismic design (PBSD) of structures in 1990's aiming at providing design methodologies and criteria to provide different performance levels (not only life safety) to be achieved with certain probabilities for a specific design earthquake thereby providing uniform-risk designs.

Adoption of PBSD principles partly requires a paradigm shift from current seismic design approaches, to a more in depth understanding of the actual seismic behaviour of structural components and systems, and development of analytical

models to more accurately predict the seismic response of different structures in terms of specific physical parameters known as *performance indicators*.

Masonry systems comprise one of the most common types of construction in urban areas for low- and mid-rise buildings. In terms of potential seismic hazard, there is a perception that masonry buildings, in general, possess little ductility and are particularly vulnerable to earthquake events primarily due to the brittle nature of unreinforced masonry (URM) construction. However, over the past four decades, the growing seismic performance database (SPD) of experimental results have shown that capacity design and seismic detailing can significantly improve the performance of reinforced masonry (RM) in terms of displacement ductility, and energy dissipation capabilities during seismic events. These findings are expected to facilitate the adoption of RM construction as a viable seismic force resisting system (SFRS) alternative (Drysdale and Hamid, 2005; Paulay and Priestley, 1992), especially for low- and mid-rise buildings.

Translating the seismic performance of structures to seismic codes requires a more comprehensive and in-depth understanding of the component- and system-level behaviour and their displacement capacities and energy dissipation mechanisms. This understanding is even more critical and challenging in the case of masonry construction due to its complex anisotropic and composite nature as well as the observed extensive damage to the structural and non-structural masonry components during previous earthquakes. As such, there is a critical need for masonry research, and specifically RM shear wall SFRS, to quantify the

different aspects of its seismic performance and energy dissipation mechanisms. Investigation of the seismic performance of RM shear walls as isolated components is the first step to understanding of the system-level seismic performance. This understanding can be facilitated through quasi-static and shake table lateral tests (ATC 2007), where relevant experimental investigations can be found in several documents (e.g. Seible, et al. 1994, S. Jo 2010).

Similar to other international codes, the current Canadian masonry design code (CSA-S304.1 2004) has specific design prescriptions regarding reinforcement ratio, vertical and horizontal bar spacing, masonry strain limits, and aspect ratio for design of RM shear walls with limited and moderate ductility. However the use of these walls in areas of moderate and high seismicity is penalized by the National Building Code of Canada (NRCC 2010) because of their perceived limited ductility for such walls compared to other SFRS. This leads to increased seismic design demands on RM and makes their construction less economical compared to other similar SFRS (e.g. reinforced concrete).

Recent research work on the ductility of RM shear walls has shown that unexpected ductility can be achieved from RM shear walls, even when not conforming to requirements prescribed by the current Canadian masonry design code (Kasparik et al. 2012. The test program on RM shear walls in the Applied Dynamics Laboratory (ADL) of McMaster University has demonstrated the superior seismic performance of RM shear walls in terms of strength, hysteretic

energy dissipation, and ductility (Shedid et al. 2008 and 2010 and Banting and El-Dakhakhni 2012).

1.2 Research objectives and significance

Among the available experimental methods to investigate the seismic performance of structures, shake table testing is believed to provide the most realistic data through simulation of the actual dynamic excitation experienced by the structure. As such, shake table testing of RM wall systems was identified as a key research thrust by the Canadian Masonry industry and code committees. The current thesis aims at drawing a clear picture of the performance of third-scale fully grouted lightly-reinforced RM shear walls tested on one of the a shake tables at McMaster University.

The shake table tests aimed at providing the necessary data to quantify the seismic performance of the walls in terms of ductility, displacement capacity, and energy absorption and dissipation. The amount of damage to the walls, their cracking pattern and failure modes were also tracked during the tests. The results were then used to develop and calibrate simple analytical models to predict the seismic response of the walls, which were subsequently utilized to develop a fragility assessment tool for the class of RM walls studied herein.

Results from this study are believed to provide more realistic data on the seismic performance of RM shear walls, which will eventually aid in gaining a better understanding of the seismic behaviour of RM walls and developing of the necessary tools required for performance-based seismic design of RM

construction. The results of the study also provides information on the seismic performance of the RM shear walls conforming and non-conforming to the minimum provisions prescribed by Canadian masonry design code.

1.3 Scope

In order to accomplish the research objectives as stated above, five two-story and one single story RM shear walls were designed with seismic detailing based on the minimum and less-than-the-minimum prescribed by the Canadian masonry design code for RM shear walls designated as *conventional construction*. The research mainly focuses on the dynamic response of the walls to ground motions based on performance indicators including displacement and energy dissipation. It also investigates the yield and ultimate flexural strength, damage, and failure modes of the walls in order to provide the reference data to develop analytical models and to subsequently perform fragility assessments.

1.4 Organization of the thesis

The dissertation has been assembled into a sandwich thesis format comprised of three separate journal articles. Chapters 3, 4, and 5 comprise the submitted journal articles and hence some overlap exists between parts of these chapters, mainly in the introduction, literature review, experimental program, and references, as they all focus on the same RM wall specimens.

The necessary background knowledge in the fields of PBSD and RM construction, required to follow the contents of this report, is provided in Chapter

2. In Chapter 2, the history and concepts pertaining to PBSD are reviewed. Then different seismic quantification testing methods and their applications are discussed. Finally, the state-of-the-art -knowledge and -research pertaining to seismic performance of RM shear walls are reviewed. The seismic design provisions of different codes for RM shear walls are also discussed and compared.

Chapter 3 contains the work summarized in the following article:

Mojiri, S., El-Dakhakhni, W. W., Tait, M. J. (2013). "Shake Table Seismic Performance Assessment of Fully Grouted Lightly Reinforced Concrete Block Shear Walls." ASCE Journal of Structural Engineering*, Under Review.*

In this chapter a report on the experimental program undertaken within this research study, including information on the design and construction procedures of the wall models, material properties, design and fabrication of the test setup, and the instrumentation scheme is provided. The chapter also reports on the shake table test results in terms of general observations, cracking patterns, and failure modes for each wall tested. Results on the lateral strength of the walls, their hysteretic response, and dynamic properties based on the experimental data, and the contributions of different displacement components are also discussed.

Chapter 4 contains the work presented in the following article:

Mojiri, S., Tait, M. J., El-Dakhakhni, W. W. (2013). "Seismic Response Analysis of Fully Grouted Lightly Reinforced Concrete Block Masonry Shear Walls Based on Shake Table Tests." ASCE Journal of Structural Engineering*, Under Review.*

This chapter includes detailed analyses of the experimental results reported in Chapter 3 based on which the performance of the tested RM shear walls are investigated in terms of their inelastic behavior characteristics, various energy dissipation components, and the effective dynamic properties of the walls including the effective secant stiffness, period, and equivalent viscous damping.

Chapter 5 contains the work described in the following article:

Mojiri, S., Tait, M. J., El-Dakhakhni, W. W. (2013). "Seismic Fragility Assessment of Lightly-Reinforced Concrete Block Masonry Shear Walls." ASCE Journal of Structural Engineering, Submitted..

This chapter focuses on development of analytical fragility curves whereas the seismic response of the shear walls is modeled by a simplified analytical model that was calibrated based on the shake table test results and the predicted response history of the walls using the developed models were verified against the experimental test results.

Chapter 6 includes the summary of the report and conclusions based on the findings of this research study, along with their applications and implications on the PBSD of RM construction, and proposed future work to extend and compliment this research work.

1.5 References for Chapter 1

ATC. (2007). "Interim Testing Protocols for Determining the Seismic Performance Characteristics of Structural and Nonstructural Components (FEMA-461)." Applied Technology Council. Federal Emergency Management Agency, Washington D.C., USA.

Banting, B. R., El-Dakhakhni, W. W. (2012). "Force-and Displacement-Based Seismic Performance Parameters for Reinforced Masonry Structural Walls with Boundary Elements." *Journal of Structural Engineering* , 138(12), 1477-1491.

Canadian Standard Association, (CSA S304.1)."Design of Masonry Structures. S304.1." Mississuaga, ON: CSA, 2004.

Drysdale, R., and Hamid, A. (2005). "Masonry Structures- Behavior and Design." 3rd ed., Canada Masonry Design Centre, Mississauga, Canada.

Jo, S. (2010). "Seismic Behavior and Design of Low-rise Reinforced Concrete Masonry with Clay Masonry Veneer." PhD Thesis, Civil Engineering Department of University of Texas at Austin, Austin, Texas, USA.

Kasparik, T., Tait M. J., and El-Dakhakhni W. W. (2012). "Seismic Performance Assessment of Partially-Grouted Nominally-Reinforced Concrete Masonry Structural Walls Using Shake Table Testing." *Journal of Performance of Constructed Facilities*.

National Research Council of Canada (NRCC) (2010). "National Building Code of Canada (NBCC) .", Institute for Research in Construction, Ottawa, Canada.

Paulay, T., and Priestley, M., J., N. (1992). "Seismic Design of Reinforced Concrete and Masonry Buildings." John Wiley & Sons, Inc., New York and Toronto, 139-142.

Seible, F., Priestley, M., Kingsley, G., and Kürkchübasche, A. (1994). "Seismic Response of Full-Scale Five-Storey Reinforced-Masonry Building." *Journal of Structural Engineering (ASCE)*, 120 (3). 925-946.

Shedid, M. T., El-Dakhakhni, W. W., and Drysdale, R. G. (2010). "Seismic Performance Parameters for Reinforced Concrete-Block Shear Wall Construction." *Journal of Performance of Constructed Facilities*, 24(1), 4-18.

CHAPTER 2: BACKGROUND

2.1 Introduction

In this chapter the relevant background on the main theoretical concepts of the research project is provided through a review of some of the key studies available in literature relevant to each field investigated in this thesis.

This chapter starts with a brief review on the history of development and main concepts of performance-based seismic design. In the second part, the two most common laboratory testing methods for performance identification of structural systems (i.e. quasi-static testing and dynamic shake table testing) are reviewed and a brief summary of their application to reinforced concrete (RC) and RM walls and buildings as found in the literature is presented. In the third part, some technical aspects regarding the shake table testing of structures pertaining to the present research project including similitude requirements, scaling effects, and inertial mass supporting systems are discussed. Basic concepts of masonry construction pertaining to the seismic performance and failure modes specifically for RM shear walls are discussed in the fourth part based on the state-of-the-art review of the relevant literature and research projects. The fifth and final part discusses and compares the prescriptions of some modern codes for the seismic design of RM shear walls. The chapter concludes with some remarks on the need for further research for development of PBSD database and tools for RM construction based on the presented literature review.

2.2 Performance-based seismic design (PBSD)

2.2.1 Development

PBSD was initially developed in response to the need to seismic upgrade and retrofit of the damaged buildings after major earthquakes in 1990's, such as Kobe in Japan and Northridge in California, USA, and inability of the strength and ductility based design guidelines to overcome this issue. The SEAOC Vision 2000 (Vision 2000 1995), ATC-40 (ATC 1996), and FEMA-273 (ATC 1997) were mainly the first documents that attempted to develop performance-based procedures suitable to be used in seismic codes. These documents mainly developed the main concepts of PBSD, the methods to design and retrofit of structures to meet certain target performance levels, and the tools for performance evaluation of structures. While these documents mainly developed the first generation of PBSD, the second generation of PBSD was developed by FEMA-356 (ASCE 2000) involving certain incremental improvements in terms of technical updates to the analytical requirements and acceptance criteria of FEMA-273 based on experiences obtained from the engineering practice of previous guidelines and from case studies like FEMA-343 (BSSC 1999). These regulations has been recently updated and extended to *NEHRP Recommended Seismic Provisions for New Buildings and Other Structures* (BSSC 2009).

Recently, a project has been undertaken by Applied Technology Council in USA for the development of *Next-Generation Performance-Based Seismic Design Guidelines for New and Existing Buildings*. This project is in response to

certain limitations and inefficiencies of second generation PBSD. These limitations, as stated in ATC-58, (Hamburger, et al. 2004) and FEMA-445 (ATC 2006) include the accuracy of proposed analytical procedures for performance evaluation of buildings, the conservatism of the defined performance acceptance criteria, limitations on the application of PBSD for design of new buildings, and the need for probabilistic methods to quantify the seismic performance of existing and new buildings in terms of possible economic losses that can be communicated to insurance companies and stake holders for decision-making purposes.

2.2.2 Performance levels and objectives

The concept of PBSD was implicitly incorporated in most of the modern seismic codes through incorporation of *limit states.* However, such design mainly was attributed to fulfillment of only one performance level aimed to preserve the life safety. In response to the problems attributed to consideration of one performance level, as stated above, several performance levels were considered in PBSD.

PBSD mainly consists of design guidelines that can result in structures that can fulfill several performance levels with certain probability thereby providing the necessary tools to communicate the probable state of the structure in terms of damage and casualties and the corresponding costs after an earthquake with certain probability of occurrence (ATC 2006). This is expressed in the form of performance objectives. Performance objectives summarize the acceptable

performance of the structure under a probable seismic demand depending on the type and importance of each structure (Ghobarah 2001). For instance, based on the FEMA-356 (ASCE 2000) document, the basic safety objective (BSO) should be fulfilled for structures of normal importance, which is in turn accomplished by preserving the *Life Safety* performance level under earthquake intensities with 5% probability of exceedence in 50 years (*BSE-1* level) and the *Collapse Prevention* performance level under earthquake intensities with 2% probability of exceedence in 50 years (*BSE-2* level).

2.2.3 Performance indicators

The seismic performance of a structure depends on the amount of damage caused during an earthquake to its structural and nonstructural elements (i.e. the nonstructural elements and structural content). Therefore, any physical parameter that can represent the state of this damage can be used as a *performance indicator* (Ghobarah 2001). There have been ongoing discussions within the research community to establish the best performance indicator. One of the best performance indicators is the displacement of the structure or structural members expressed in terms of maximum top floor or inter-story drift, maximum strain, rotation, and curvature of members. The inter-story drift can also represent the extent of damage to nonstructural elements. These response parameters are used by documents such as FEMA-356 (ASCE 2000) for both structural and nonstructural elements as acceptance criteria for different performance levels.

However, in most cases, it is oversimplification to relate the extent of damage in the structural and nonstructural elements to only the displacement. For instance, the amount of damage also depends on the number of cycles in which the structure goes into the plastic response range. This type of damage in most of the cases can be well identified by the amount of residual drift in the structure. These permanent deformations depend mainly on the maximum ductility level in the structure reached during an earthquake. The amount of residual drift in the structure after an earthquake can have a substantial effect on the operation of the building and the repair costs. High values of residual strain in the structure after an earthquake can result in complete demolish of the structure even if the extent of damage in the main structural elements are not significant or the life safety of the occupants are preserved. On the other hand, the seismic performance of the structure can be defined based on the damage to its contents the repair costs of which in some cases can even be more than the total value of the structure itself. The damage to such structural contents depends on the amount of floor inertial loads during an earthquake expressed by the floor acceleration level (Ghobarah 2001, Christopoulos and Filiatrault 2006).

Based on the above, the extent of damage during an earthquake can better be identified by *damage indexes* that can be obtained based on relevant damage and performance indicators. Such indexes can incorporate parameters such as the displacement ductility, the hysteretic energy, the floor acceleration level for example (Ghobarah et al. 1997, Cosenza and Manfredi 1997).

2.2.4 Seismic performance verification

In order to verify that the performance of a designed structure meets specific target requirements, different types of analysis can be performed. The FEMA-356 (ASCE 2000) document proposes linear static dynamic analysis, nonlinear pushover analysis, and nonlinear dynamic response history analysis. However it recommends that the linear methods should be used for the cases when the nonlinear response of the structure is expected to be low and the static methods should be applied to simple regular structures and when the higher mode effects are expected to be low like in low-rise buildings. In such analysis the structure is exposed to the target seismic demands and the level of performance indicator parameters in the structure are computed and compared to the thresholds relevant to the targeted performance levels.

Nonlinear response history analysis is the most realistic method for seismic performance verification of structures, but some of its limitations are the complicated nature of the analysis, selection of the response histories representing the seismic hazard in the area, and the approximate nature of the models for the nonlinear behaviour of the elements.

2.2.5 Seismic risk and fragility assessment

Seismic risk can be defined as the potential for damage and losses that can occur in a region following a seismic event and is mainly a function of seismic hazards, the value of assets, and the fragility of assets (Jacob 1992). Seismic risk

and loss estimation is essential for seismic risk planning and is key to performance based seismic evaluation and design of structures (ATC 2011). Evaluation of seismic fragility curves, defined as the probability that a structure or class of structures exceeds certain limit state or damage level if an earthquake with certain intensity occurs, is a crucial step in seismic risk and loss estimation.

The seismic performance of a structure mainly depends on the seismic demand and capacity but due to the uncertainties in both seismic demand and capacity pertaining to the uncertainties in the level of future ground motion, material behavior, and structural response, the seismic performance of the structure only can be expressed with probabilistic functions (Hamburger, et al. 2004). In the *Next Generation PBSD* currently under development as ATC-58 project where the aim is to develop procedures to communicate the performance levels to the decision-making authorities, it is important to be able to provide the level of the uncertainty included in the data. Therefore, probabilistic functions should be employed to relate the uncertainties involved in each of the parameters affecting the performance of the structure. In this context, fragility functions are one of the main probabilistic functions required to express the performance of the structures.

Fragility curves as defined above can be generated using three main approaches (Nielson 2005). The first is a judgment-based approach that is generated by expert opinion surveys (ATC 1985). There is a level of uncertainty inherent in this approach resulting from the level of experience of the considered

experts and their subjectivity as well as their perspective of damage. The second approach to develop fragility curves is the empirical one and is based on post-earthquake observational surveys (Erberik 2008). Since this approach deals with the damage data after actual earthquakes, the resulting fragility curves are thought to be more realistic. However, such fragility curves cannot be generalized, as the data pertaining to documenting different damage states of various structural systems following seismic events is very limited. The third approach is the analytical one that is more general and can be used when no actual post-earthquake damage datasets are available. However, the analytical approach can easily deal with uncertainties resulting from the accuracy of the model used and consideration of variability of different parameters. In analytical fragility assessment, the damage states are related to structural capacity and the seismic intensities are related to structural demands. The former considers the uncertainties in the structural design parameters, material, and geometry for a specific structure or class of structures (ATC 2011) while the latter should account for the uncertainties in the level of ground motion and nonlinear response of the structure (Shome 1999). Subsequently, Probabilistic Seismic Demand Analysis (PSDA), utilizing nonlinear response history analysis of numerical models of the structures, can be employed. With the availability of computational power and the development of reliable analysis tools, PSDA based on response history analysis of numerical models of the structures has been attracting more research attention (Shome 1999, Nielson 2004, and Kwon 2007).

2.2.6 Displacement-based design (DBD)

In most of the current modern codes like National Building Code of Canada (NRCC 2010), the maximum top floor and inter-story drifts are used as a design check in the final step of the design of the structure. The efficiency of displacement of structure as a performance indicator has been the motivation for development of seismic design approaches based on displacement called *Displacement-Based Design (DBD)* methods. In fact DBD methods were developed in response to the need for the development of seismic design approaches that can simply and efficiently accommodate PBSD principles and to overcome the limitations of current force-based design approaches. Discussions regarding the limitations of current force-based seismic design codes can be found in several documents like Medhekar and Kennedy (2000), Priestley (2000), and Priestley et al. (2007).

In DBD, the design outcomes, including the levels of strength and stiffness required, aim at achieving a target displacement bounded to a target performance level. This procedure significantly reduces the number of iterations required in current seismic design methods to ensure that the targeted seismic performance level in the form of displacement is satisfied. Most of the DBD methods use the principle of *substitute structure* (Gulkan and Sozen 1974, Shibata and Sozen 1976) in order to represent the strain based performance levels by the displacement of the structural system and use the single degree of freedom (SDOF) response spectrum to obtain the required design parameters of the

structure (Medhekar and Kennedy 2000, Priestley 2000, Priestley et al. 2007, and Panagiotou and Restrepo 2010).

Displacement-based design methods differ in some aspects like the approach for determination of fundamental period of the structure and if they use an elastic response spectrum with equivalent viscous damping or a nonlinear response spectrum. A discussion of the different methods can be found in Moehle (1992) and Sullivan, et al. (2003)

2.2.7 Challenges

The main challenges in the development of PBSD as stated by Ghobarah (2001), ATC (2006), and Hamburger, et al. (2004) are in the areas of design criteria, probabilistic characterization of capacity and performance, development of general design procedures for multi-performance and hazard levels, and analysis and modeling of the inelastic behaviour of structures for the realistic determination of transient and residual deformations. In order to overcome these challenges research is required to investigate the relationship between the response parameters and damage in different structural members in order to determine the design criteria. More investigations are also required to develop probabilistic relationships to represent the seismic demands based on the field location. Finally, analytical investigations are required to develop simplified and robust design guidelines capable of incorporating PBSD concepts into engineering design practice practically and efficiently.

2.3 Testing methods for seismic performance assessment of structural components and systems

2.3.1 Laboratory testing of structures

Although there have been considerable improvements in recent years in analytical modeling and simulation of structures as a result of improvements in the techniques and the computational capabilities, the experimental testing of structures is still a necessary and inseparable requirement for the development, calibration, and validation of such models. This is particularly true and inevitable for the cases when the structural or the material behaviour is largely nonlinear and there are considerable uncertainties in the accuracy of their analytical models. This fact is more essential for the case of seismic performance evaluation of structures where there are inelastic, rate dependent, history dependent behaviour of the structure and material involved.

For the case of seismic performance assessment of structures, experimental data are required to investigate the seismic capacity of the structure and also state of damage for different levels of demand in the structure based on which the relevant performance levels and fragility functions can be developed. The experimental results are also the only source of data that can assist in identification of relevant performance and damage indicators. They can also facilitate the development of more realistic models of the nonlinear behaviour of the structural elements that are required for nonlinear response history analysis.

Structures can be tested in the laboratory in a system level or element level in the form of subassemblages. System-level testing requires more expensive specimens and instrumentation. It is mainly used to obtain the global responses of the structure like the inter-storey drift, maximum top floor drift, etc. which are most suitable data for the verification of analytical models. System-level testing can provide the most accurate structural configuration for testing in terms of boundary conditions and the interactions between different structural elements. On the other hand, testing structural elements or subassemblages is less expensive and provides data on the local response of specific structural members within the structure that is most suitable for the calibration of analytical models. However, there are difficulties in providing the same boundary conditions as when the element is located in a structural system.

There are several laboratory test methods to assess the seismic performance evaluation and characterization of structures. They can be considered as complementary to each other and should be selected based on the needs of the project. An overview of the two most common experimental methods for seismic performance evaluation of structures is discussed and some of their applications to different types of structure as found by the author in the literature are presented in the next sections. A complete discussion on different dynamic experimental methods can be found in Carvalho (1998) and Williams and Blakeborough (2001).

2.3.2 Quasi-static cyclic testing

Quasi-static cyclic testing is mostly used to evaluate the performance of structural systems and elements under cyclic lateral loads occurring during earthquakes. In this method the excitation is normally imposed in the form of predetermined cyclic history of displacement at one or several points of the structure. This method of testing is simpler and less expensive compared to other test methods both in equipment and control. It is suitable for the identification of force-displacement behaviour of structural components to be used for calibration of analytical models and for determination of seismic capacity of a class of structures used for fragility assessment purposes. However, as the excitations are applied at slow rates this method can not simulate the dynamic behaviour of the structure and therefore, should not be used for the cases where strain rate, velocity, or acceleration dependant behaviours are involved like for fatigue behaviour, viscous dampers, and performance of non-structural elements and contents (Carvalho 1998, ATC 2007). Quasi-static cyclic testing has been widely used by researchers for different structural system like RC shear walls (Taylor et al. 1998, Thomsen and Wallace 2004, Massone and Wallace 2004) and RM shear walls (Shedid et al. 2008, 2010, Banting and El-Dakhakhni 2012)

2.3.3 Dynamic shake table testing

Dynamic shake table testing is the most realistic dynamic testing method. It involves the simulation of the real or scaled ground motions at the base of the

structure. A model of the structure is mounted on a stiff platform that provides the appropriate displacements through shaking. The shaking of the platform can be consist of up to six independent degrees of freedom by independent servo-hydraulic actuators. This method can provide the real dynamic response of the structure and hence is most suitable for characterization of seismic performance of structures or structural elements with strain rate, velocity, and acceleration dependent behaviour. However, it is more complicated and expensive both for the equipment and the control compared to quasi-static testing, which poses limitations for performing large number of tests. Moreover, due to the restrictions on the gravity and lateral load capacity of most of the shake tables, full-scale testing of the structures may not be affordable and hence reduced-scale models of structures are mostly used as specimens. This can be a source of error for size-dependant response of structures like the dynamic nonlinear response. Nevertheless, shake table testing, if well performed, can provide the most realistic and trusted data on seismic performance for all structural and non-structural elements and systems (Carvalho 1998, ATC 2007, and Williams and Blakeborough 2001).

With the advances in both the equipment and control technology, shake table testing has been used more often in the recent decade for investigation and characterization of seismic performance of different structural systems and components. It has been used for testing RC shear walls (Bisch and Coin 1998, Lestuzzi and Bachmann 2007, Carrillo and Alcocer 2008, Panagiotou et al. 2010,

Ghorbanirenani et al. 2012), precast concrete large panel buildings (Harris and Caccese 1984), masonry infilled RC frame buildings (Žarnić, et al. 2001), and for evaluation of seismic retrofit techniques for RC walls (Elnashai, et al. 2000). A brief summary of the techniques used for shake table testing of reduced-scale concrete structures like the issues with modeling, similitude requirements, and choice of model scale with some relevant case studies are also discussed by Caccese and Harris (1990).

2.3.4 Shake table testing of RM walls and systems

There are numerous shake table tests reported in literature for as-built URM construction (Iiba, et al. 1996, Alcocer et al. 2004, Sweeney et al. 2005, Lihong, et al. 2008, Bothara et al. 2010) and FRP-strengthened and retrofitted URM buildings (ElGawady et al. 2005 and Turek et al. 2007). However, the number of experimental research projects conducted to investigate the seismic performance of RM construction is far less than those focusing on URM construction. In fact, very few shake table tests are reported for RM components and systems. Below a review of some of the shake table research projects on RM construction is provided:

Abrams and Paulson (1991) performed shake table tests on one-quarter scale models of fully grouted reinforced concrete block three-story masonry buildings. Their tests were part of a larger research program on seismic response of masonry buildings at the University of Illinois at Urbana-Champaign. Two

model buildings were designed and tested. The design of the two models mainly differed in the layout of the window and door openings and distribution of horizontal reinforcement. For each test, they used the N-S components of El Centro (1940) earthquake with increasing amplitudes to investigate the response of the structures at different states of damage (i.e. pre-cracking, post-cracking, yielding, etc.). They also investigated the dynamic properties of the structures like the natural frequencies and damping through free vibration tests before and after each shake table run. They investigated the seismic response of the structures in terms of maximum response, change of fundamental frequencies and damping, apparent spectral accelerations, lateral drift ratios, and values of shear and moment forces t the base of the structures. In their report they also discussed the dynamic modeling techniques and the specific considerations for reduced-scale RM buildings. They also evaluated the trends in observed response of reduced-scale models to investigate the appropriateness of the modeling techniques and reliability of data on dynamic response of such models to represent the nonlinear hysteretic behaviour of real-scale structures.

In an attempt to characterize the effect of reinforcement on the seismic response of masonry buildings, Tomaževič and Weiss (1994) performed shake table tests on plain and reinforced masonry buildings with identical structural configuration. They tested two three-story plain and reinforced masonry building models with light weight ceramic perforated blocks. The models were parts of a prototype building at one fifth-scale and consisted of peripheral walls and a cross-

shaped wall in the middle of the plan section. They ran artificial low-intensity earthquakes and real earthquakes to derive the model buildings to the linear and nonlinear range of response respectively. They also used the free vibration response of the models to identify the changes in the dynamic properties of the specimens after each shake table run. Using the test data, they investigated the effect of reinforcement on the failure mechanism of the buildings. The also investigated the evolution of extent of damage in both buildings based on the change in frequency and damping of buildings and the change of effective stiffness. Moreover, they investigated the effect of reinforcement on ductility and the energy dissipation capacity of the buildings and derived *behaviour factors* (*force modification factor*) to be used for seismic design purposes.

As a part of multi-university project on performance-based seismic design of new masonry structures, shake table tests have been performed on full-scale reinforced concrete masonry structures at the University of California at San Diego (UCSD). In-plane and out-of-plane dynamic tests were performed on single-story isolated RM walls with clay veneer as well as a single-story RM building with clay veneer. Different configurations of clay veneer connectors to the backing walls were investigated in this study. The experimental results were analyzed by S. Jo (2010). In his work the results of the dynamic tests were used to calibrate nonlinear analytical models based on macro elements, which were eventually used for parametric studies intended to supply information on seismic performance of low-rise RM residential buildings with clay veneer.

More recently, Kasparik et al. (2012) carried out shake table tests to investigate the overall seismic performance of five reduced-scale partially grouted nominally-reinforced concrete block masonry shear walls. They documented a ductile response, even in several walls that had reinforcement ratio values that were much less than the minimum specified by the Canadian masonry design code (CSA S304.1, 2004) and NBCC (NRCC 2010) for seismic zones.

2.4 Technical aspects of shake table testing of model structures

2.4.1 Similitude requirements

Due to limitations of payload capacity of the shake tables, most of the time, full-scale testing of structures is not feasible and small-scale models of prototype structures should be used. However, in order to build a model that is representative of the prototype structures both in dynamic properties and failure modes, laws of dynamic similitude should be employed. Dynamic similitude can be conveniently expressed using Cauchy and Froude dimensionless numbers (Harris and Sabnis 1999). The Cauchy number is the ratio between the dynamic inertia forces (F_i) and the elastic restoring forces (F_e) and is defined as

$$\frac{F_i}{F_e} = \frac{\rho v^2}{E} \tag{2.1}$$

where ρ is the material density, v is the velocity, and E is the Young's modulus. The Froude number is the ratio between the inertia and gravity forces (F_i and F_g) and is defined as

$$\frac{F_i}{F_g} = \frac{v^2}{Lg} \quad (2\text{-}2)$$

where L is the length and g is gravitational acceleration. The Dynamic similitude will be satisfied if the Cauchy and Froude numbers for both model and prototype structures are the same. Based on this, the scaling factors for dynamic similitude will be as presented in Table 2.1 where the length scale factor is defined as $S_L = L_{prototype}/L_{model}$ and the modulus of elasticity scale factor is defined as

Table 2.1: Scale factors required for dynamic similitude

Scaled quantities	Dimension	Scale factor	Scaled quantities	Dimension	Scale factor
Force (F)	F	$S_E S_L^2$	**Frequency (f)**	T^{-1}	$S_L^{-\frac{1}{2}}$
Acceleration (a)	LT^{-2}	1	**Stress (σ)**	FL^{-2}	S_E
Gravitational acceleration (g)	LT^{-2}	1	**Strain (ϵ)**	-	1
Velocity (v)	LT^{-1}	$S_L^{\frac{1}{2}}$	**Poisson ratio (ν)**	-	1
Time (T)	T	$S_L^{\frac{1}{2}}$	**Modulus (E_s)**	FL^{-2}	S_E
Length (L)	L	S_L	**Mass density (ρ)**	$FL^{-4}T^2$	S_E/S_L
Displacement (δ)	L	S_L	**Energy (E)**	FL	$S_E S_L^3$

$S_E = E_{prototype}/E_{model}$. Due to the difficulties in production of model materials with scale properties as defined by similitude requirements, it is a good practice to use the same material for both the model and prototype structure. Therefore, due to the similarity of the mechanical properties of the model and prototype materials, the modulus of elasticity scale factor (S_E) will become unity. On the other hand, as a result, the mass density of both materials will also be the same, which is in contrast to the similitude requirements stated in Table 2.1 ($S_\rho = S_E/S_L = 1/S_L$). To compensate for this problem, additional mass of $\Delta m = m_p(1/S_L^2 - 1/S_L^3)$ should be added to the model. As a general practice for building models, this amount of mass is added as lumped mass to the story floors.

2.4.2 Scaling effects

Even with perfect dynamic similitude between full-scale prototype and reduced-scale model structures, there are uncertainties regarding the extrapolation of nonlinear dynamic response of reduced-scale models to full-scale prototypes mainly due to *scale-sensitive* problems. Scale-sensitive problems arise when the mechanical behaviour of the material or the structure varies with the size of specimen and is often observed in quasi-brittle cementitious and heterogeneous materials like concrete and masonry. Examples of such properties are crack propagation in masonry materials or bond and anchorage of reinforcing bars in RC and RM structures. In order to investigate the level of confidence in extrapolation of the response of model structures to their prototype counterparts,

the response of reduced-scale model structures should be compared and correlated to the behaviour of their real-scale prototypes based on experimental data. A summary of some of the research projects of this kind is presented below.

Ghorbanirenani, et al. (2009) performed cyclic and monotonic quasi-static tests on two full-scale and two reduced-scale ductile RC shear walls. The aim of the tests was to investigate the capability of the reduced-scale shear wall models to represent the behaviour of their full-scale counterparts in terms of shear/flexural capacity/response, ductility, energy dissipation, etc. The tests were conducted as a preliminary stage for future shake table dynamic tests on model walls. Excellent agreement was observed between the behaviour of the full-scale and reduced-scale walls under both monotonic and cyclic loading.

As a part of a research project in McMaster University to investigate the seismic performance of reduced-scale RM walls, Hughes (2010) performed tests on reduced-scale masonry material, assemblages, and wall elements. Tests on third-scale concrete masonry blocks, grout, mortar, and steel reinforcing bars and compression and shear tests on third-scale concrete block masonry prism assemblages were also performed. Finally, the behaviour of third-scale masonry wall elements through monotonic tests on RM concrete block shear walls was investigated. The test results were subsequently compared to the full-scale material, assemblages, and shear walls previously tested in McMaster University. The investigations revealed that in general the behaviour of the third-scale models correlated well with their full-scale counterparts.

2.4.3 Shake table mass supporting system

The weight of the mass in shake table testing sometimes becomes beyond the bearing capacity of the table platform. This issue becomes worse in reduced-scale model testing were based on dynamic similitude requirements between the prototype and the model as discussed in previous sections, additional amount of mass should be added to the model. In order to overcome this problem and keep the weight of the structural models within the table bearing capacity in shake table testing the inertial mass can be placed outside the table platform. To accomplish this a mass supporting system is usually constructed adjacent to the shake table to support the weight of the required inertial mass. The inertial masses are then connected to the main structure using loading beams that transmit the lateral inertial forces to the main structural model. This system not only enhances the performance of the table, but also it increases the safety under collapse of the walls, reduces the out-of-plane deformations, and provides a simple and easy to setup system for transmitting the in-plane lateral loads to the walls. Furthermore, it facilitates decoupling the gravity loads and the inertial masses. Such situation typically arises in low-rise construction where gravity-loaded RC or steel columns would carry a significant portion of the gravity loads, while the SFRS is required to carry the majority of the lateral inertial masses, which are not consistent with the gravitational loads.

The separation of the inertial model mass from the shaking table has been used by a number of other researchers (Lestuzzi and Bachmann 2007, Carrillo and

Alcocer 2011, and Ghorbanirenani et al. 2012). Carrillo and Alcocer (2011) presented and discussed different techniques for supporting the inertial mass outside of the shake table like linear sliding systems using Teflon® pads and roller bearings, rotational systems, pendulum systems, and linear motion guide systems (LMGS). They investigated the efficiency of each technique and concluded that using LMGS resulted in only 2% of the total added damping developed in the model. However, one of the main drawbacks of the LMGS system is the inability of applying high axial forces on the system. Nonetheless, his issue can be resolved using post-tensioned tendons or threaded rods attached in series to a soft spring (to control axial load fluctuations) on top of the model.

2.5 Masonry construction

Masonry construction is one of the oldest methods of construction in the world. In addition to the ease and simplicity of construction, the excellent thermal and architectural aesthetic properties of masonry have been the main reasons for its popularity worldwide. On the other hand, due to the anisotropic behaviour of masonry materials and the composite and non-homogeneous nature of masonry material, the structural behaviour of engineered masonry is complex and has not been well understood until the past few decades. One of the key drawbacks of masonry materials is their brittleness. This property has made the perception that masonry structures are vulnerable to seismic hazards. Therefore, with the advance of technology and development of more ductile structural systems like RC and

steel, there has been a common practice in most codes to avoid masonry construction in areas with high seismic hazard risks.

Recent research studies focusing on the behaviour of masonry buildings have shown that although the constituents of masonry buildings are of brittle nature, if well designed, masonry buildings can provide ductile behaviour. This behaviour was more enhanced by other advances in masonry building construction like incorporation of RC slabs allowing formation of rigid diaphragms, incorporation of steel reinforcement to enhance the tensile strength and ductility of masonry components and the possibility of manufacturing masonry units with higher compressive strength allowing for design of thinner components (Casabonne 2000). Acceptable ductility capacities provided by masonry buildings while maintaining other excellent properties of masonry construction has recently made masonry construction a preferred construction method for low and medium rise buildings throughout the world, and specifically in Latin and North America.

2.5.1 Seismic performance of masonry buildings

As the ductility of RM buildings becomes more recognized by the structural engineering community, RM construction is becoming a competitive alternative to other construction materials in seismic prone areas. On the other hand, the importance of adoption of seismic performance of structures in seismic codes as outlined in previous sections requires more comprehensive and in-depth

understanding of both the strength and displacement capacities at different performance levels. As such, extensive research is required to investigate the seismic performance of RM components and buildings and the factors affecting their performance, leading to design approaches more suited for PBSD.

2.5.2 Seismic performance of masonry shear walls

Masonry loadbearing buildings (systems) are usually constructed from structural masonry walls and in some cases with additional RC columns to carry some/most of the gravity loads where structural walls are not needed. The whole system is typically connected by either flexible or rigid diaphragms with the system's lateral resistance and seismic performance of the buildings being primarily governed by the in-plane lateral resistance and stiffness of the walls. Hence, investigating the seismic performance of masonry shear walls as isolated components can help in better understanding the seismic performance of masonry systems as a whole. This understanding can be obtained by performing quasi-static and shake table lateral tests on masonry shear walls. In the following sections, important design factors, seismic performance parameters and desired failure modes of RM shear walls are discussed in detail.

2.5.3 Reinforced masonry shear walls

In masonry shear walls made of hollow core units, horizontal and vertical reinforcement can be distributed inside the wall improving the strength and ductility capacities of the walls. RM shear walls provide better seismic

performance than URM shear walls and hence are preferred and prescribed by masonry design codes for areas with moderate levels of seismic risk.

2.5.3.1 Failure modes

The failure modes of RM shear walls as outlined by Drysdale and Hamid (2005) are as follows:

Flexural failure: This failure mode is characterized by cracking in bed joint followed by yielding of vertical reinforcement and toe crushing at the end of failure. Due to yielding of reinforcement this failure mode involves extensive energy dissipation and large ductility capacity.

Shear failure: This failure mode is characterized by either diagonal cracking or bed joint sliding which are both of non-ductile nature. In the case of diagonal cracking the shear strength is provided by both masonry and horizontal reinforcement while in the case of bed joint sliding it is provided by the doweling action of the vertical reinforcing bars and the friction in the plane of cracking (mainly between mortar and units), which in turn depends on the amount of axial force on the wall and clamping pressure provided by vertical reinforcement.

As noted above the flexural failure provides more ductility capacity and energy dissipation, thus is desired for seismic design. Therefore, brittle shear failure either characterized by diagonal cracking or bed joint sliding should be avoided. The shear failure due to diagonal cracking can be well controlled by horizontal reinforcement and shear failure due to bed joint sliding is not critical

for tall buildings due to high level of axial loads. But investigations (Shing et al. 1990) have shown that in low-rise masonry buildings, due to small amount of axial loads, the bed joint sliding failure in most of the cases becomes critical and prevents development of the flexural capacity of the building. In order to avoid this brittle failure mode, it is suggested in some documents (Leiva and Klingner 1994, Jo 2010) to use shear keys and to roughen the bed joint at the wall base. In order to provide more shear-friction and control on cracking, it is also recommended to use uniformly distributed instead of concentrated vertical reinforcement in RM shear walls (Drysdale and Hamid 2005).

In order to better represent the actual behaviour of structure as required in PBSD, the failure mode should be predicted and the amount of ductility and energy dissipation corresponding to the predicted failure modes should be taken into account for design provisions and seismic demand and capacity assessments.

2.5.4 Investigations on seismic performance of RM shear walls

One of the first major research projects towards development of seismic design guidelines and characterization of seismic response of RM shear walls was the US Coordinated Program for Masonry Building Research established in mid 1980s under the direction of the Technical Coordinating Committee for Masonry Research (TCCMR). The main objective of this program was to develop seismic design guidelines and analytical models based on limit states and capacity design principles resulting in ductile response of the RM buildings (Noland 1987). Under

this program, Shing et al. (1989, 1990) investigated the flexural and shear strength of RM panels and examined the effect of axial stress and vertical and horizontal reinforcement ratios on the ductility, energy dissipation, lateral strength, and failure modes of RM shear walls, based on quasi-static cyclic tests. Subsequently, Seible, et al. (1994) tested a full-scale five-story RM building using pseudo-dynamic method. The RM building model provided the necessary experimental data on the system-level real seismic response of RM shear walls including the interaction of different elements and the higher mode effects which were used for the evaluation of TCCMR design guidelines and analytical models. The building model was a subsection of a symmetric prototype building including two flanged shear walls and precast concrete floor slabs. The overall ductile response of the building confirmed the successful implementation of a ductile capacity design for RM buildings and ability of analytical models to predict their seismic response.

The research programs discussed above established the effectiveness of applying capacity design principles to RM construction and identified the enhanced lateral strength, ductility, and energy dissipation levels of RM construction, which lead to their corresponding currently adopted levels in North American codes. However, the growing database of more recent test results has revealed that well-detailed RM shear walls can possess seismic performance qualities that are significantly higher than what is currently recognized and adopted by current seismic design codes. Consequently, and as a part of a larger research program focused on investigating the seismic response of RM shear

walls from a PBSD perspective, Shedid, et al. (2008 and 2009) performed quasi-static cyclic tests on real-scale RM shear walls. The experimental results confirmed the well-defined flexural response and ductility and energy dissipation characteristics of these walls under cyclic lateral loads. It was observed that if well reinforced, RM shear walls can benefit from almost the same ductility and energy dissipation mechanisms resulting from formation of plastic hinge at the base of the walls commonly observed in RC shear walls. Based on the amount of ductility observed, the *force modification factors* used as a seismic design parameter for structures were observed to well exceed the values recommended by NBCC 2010. Shedid, et al. (2010-a) also indicated that the seismic performance of RM shear walls can be quantified based on the same parameters used for RC walls like *equivalent plastic hinge length*, which is based on the plastic hinge model and can be used for the prediction of the seismic response of the walls aiding in development of simple and robust seismic design guidelines.

Shedid, et al. (2010-b) also investigated the effect of aspect ratio and added boundary elements on the seismic performance of RM walls through quasi-static cyclic tests on half-scale two- and three-storey walls. They observed that the boundary conditions are quite effective in increasing the ductility of the walls but the nonlinear behaviour of the walls failing in flexure is not sensitive to the wall height but is rather a function of wall length. Similar findings were subsequently reported by Banting and El-Dakhakhni (2012) who tested four specially detailed RM structural walls under quasi-static cyclic loads. The study aimed at providing

experimental evidence required for establishment of a new category of RM seismic force resisting systems in North American building codes.

More recently, Kasparik et al. (2012) carried out shake table tests to investigate the overall seismic performance of five reduced-scale partially grouted nominally-reinforced concrete block masonry shear walls subjected to in-plane seismic loading. They documented a type ductile response, even in several walls that had reinforcement ratio values that were much less than the minimum specified by the Canadian masonry design code (CSA S304.1, 2004) and the NBCC (NRCC 2010) for seismic zones. The effectiveness of incorporation of reinforcing steel on ductility and energy dissipation of RM shear walls were also investigated by Long (2006), Wierzbicki (2010) and by Haach, et al. (2010).

2.6 Code-based seismic design requirements for RM shear walls

Modern masonry seismic design provisions such as those in the Canadian masonry standards (CSA-S304.1 2004), the USA masonry code (MSJC 2011) and the New Zealand masonry standards (NZS4230 2004) allow seismic design of RM walls based on the *capacity design* philosophy. They allow for reduction of seismic lateral forces based on nonlinear deformations and energy dissipation in the plastic hinge region through application of so called *force modification factors*. Based on this, they define different categories of shear walls with certain requirements for dimension, reinforcement content, etc. Some of the main seismic requirements of Canadian, USA, and New Zealand codes for different categories of RM shear walls are presented in Table 2.2. Note that the *force modification*

Table 2.2: Seismic requirements of Canadian, USA, and New Zealand codes for RM shear walls

Code	Wall Type	$A_{sh,min}$	$A_{sv,min}$	ρ_{min}	$S_{v,max}$ (mm)	$S_{h,max}$ (mm)	ε_{mu}	l_p	R (R_dxR_o) μ
CSA S304.1-04	Conventional	$0.13\%A_g$	N.A.	N.A.	2400	Bond Beam: 2400 Joint Reinf.: 400	0.003	N.A.	2.25
	Limited Ductile	$0.067\%A_g$	$0.067\%A_g$	0.2%	min $\begin{cases} 6(t+10) \\ 1200 \\ l_w/4 \end{cases}$ < 600	Bond Beam: min $\begin{cases} 1200 \\ l_w/2 \end{cases}$ Joint Reinf.: 400	0.0025	max $\begin{cases} l_w/2 \\ h_w/6 \end{cases}$	2.25
	Moderate Ductile							max $\begin{cases} l_w \\ h_w/6 \end{cases}$	3
MSJC 2011	Ordinary	2 W1.7	129 mm^2	N.A.	3048	406	0.0025	l_w	2
	Intermediate				1219				3.5
	Special	$0.07\%A_g$	max $\begin{cases} 0.33A_{sh,req} \\ 0.07\%A_g \end{cases}$	0.2%	min $\begin{cases} l_w/3 \\ 1219 \\ h_w/3 \end{cases}$	min $\begin{cases} l_w/3 \\ 1219 \\ h_w/3 \end{cases}$			5
NZS 4230:2004	Limited Ductile	$0.07\%A_g$	$0.07\%A_g$	0.2%	400	3 story or < 12m: 400 More: 200	0.003	max $\begin{cases} l_w \\ 600 \\ h_w/6 \end{cases}$	2
	Ductile								4 < $2(1\text{-}T_1)$ < 6

factor (*R*) in the right end column in this table is essentially equivalent to the product of the *over-strength related force modification factor* (R_0) and the *ductility related force modification factor* (R_d) in the Canadian code. This parameter is the *structural ductility factor* (μ) in the New Zealand code.

Based on the requirements presented in Table 2.2, it can be observed that although there is minimal scatter in the minimum horizontal and vertical reinforcement requirements in the codes, but they considerably differ in their proposed formulas for the plastic hinge length and the force modification factor (*R*). The Canadian code seems to be generally more conservative in terms of these parameters compared to the other two codes. Considering the great effect of these parameters on the seismic design of the RM walls, such scatter can not be justified and can result in different designs for the same seismic demands. It is also observed that while the New Zealand code and the Canadian code are more conservative in terms of the maximum spacing of the vertical reinforcement for consideration of ductility levels, the code of USA specifies greater maximum distance between vertical reinforcement for ductile walls.

2.7 Conclusions

Based on the literature review presented in this chapter the following can be concluded:

- In order to achieve design of structures with predictable seismic performance, there is a need to make further developments in seismic design of structures in the context of performance-based seismic design and find

simple and practical methods to implement code-based performance-based design guidelines for different types of structural systems.

- Adoption of seismic performance of structures in seismic codes requires more comprehensive and in-depth understanding from strength and displacement capacities of different structural systems and masonry is of no exception for this. This understanding is even more critical in the case of masonry construction due to its complex composite anisotropic behaviour and the possible extensive damage to structural and non-structural masonry components during earthquakes that may comprise a major seismic hazard.
- The required understanding for PBSD is far beyond the existing knowledge of masonry construction. Therefore, there is a need for research in the field of masonry construction and specifically on reinforced masonry (RM) shear walls to evaluate the ductility and performance provided by such construction in the case of seismic loading.
- Investigation of the seismic performance of RM shear walls as isolated components can help in better understanding of the seismic performance of the whole building. This understanding can be obtained by performing quasi-static and shake table tests on RM shear walls as isolated components.
- The failure modes of RM shear walls greatly affect the behaviour and type and extent of damage incurred during an earthquake. Therefore, in order to better predict the actual performance of RM shear walls as required in PBSD, their failure modes should be predicted and the amount of ductility

and energy dissipation corresponding to the predicted failure modes should be taken into account for design provisions and seismic demand and capacity assessments. Thus, identification of failure modes of RM shear walls and the effect of parameters like the amount of axial load, aspect ratio, and reinforcement arrangement through experimental testing is necessary for development of PBSD concepts for RM construction.

- There are numerous quasi-static and shake table tests reported in literature for URM construction. However, the number of experimental projects conducted for investigation of seismic performance of RM construction is far less than URM. In fact there are rare shake table tests reported for RM buildings especially for RM subassemblages like isolated RM shear walls. In addition, most of these tests pertain to construction techniques that are not representative of those currently employed or focused mainly on evaluating and reporting force-based design parameters.. Therefore, there is urgent need for conducting seismic tests on RM buildings and isolated walls with a performance-based point of view specially using shake table testing as the most realistic method for dynamic testing.

  Some modern codes do not give full credit for the ductility of RM shear walls. However, recent research projects have shown clear evidences of the inherent ductility capacity of RM walls that is significantly more than what is recognized by the codes even without special detailing. Nevertheless, more experimental data is required though to provide more evidence and

support the ductility capacity of RM walls in order to promote RM construction as a competitive SFRS in regions of high seismicity.

2.8 Notations for Chapter 2

A_g = Gross cross section are perpendicular to the reinforcement
$A_{sh,min}$ = Horizontal reinforcement minimum area
$A_{sh,min}$ = Required horizontal reinforcement
$A_{sv,min}$ = Vertical reinforcement minimum area
E = Young's modulus
F = Force
F_i = Dynamic inertia force
F_e = Elastic restoring force
F_g = Gravity force
L = Length
R = Force modification factor
R_0 = Overstrength related force modification factor
R_d = Ductility related force modification factor
S_x = Scale factor for parameter x
$S_{v,max}$ = Maximum distance between centers of vertical reinforcement
$S_{h,max}$ = Maximum distance between centers of horizontal reinforcement
T = Time
a = Acceleration
f = frequency
g = Gravitational acceleration
h_w = Wall height
l_p = Plastic hinge length
l_w = Wall length
m = Mass
t = Wall thickness
v = Velocity
ρ = Material density
ρ_{min} = Minimum total reinforcement ratio
ε_{mu} = Compressive strain of masonry at ultimate states
μ = Structural ductility factor
δ = Displacement
σ = Stress
ϵ = Strain
ν = Poisson ratio

Subscripts:

$protptype/p$ = Related to prototype
$model/m$ = Related to model

2.9 References for Chapter 2

Abrams, D. P., & Paulson, T. J. (1991). "Modeling Earthquake Response of Concrete Masonry Building Structures." *ACI Structural Journal* , 88 (4), 475-485.

Alcocer, S. M., Arias, J. G., and Vázquez, A. (2004). "Response Assessment of Mexican Confined Masonry Structures through Shaking Table Tests." *13thWorld Conference on Earthquake Engineering*. Vancouver, B.C., Canada. Paper, no. 2130.

ASCE. (2000). "Prestandard and Commentary for The Seismic Rehabilitation of Buildings (FEMA-356)." American Society of Civil Engineers, Federal Emergency Management Agency.

ATC. (1985). "Earthquake Damage Evaluation Data for (ATC-13)." Applied Technology Council. Federal Emergency Management Agency, Washington D.C., USA.

ATC. (1996). "Seismic Evaluation and Retrofit of Existing Concrete Buildings (ATC-40)." Applied technology Council, Redwood City, California.

ATC. (1997). "NEHRP Guidlines for The Seismic Rehabilitation of Buildings (FEMA-273)." Applied Technology Council, Federal Emergency Management Agency.

ATC. (2006). "Next-Generation Performance-Based Seismic Design Guidlines: Program Plan for New and existing Buildings (FEMA-445)." Applied Technology Council. Federal Emergency Management agency, Washington D.C., USA.

ATC. (2007). "Interim Testing Protocols for Determining the Seismic Performance Characteristics of Structural and Nonstructural Components (FEMA-461)." Applied Technology Council. Federal Emergency Management Agency, Washington D.C., USA.

ATC. (2011). "Seismic Performance Assessment of Buildings Volume 1- Methodology (ATC-58-1 75% Draft)". Applied Technology Council. Federal Emergency Management Agency, Washington D.C., USA.

Banting, B. R., El-Dakhakhni, W. W. (2012). "Force-and Displacement-Based Seismic Performance Parameters for Reinforced Masonry Structural Walls with Boundary Elements." *Journal of Structural Engineering*, 138(12), 1477-1491.

Bisch, P., Coin, A. (1998). "The CAMUS research." *Proceedings of the Eleventh European Conference on Earthquake Engineering.* Paris.

Bothara, J. K., Dhakal, R. P., and Mander, J. B. (2010). "Seismic Performance of an Unreinforced Masonry Building: An Experimental Investigation." *Earthquake Engineering and Structural Dynamics*, 39, 45-68.

BSSC. (1999). "Case Studies: An Assessment of the NEHRP Guidelines for the Seismic Rehabilitation of Buildings (FEMA-343)." Building Seismic Safety Council, Washington D. C.: Federal Emergency Management Agency.

BSSC. (2009). "*NEHRP Recommended Seismic Provisions for New Buildings and Other Structures (FEMA P-750)."* Building Seismic Safety Council of the National Institute of Building Sciences, Washington D. C.: Federal Emergency Management Agency.

Carrillo, W. J., Alcocer, S. M. (2008). "Shaking Table Tests of Low-Rise Concrete Walls for Housing." *14th World Conference on Earthquake Engineering.* Beijing, China.

Carrillo, J., and Alcocer, S. (2011). "Improved External Device for a Mass-Carrying Sliding System for Shaking Table Testing." *Journal of Earthquake Engineering and Structural Dynamics,* 40, 393-411.

Caccese, V., Harris, H. G. (1990). "Earthquake Simulation Testing of Small-Scale reinforced Concrete Structures." *ACI Structural Journal*, 87(1).

Canadian Standard Association, S304.1 (2004). “Design of Masonry Structures”. Mississuaga, ON: CSA.

Carvalho, E. (1998). “Seismic Testing of Structures.” *Proceedings of the Eleventh European Conference on Earthquake Engineering.* Paris, France, 53-64.

Casabonne, Carlos (2000). “Masonry in the seismic areas of the Americas, recent investigation and developments.” *Progress in Structural Engineering and materials*, 2(3), 319-327.

Cosenza, E., Manfredi, G. (1997). “The Improvement of the Seismic Resistant Design for Existing and New Structures Using Damage Concepts.” *Seismic Design Methodologies for the Next Generation of Codes.* Rotterdam: AA Balkema, 119-1130.

Christopoulos, C. Filiatrault, A. (2006). “Principles of supplemental damping and base isolation”, IUSS Press, Milan, Italy.

Drysdale, R., and Hamid, A. (2005). “Masonry Structures- Behavior and Design.” 3rd ed., Canada Masonry Design Centre, Mississauga, Canada.

Elnashai, A., Pinho, R., and Vaz, C. T. (2000). “Experimental Observations from Shaking-Table Tests on Selective techniques for Repair and Strengthening of RC Walls.” *Proceedings of 12th World Conference on Earthquake Engineering.* Auckland, New Zealand.

ElGawady, M. A., Lestuzzi, P., and Badoux, M. (2005). “In-Plane Seismic Response of URM Walls Upgraded with FRP.” *Journal of Composites for Construction*, 9 (6), 524-535.

Erberik, M. Altuğ (2008). “Generation of Fragility Curves for Turkish Masonry Buildings Considering In-plane Failure Modes.” *Earthquake Engineering and Structural Dynamics*, 37(3), 387-405.

Ghobarah, A., Aly, N. M., and El-Attar, M. (1997). "Performance Level Criteria and Evaluation." *Seismic Design Methodologies for the Next Generation of Codes.* Rotterdam: AA Balkema, 207-215.

Ghobarah, Ahmed. (2001). "Performance-Based Design in Earthquake Engineering: State of Development." *Engineering Structures,* 23(March), 878–884.

Ghorbanirenani, I., Velev, N., Tremblay, R., Palermo, D., Massicotte, B., and Léger, P. (2009). "Modeling and Testing Influence of Scaling Effects on Inelastic Response of Shear Walls." *ACI Structural Journal*, 106(3).

Ghorbanirenani, I., Tremblay, R., Léger, P., and Leclerc, M. (2012). "Shake Table Testing of Slender RC Shear Walls Subjected to Eastern North America Seismic Ground Motions." *Journal of Structural Engineering*, 138(12), 1515–1529.

Gulkan, P., Sozen, M. A. (1974). "Inelastic Response of Reinforced Concrete Structures to Earthquake Motions." *Journal of the American Concrete Institute*, December, 604-610.

Haach, V. G., Vasconcelos, G., and Lourenço, P. B. (2010). "Experimental Analysis of Reinforced Concrete Block Masonry Walls Subjected to In-Plane Cyclic Loading." *Journal of Structural Engineering*, 136(4), 452-462.

Hamburger, R., Rojahn, C., Moehle, J., Bachman, R., Comartin, C., and Whitakker, A. (2004). "ATC-58 Project: Development of Next-Generation Performance-Based Earthquake Engineering Design Criteria for Buildings." *13thWorld Conference on Earthquake Engineering*.Vancouver, B.C., Canada, Paper, no. 1819.

Harris, H. G., and Caccese, V. (1984)."Seismic Behaviour of Precast Concrete Buildings Using a Small Shake Table." *8thWorld Conference on Earthquake Engineering*, San Fransisco, USA

Harris, H. G., and Sabnis, G. (1999). "Structural Modeling and Experimental Techniques." Second ed., CRC Press.

Hughes, K. J. (2010), "Behaviour of Reduced-Scale Reinforced Concrete Masonry Shear Walls and Components." M.A.Sc Thesis, Civil engineering Department of Mcmaster University, Hamilton, Canada.

Iiba, M., Mizuno, H., Goto, T., and Kato, H. (1996). "Shake Table Test on Seismic Performance of Confined Masonry Wall." *11thWorld Conference on Earthquake Engineering*, Mexico, Paper, no. 659.

Jacob, Klaus H. (1992). "Seismic Hazards in the Eastern US and the Impact on Transportation Lifelines." *In Lifeline Earthquake Engineering in the Central and Eastern US*, ASCE, 58-71.

Jo, S. (2010). "Seismic Behavior and Design of Low-rise Reinforced Concrete Masonry with Clay Masonry Veneer." PhD Thesis, Civil Engineering Department of University of Texas at Austin, Austin, Texas, USA.

Kasparik, T., Tait M. J., and El-Dakhakhni W. W. (2012)."Seismic Performance Assessment of Partially-Grouted Nominally-Reinforced Concrete Masonry Structural Walls Using Shake Table Testing." *Journal of Performance of Constructed Facilities*, Accepted for publication.

Kwon, O.S. (2007). "Probabilistic Seismic Assessment of Structure, Foundation and Soil Interacting Systems." PhD Thesis, Civil Engineering Department, University of Illinois at Urbana-Champaign, Urbana, Illinois, USA.

Leiva, G., Klingner, R. (1994). "Behaviour and design of multi-storey masonry walls under in-plane seismic loading. " *The Masonry Society Journal*, August, 13(1), 15–24.

Lestuzzi, P., Bachmann, H. (2007). "Displacement Ductility and Energy Assessment from Shaking Table Tests on RC Structural Walls." *Journal of Engineering Structures*, 29, 1708-1721.

Lihong, X., Xiong, D., Ruifeng, W., and Jingqian, X. (2008). "Shaking Table Tests and Dynamic Analyses of Masonry Wall Buildings with Frame-Shear Walls at Lower Stories." *Earthquake Engineering and Engineering Vibration*, 7, 271-283.

Long, L. (2006). "Behaviour of Half-Scale Reinforced Concrete Masonry Shear Walls." M.A.Sc. Thesis, Civil Engineering, McMaster University, Hamilton, Canada.

Massone, L. M., Wallace, J. W. (2004). "Load-Deformation Responses of Slender Reinforced Concrete Walls." *ACI Structural Journal*, 101(1).

Medhekar, M. S., Kennedy, D. J. L. (2000). "Displacement-Based Seismic Design of Buildings-Theory." *Journal of Engineering Structures* 22, 201-209.

Moehle, J. P. (1992). "Displacement-Based Design of RC Structures Subjected to Earthquakes." *Earthquake Spectra*, 8(3), 403-428.

MSJC, 2011. "Building Code Requirements for Masonry Structures (TMS 402-11 / ACI 530-11 / ASCE 5-11)." The Masonry Society, Boulder, Colorado, USA, the American Concrete Institute, Farmington Hills, Michigan, USA, and the American Society of Civil Engineers, Reston, USA, 2011.

National Research Council of Canada (NRCC) (2010). "National Building Code of Canada (NBCC) ."Institute for Research in Construction, Ottawa, Canada.

Nielson, Bryant G. (2005). "Analytical Fragility Curves for Highway Bridges in Moderate Seismic Zones." PhD Thesis, School of Civil and Environmental Engineering, Georgia Institute of Technology, Atlanta, Georgia, USA.

Noland, J. L. (1987). "A Review of the U.S. Coordinated Program for Masonry Building Research." *Proceedings of Fourth North American Masonry Conference*, The Masonry Society,University of California, Los Angeles, Ca, USA, 38-1.

NZS4230 (2004). "New Zealan Standard: Design of Reinforced Concrete Masonry Structures." Wellington, New Zealand: Standards New Zealand.

Panagiotou, M., Restrepo J. I. (2010). "Displacement-Based Method of Analysis for Regular Reinforced-Concrete Wall Buildings: Application to a Full-Scale 7-Story Building Slice Tested at UC–San Diego." *Journal of Structural Engineering*, 137(6), 677-690.

Panagiotou, M., Restrepo, J. I., and Conte, J. P. (2010). "Shake-Table Test of a Full-Scale 7-Story Building Slice. Phase I: Rectangular Wall." *Journal of Structural Engineering*, 137(6), 691-704.

Priestley., M. J. N. (2000). "Performance Based Seismic Design." *Bulletin of the New Zealand Society for Earthquake Engineering,* 33(3), 325-346.

Priestley, M.J.N., Calvi, G. M., and Kowalsky, M. J. (2007). "Displacement-Based Seismic Design of Structures." , IUSS Press, Pavia, Italy.

Seible, F., Priestley, M., Kingsley, G., &Kürkchübasche, A. (1994). "Seismic Response of Full-Scale Five-Storey Reinforced-Masonry Building." *Journal of Structural Engineering*, 120 (3). 925-946.

Shedid, M., Drysdale, R., and El-Dakhakhni, W. W. (2008). "Behaviour of Fully Grouted Reinforced Concrete Masonry Shear Walls Failing in Flexure: Experimental Results." *Journal of Structural Engineering*, 134 (11), 1754-1767.

Shedid, M. T., El-Dakhakhni, W. W., and Drysdale, R. G. (2009). "Behavior of Fully Grouted Reinforced Concrete Masonry Shear Walls Failing in Felxure: Analysis." *Engineering Structures*, 31, 2032–2044.

Shedid, M. T., El-Dakhakhni, W. W., and Drysdale, R. G. (2010-a). "Seismic Performance Parameters for Reinforced Concrete-Block Shear Wall Construction." *Journal of Performance of Constructed Facilities*, 24 (1), 4-18.

Shedid, M. T., El-Dakhakhni, W. W., and Drysdale, R. G. (2010-b). "Alternate Strategies to Enhance the Seismic Performance of Reinforced Concrete-Block Shear Wall Systems." *Journal of Structural Engineering*, 136(6), 676-689.

Shibata, A., Sozen, M. A. (1976). "Substitute-Structure Method for Seismic Design in R/C." *Journal of the Structural Division (ASCE)*,102(ST1), 1-18.

Shing, P. B., Noland, J. L., Klamerus, E., and Spaeh, H. (1989). "Inelastic behavior of concrete masonry shear walls." *Journal of Structural Engineering* 115(9), 2204-2225.

Shing, P. B., Schuller, M., and Hoskere. V. S. (1990). "In-plane resistance of reinforced masonry shear walls." *Journal of Structural Engineering*,116(3), 619-640.

Shome, Nilesh (1999). "Probabilistic Seismic Demand Analysis of Nonlinear Structures." PhD Thesis, Department of Civil and Environmental Engineering, Stanford University, Redwood City, California, USA.

Sullivan, T. J., Calvi, G. M., Priestley, M. J. N., and Kowalsky, M. J. (2003). "The Limitations and Performances of Different Displacement Based Design Methods." *Journal of earthquake Engineering*,7, 201-241.

Sweeney, S. C., Horney, M. A., and Orton, S. L. (2005). "Seismic Response of a Half-Scale Masonry Building with Flexible Diaphragms." Engineer Research and Development Center. Champaign, IL, USA: Military Facilities Engineering Technologies, no. ERDC/CERL-TR-05-25.

Taylor, C. P., Cote, P. A., and Wallace, J. W. (1998). "Design of Slender Reinforced Concrete Walls with Openings." *ACI Structural Journal*, 95(4).

Thomsen, J. H., Wallace, J. W. (2004). "Displacement-Based Design of Slender Reinforced Concrete Structural Walls: Experimental Verification." *Journal of Structural Engineering*, 130(4), 618-630.

Tomaževič, M., and Weiss, P. (1994)."Seismic Behaviour of Plain- and Reinforced- Masonry Buildings." *Journal of Structural Engineering*, 120 (2), 323-338.

Turek, M., Ventura, C. E., and Kuan, S. (2007). "In-Plane Shake-Table Testing of GFRP Strengthened Concrete Masonry Walls." *Earthquake Spectra*, 23 (1), 223–237.

Wierzbicki, J.C. (2010). "Behaviour of Reduced-Scale Fully Grouted Concrete Block Shear Walls." M.A.Sc. Thesis, Civil Engineering, McMaster University, Hamilton, Canada.

Williams, M. S., Blakeborough, A. (2001). "Laboratory Testing of Structures under Dynamic Loads: An Introductory Review." *Philosophical Transactions:Mathematical, Physical, and engineering Sciences (The Royal Society)* 359(1786), 1651-1669.

Žarnić, R., Gostič, S., Crewe, A. J., and Taylor, C. A. (2001). "Shaking Table Tests of 1:4 Reduced-Scale Models of Masonry Infilled Reinforced Concrete Frame Buildings." *Earthquake Engineering & Structural Dynamics*, 30(6), 819–834.

CHAPTER 3: SHAKE TABLE SEISMIC PERFORMANCE ASSESSMENT OF FULLY GROUTED LIGHTLY REINFORCED CONCRETE BLOCK SHEAR WALLS

3.1 Introduction

In this chapter a report on the experimental program undertaken for this research including information on the design and construction procedures of the wall models, material properties, design and fabrication of the test setup, and the instrumentation scheme is provided. The chapter also reports on the shake table test results in terms of general observations, cracking patterns, and failure modes for each wall tested. Results on the lateral strength of the walls, their hysteretic response, and dynamic properties based on the experimental data, and the contribution of different displacement components to the response of the walls are also discussed in this chapter.

This chapter contains the work in the following article:

Mojiri, S., El-Dakhakhni, W. W., Tait, M. J. (2013). "Shake Table Seismic Performance Assessment of Fully Grouted Lightly Reinforced Concrete Block Shear Walls." ASCE Journal of Structural Engineering, Under Review.

3.2 Experimental Program

3.2.1 Archetype Building

The archetype (prototype) buildings considered for the experimental program were single and two-storey buildings sharing the same footprint configuration

shown in Fig. 3.1-a in plan. The buildings each have ten peripheral and two internal RM shear walls to resist seismic loads and two gravity columns to carry significant parts of the gravity loads. Similar archetypal buildings have been recently used (NIST 2010) to evaluate the seismic performance of RM SFRS according to the FEMA P695 (ATC, 2009) methodology. The numbers in the figure refer to the prototype shear walls of the models considered for the current experimental program.

3.2.2 Similitude Requirements

The scaling of the third scale model walls ($S_L = 3$) and the dynamic tests were performed based on laws of dynamic similitude (Harris and Sabnis 1999).

Table 3.3: Scale factors required for dynamic similitude

Scaled quantities	Dimension	Scale factor	Scaled quantities	Dimension	Scale factor
Force (F)	F	$S_E S_L^2$	**Frequency (f)**	T^{-1}	$S_L^{-\frac{1}{2}}$
Acceleration (a)	LT^{-2}	**1**	**Stress (σ)**	FL^{-2}	S_E
Gravitational acceleration (g)	LT^{-2}	**1**	**Strain (ϵ)**	**-**	**1**
Velocity (v)	LT^{-1}	$S_L^{\frac{1}{2}}$	**Poisson ratio (ν)**	**-**	**1**
Time (T)	T	$S_L^{\frac{1}{2}}$	**Modulus (E_s)**	FL^{-2}	S_E
Length (L)	L	S_L	**Mass density (ρ)**	$FL^{-4}T^2$	S_E/S_L
Displacement (δ)	L	S_L	**Energy (E)**	FL	$S_E S_L^3$

Table 3.2: Details of the prototype and model walls

Wall	Number of Stories	Length P/M[1](mm)	Aspect ratio	Ver. Reinf. P/M[1]	ρ_v P/M[1](%)	S_v P/M[1](mm)	Hor. Reinf. (First floor)	Axial stress
1	2	1,800/598	3.77	3M15/3-D4*	0.18/0.20	798/266	M10 @ 390 mm/ W1.7 @ 130 mm	$0.02f'_m$
2				2M15/2-D4	0.12/0.13	1596/532		
3	1		1.88	3M15/3-D4*	0.18/0.20	798/266		
4	2	2,600/865	2.62		0.12/0.14	1197/399		
5		1,800/598	3.77	2M25/2-D7**	0.29/0.24	1596/532		
6				3M15/3-D4*	0.18/0.20	798/266		0.05 f'_m

1-Prototype/Model
***D4=26 mm^2**
****D7=45 mm^2**

The scaling factors required to maintain dynamic similitude are as presented in Table 3.1, where the length scale factor is defined as $S_L = L_{prototype}/L_{model}$ and the modulus of elasticity scale factor is defined as $S_E = E_{prototype}/E_{model}$. As the materials (i.e. concrete) for the model and the prototype walls are essentially similar ($S_E \approx 1$), additional mass of $\Delta m = m_p(1/S_L^2 - 1/S_L^3)$ lumped at different floor levels is needed to compensate for the required material density scaling.

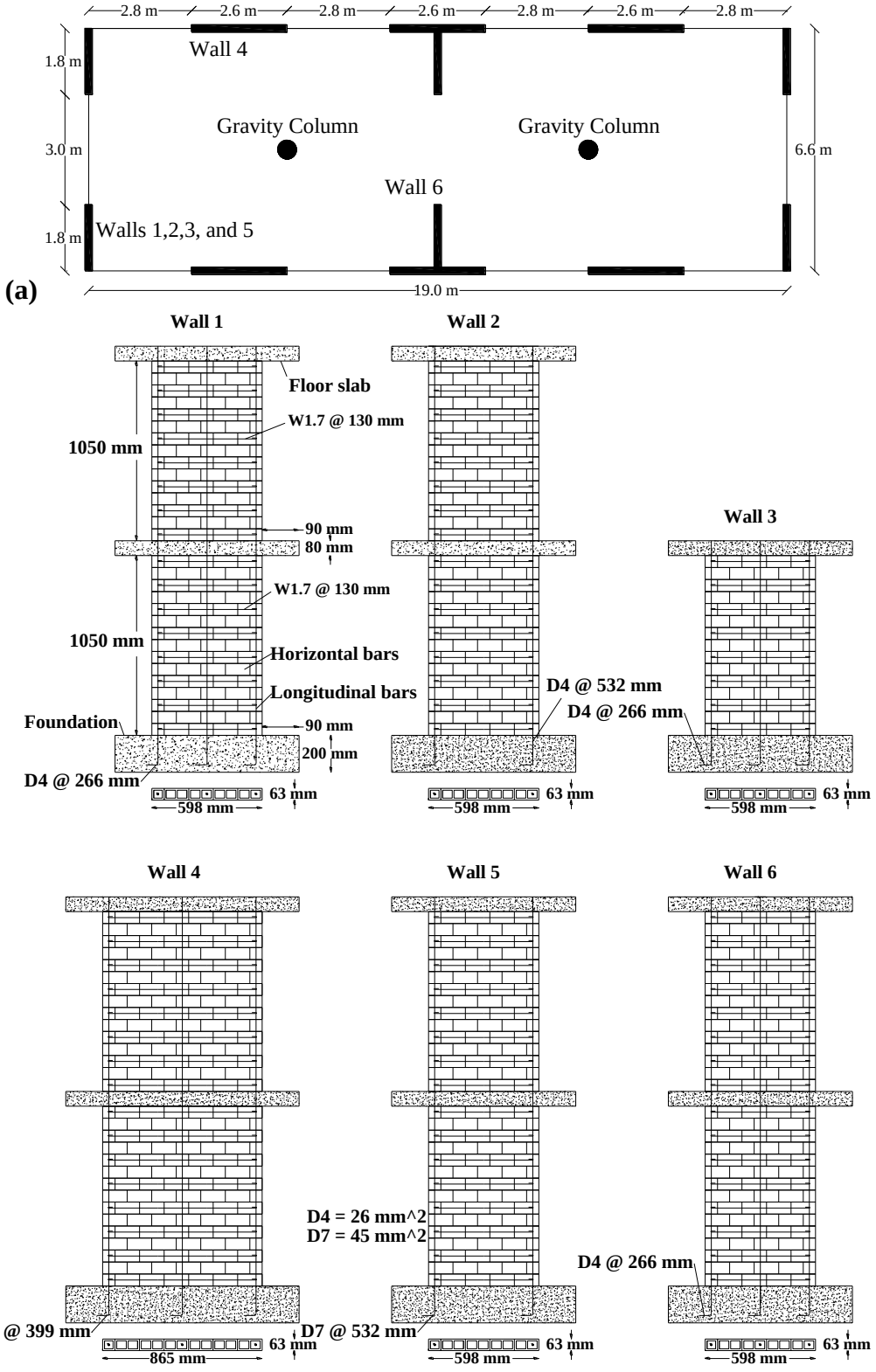

Figure 3.1: Test Walls: **a)** As located in the Archetype Building Plan; and **b)** As scaled

More detailed studies of scaling requirements for shake table testing of reduced-scale structural components and similitude requirements and choice of model scale as well as some relevant case studies of RC and RM walls are presented elsewhere by Caccese and Harris (1990) and Harris and Sabnis (1999).

3.2.3 Wall Design and Construction

Figure 3.1-b shows the elevation of the model walls with their horizontal and vertical reinforcement details and Table 3.2 summarizes the details of the prototype and model walls. The design of the walls does not meet the maximum vertical reinforcement spacing limitations of the Canadian masonry design code (CSA-S304.1-2004) for the *limited ductility* or the *moderately ductile* shear wall categories. However, the wall design meets the maximum spacing for the *conventional construction* category which is restricted to low seismic zones. The design of the model RM shear walls was focused on providing experimental data to investigate the effect of typical wall design parameters such as the wall height (Wall 1 and Wall 3), vertical reinforcement spacing (Wall 1 and Wall 5), level of axial load (Wall 1 and Wall 6), wall length (Wall 2 and Wall 4), and reinforcement ratio (Wall 2 and Wall 5) on their seismic performance.

The RM walls were constructed on RC bases and for the two-storey walls, 80 mm thick RC slabs were used between the first and second story and on top of the walls (for both the two- and single-storey walls) as shown in Fig. 3.1-b. The slabs were to simulate the discontinuity between the walls of first and second

stories in actual RM construction and to provide a means for applying the lateral inertial forces to the walls at different levels. The construction of the specimens started with pouring of the concrete bases. The walls were then constructed in a running bond and in half story stages (to allow for low-lift grouting) from third-scale concrete masonry units by a professional mason.

The vertical reinforcement was anchored to the reinforcement in the base and no lap splices were used in the vertical reinforcement. The webs of the concrete masonry units (CMU's) were notched to the mid-height of the units in every other course to allow placement of the shear (horizontal) reinforcements. This also facilitated grout flow between the cells and ensured complete grout filling of the walls. The RC slabs were cast in place between first and second stories and on the roof after the completion of the construction of each story and the vertical reinforcement in the walls were extended through the reinforcement mesh of the floor and bent inside the roof slabs.

3.2.4 Material Properties

The walls were constructed from 63 x 63 x 130 mm third-scale CMU's, which were manufactured as true replicas of the190 x 190 x 390 mm standard CMU's widely used in North America. The average CMU compressive strength was 25.9 MPa with a coefficient of variation (c.o.v.) of 13.4% (ASTM C140-122012-c). Type S mortar (CSA A179-04 2004) made with a maximum aggregate size of 1.25mm (third-scale), weight proportions of 1.0: 0.2: 3.53: 0.85 of portland

cement: lime: sand: water, and with an average flow of 125% (ASTM C1437-07 2007)was used for the construction of the walls. The average compressive strength of the 51 mm cubic mortar specimens was 24.6 MPa with a c.o.v. of 12.2% (ASTM C780-12 2012-b). High slump grout with weight proportions of1.0: 0.04: 3.9: 0.85 of portland cement: lime: sand: water and with maximum aggregate size of 2.5mm was used. The compressive strength of the cylinder grout specimens was 20.4 MPa (c.o.v. = 10.5%) (ASTM C476-10 2010-a).

Three different types of reinforcing steel were used in the wall construction. The first and second were deformed bars (D4 and D7),which were used as vertical reinforcement in the walls and as reinforcing mesh in the RC bases and the slabs. The diameter of the D4 and D7 bars were 5.74 mm and 7.6 mm, respectively. The third type of reinforcement was a smooth W1.7 wire, which had a diameter 3.8 mm, was used for horizontal (shear) reinforcement in the walls. The average yield strength and Young's modulus were 490 MPa (c.o.v. = 1%) and 195GPa (c.o.v. = 6.5%) for the D4 bars, 487 MPa (c.o.v. = 3.2%) and 202GPa (c.o.v. = 8.9%) for the D7 bars, and 281 MPa (c.o.v. = 0.4%) and 214GPa (c.o.v. = 2.4%) for the W1.7 wires respectively (ASTM A615-12 2012, ASTM E111-04 2004).

Third-scale fully grouted masonry prisms were constructed with four course running bond by the mason on each construction day. The average compressive strength of the masonry prisms (f'_m) was 17.7 MPa (c.o.v. = 13.6%) (CSA S304.1 2004)and the average value of the modulus of elasticity of the

masonry prisms obtained as the slope of the straight line between stress and strain at $0.05f'_m$ and $0.33f'_m$ stress levels was 10,250 MPa (c.o.v. = 29.1%). The average value of the modulus of elasticity to strength ratio was approximately 580 which is 32% less than the 850 value specified by CSA-S304.1 (2004) but still within its expected range of variation (Drysdale and Hamid, 2005).

3.2.5 Test Setup

The test setup shown in Fig. 3.2 has the following components: a uniaxial shake table, an external mass supporting system (frame, masses, bearings and links), lateral (out-of-plane) supports, and an axial loading system. The uniaxial shake table has a 2.0 x 2.15 m platform and a servo-controlled dynamic actuator with stroke of +/-150 mm.

Based on approximate tributary areas shown in Fig. 3.1-a, and considering a residential application for the buildings, the axial load is approximately 2% and 4% of the resistance of the nominal gross section ($i.e. 0.02A_g f'_m$ and $0.04A_g f'_m$) for peripheral and internal walls, respectively. Referring to Fig. 3.1-a, it can be inferred that the two RC columns would carry significant portions of the gravitational but not the seismic loads as they would not be designed as a part of the SFRS. As such, the RM walls would be required to carry seismic masses that are not consistent with the gravitational loads. Subsequently, an external mass supporting system was designed and constructed next to the shake table to carry the main part of the inertial (seismic) mass.

The inertial mass at each floor was connected through a loading link using real pin-type connections to both sides of the floor slabs. Each floor mass was placed on four linear bearings which facilitated the horizontal movement of the masses with minimal friction. Not only did this system enhance the test safety in the event of a wall collapse but it also reduced the possibility of out-of-plane wall instability (in case of a mass accidental, or wall damage-induced, eccentricity) and provided a simple system for transmitting the inertial loads to the walls and

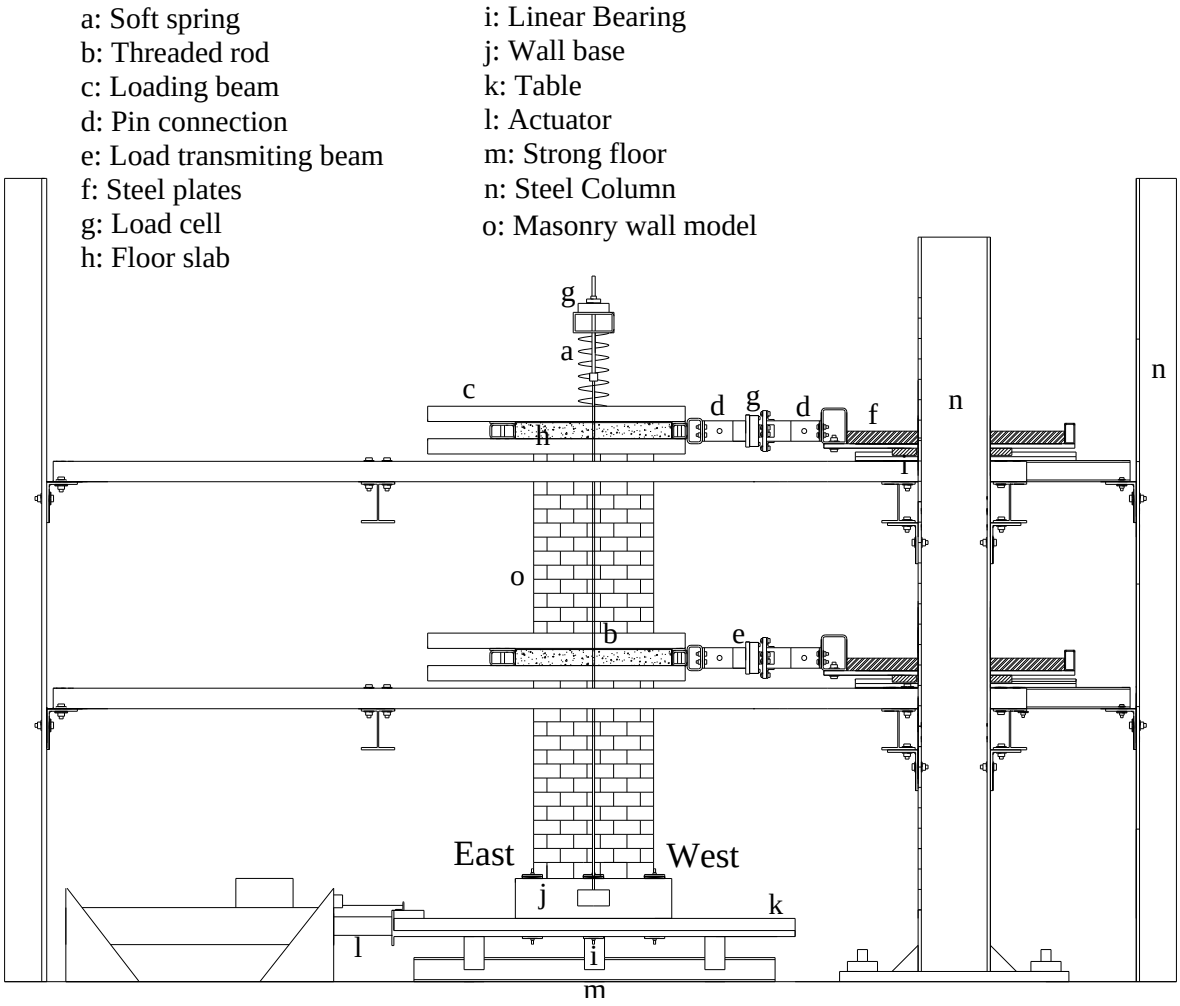

Figure 3.2: Test setup elevation

decoupled gravitational and seismic masses. The separation of the inertial model mass from the shaking table has been used by a number of other researchers (Lestuzzi and Bachmann, 2007; Ghorbani et al., 2012 and Carrillo and Alcocer, 2011).

Based on the preliminary nonlinear response history analysis conducted prior to the shake table tests (Mojiri et. al, 2012), an inertial mass of approximately 1,000 kg was necessary at each story of the model walls in order to achieve significant nonlinear response in most of the model walls. Parts of the inertial mass were provided by the mass of the walls themselves, the loading beams, and parts of the mass supporting system, and the rest was provided by four 510 mm x 510 mm x 63 mm steel plates weighing 125 kg each at different floor levels. Based on this scheme, the total inertial mass including the tributary contribution of wall mass at each story was 1,097 kg and 1,119 kg respectively for the first and second story of Walls 1, 2, 5, and 6; 1,119 kg for Wall 3, and 1,158 kg and 1,162 kg for the first and second story, respectively, of Wall 4.

In order to restrict the out-of-plane movements of the model walls at each floor slab, a lateral support system composed of lateral beams and ball bearing was used. In actual buildings, orthogonal walls that would be supporting the floor diaphragms would provide such lateral support. In order to simulate the compressive load on the model shear walls, two post-tensioned threaded rods were used to apply the required axial load on the walls. The threaded rods were connected in series with a soft spring at the top of the wall to prevent large

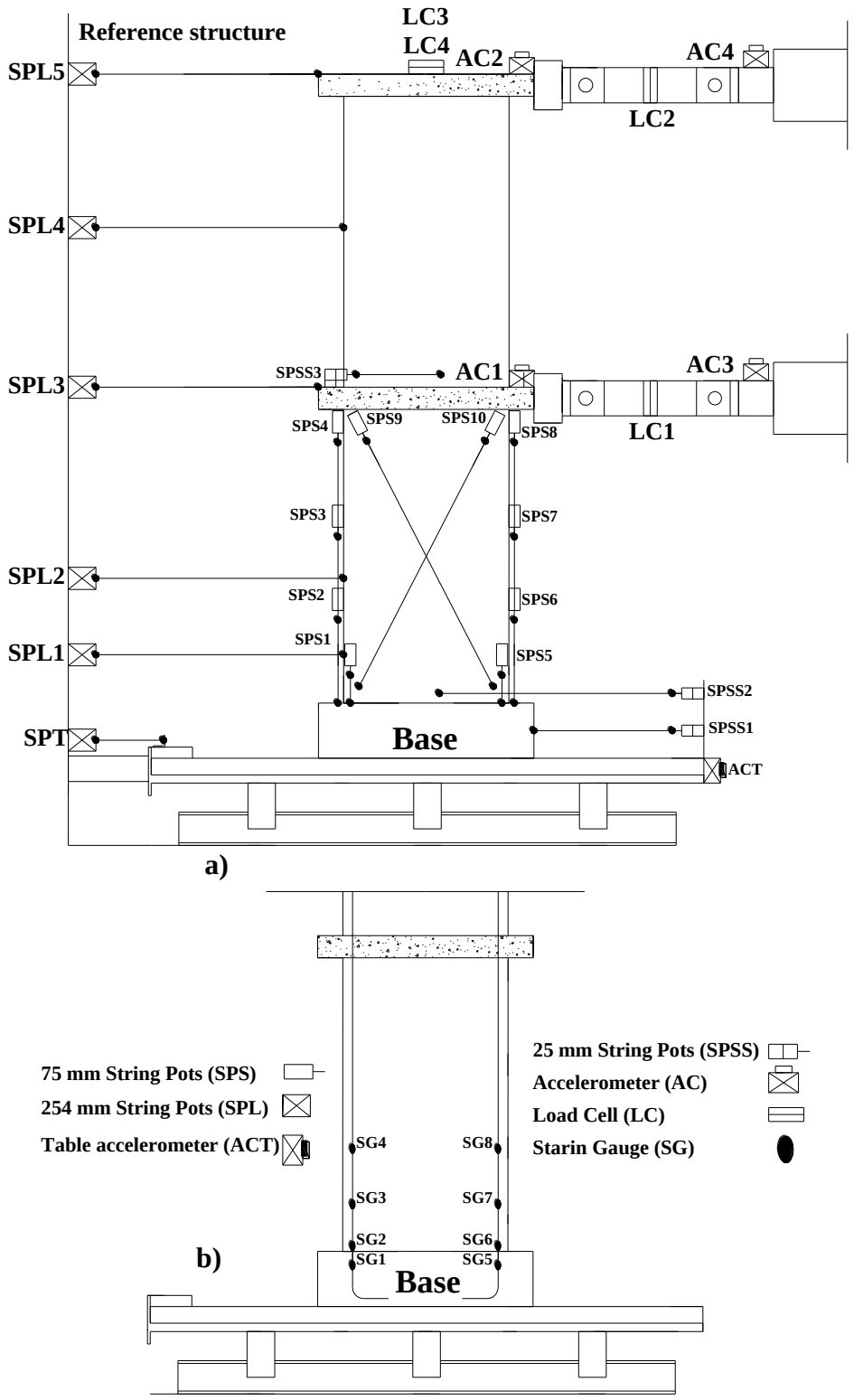

Figure 3.3: Instrumentation map: **a)** External instrumentation, **b)** Internal instrumentation

fluctuations in the amount of axial load due to extension of the rods during the shaking of the model walls.

3.2.6 Instrumentation

The experimental data was recorded at a sampling frequency of $f_s = 1{,}612$Hz and filtered using a low-pass anti-aliasing filter with a cut-off frequency of $0.45f_s$ less than the Nyquist frequency in order to avoid unnecessary aliases of the original signal. Figure 3.3 shows the instrumentation layout, where the external instrumentation was used to measure the absolute lateral displacement of the shake table as well as the walls at various locations along their heights. In addition, sliding of the base, first story and second story displacements, vertical deformations of the walls along their heights and the diagonal deformations in the first story, acceleration of the shake table and first and second story of walls, and lateral and axial forces were all recorded as indicated in Fig. 3.3-a. Internal instrumentations consisted of strain gauges installed at four different locations along the end vertical reinforcement bars as shown in Fig. 3.3-b. All data was digitally filtered (post-processed) using a low-pass Butterworth filter with a cut off frequency of 30 Hz as recommended by FEMA-461 (ATC, 2007).

3.2.7 Ground Motion Record Selection and Scaling

For this study the Loma Prieta 1989 earthquake record from PEER NGA

Table 3.3: Dynamic characteristics of the Loma Prieta earthquake at Station Gilroy Array #2

Original record				Scaled record			
Duration (sec)	PGA (g)	PGV (cm/s)	PGD (cm)	Duration (sec) (s)	PGA (g)	PGV (cm/s)	PGD (cm)
40	0.37	32.91	7.15	23	0.37	19.02	2.39

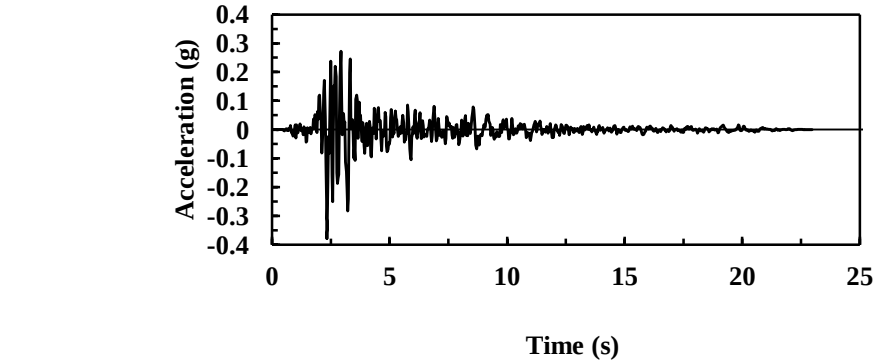

(a)

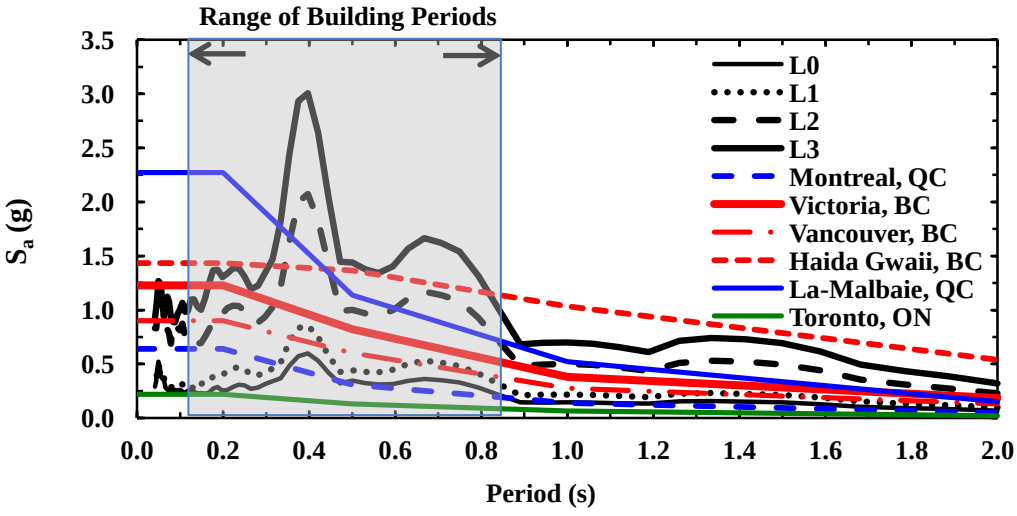

(b)

Figure 3.4: Scaled Loma Prieta 1989 earthquake: **a)** Acceleration response history; and **b)** Response spectra

strong motion database (PEER NGA Database, 2011) was selected. The third-scale model record was obtained using the scaling factors presented in Table 3.1. The dynamic characteristics of the original and model records are presented in Table 3.3 and the acceleration history of the model record is shown in Fig. 3.4a. The original record was selected and scaled to four different intensity levels, L0, L1, L2, and L3, covering a wide range of different seismic hazard levels of high seismic zones across Canada (NRCC 2010) as shown in Fig. 3.4-b. The intensity scaling for each intensity level was performed by multiplying the acceleration response history by an amplification factor. The Peak Ground Acceleration (PGA) of L0, L1, L2, and L3 intensity levels were 0.19g, 0.24g, 0.61g, and 0.84g, respectively. The dynamic tests for each specimen started with the application of the L0 level record and continuing with L1, L2, and L3 level records. Static pull-back tests were also conducted before and after each test to evaluate the dynamic properties of the walls as will be explained later.

3.3 Experimental Results

3.3.1 Crack Pattern and Failure Modes

The cracking pattern was documented for each wall after each test at different earthquake intensity levels. In general, the main cracks observed after each test were typically limited to vertical cracks in the wall toe regions and horizontal flexure and shear cracks along the wall/base interface.

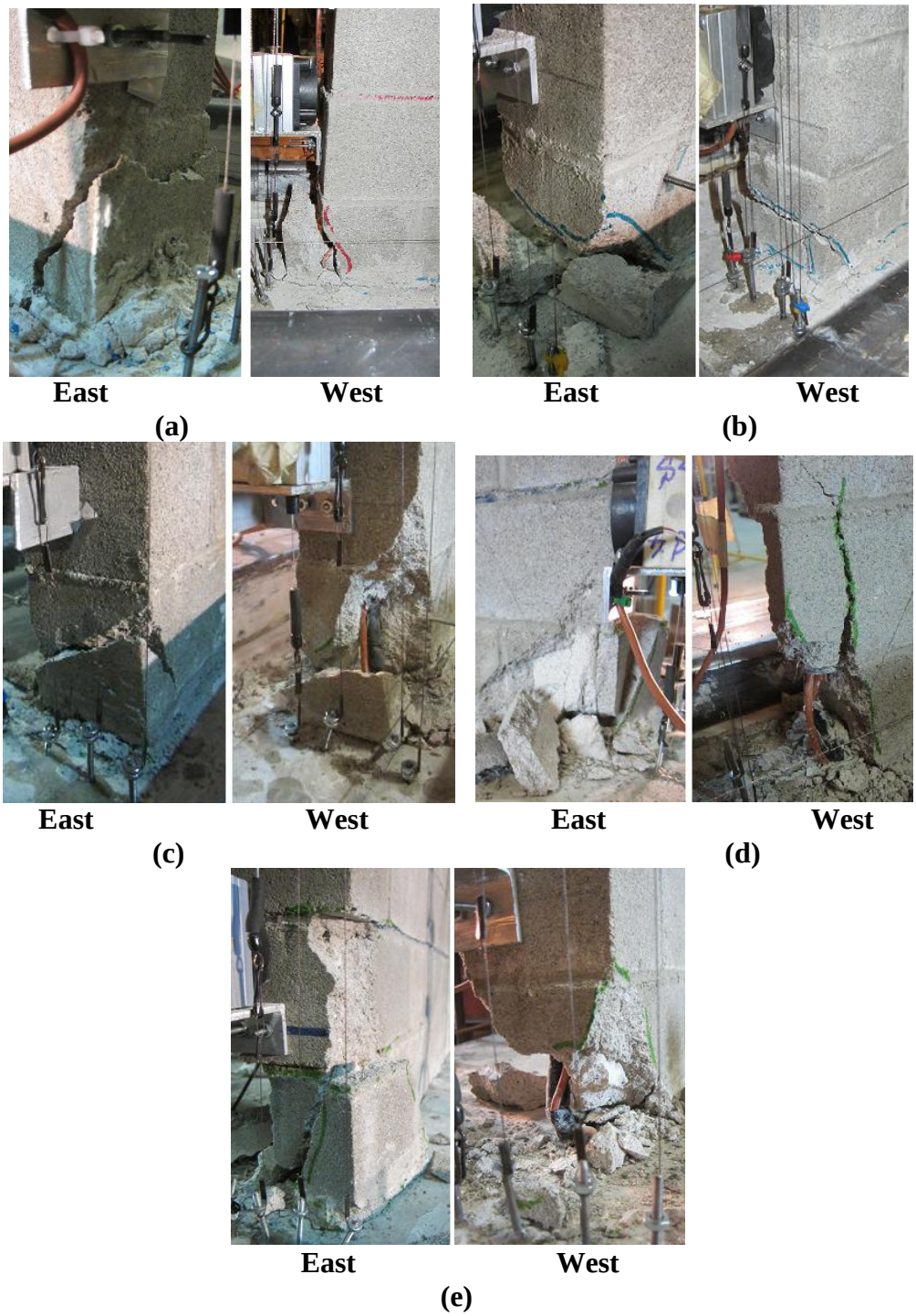

Figure 3.5: Damaged zones and bar buckling of the walls after the L3 level test: **a)** Wall 1, **b)** Wall 2, **c)** Wall 4, **d)** Wall 5 and **e)** Wall 6

The diagonal shear cracks were limited to a few minor cracks in a few walls as all walls were designed following capacity design principles with adequate horizontal reinforcement to prevent shear failures. As such, the failure modes for the walls were mainly flexural characterized by steel yielding followed by crushing of the masonry and subsequent buckling of the vertical bars located at the wall toes. Following toe crushing and bar buckling, the walls typically exhibited significant sliding and rocking resulting in even more damage to the wall toes. Walls 1, 2, and 5 started yielding at the L0 level records while Walls 3, 4, and 6 started to yield at the L3, L2, and L1 level tests, respectively. Nevertheless, all walls maintained their integrity after the L3 level test and damage was typically localized within the first and second courses at the wall toes. Figure 3.5 shows the damaged zones and bar buckling in Walls 1, 2, 4, 5, and 6 at the end of tests.

3.3.1.1 Wall 1

This wall started to develop a horizontal flexural crack at the wall/base interface following the L0 level test. The width of the base crack increased after the L1 level test and mortar spalling along the base of the wall started to occur. A narrow crack was also observed after the L1 level test at the wall/slab interface of the second story for this wall. The East vertical bar started to buckle during the L2 level test at 3.32 sec and the West toe of the wall crushed up to the first course. The horizontal cracks at the first and second stories became wider and another

horizontal crack started to develop above the second mortar course of the first story. At the beginning of the L3 level test the East vertical bar buckled at 3.14 sec, after which the wall exhibited significant rocking and sliding along its base. The damage at the wall toes was very localized, not exceeding the first course of the wall in height and half a block in length. No signs of diagonal cracking were observed even after the conclusion of the L3 level test.

3.3.1.2 Wall 2

A horizontal flexural crack started to develop at the base of this wall during the L0 level test. This crack became wider and some mortar chippings also were observed at the base of the wall after the L1 level test. A narrow horizontal crack also started to develop at the wall/slab interface of the second story after the L1 level test. The base cracks at the first and second stories widened after the L2 level test. The East vertical bar buckled at 3.32 sec and the masonry blocks at both wall toes crushed half a course in height and half a block in length during the L2 level test. The West vertical bar buckled at 3.16 sec during the L3 level test after which the wall started to rock and slide significantly. No signs of diagonal cracking were observed even after the L3 level test for this wall.

3.3.1.3 Wall 3

No damage was observed in Wall 3 except for horizontal cracking and mortar spalling at the wall/base interface during the L3 level test. The wall remained fairly elastic during the L0and L1 level tests and started yielding during

the L3 level test. No cracks were observed following any of the tests. In fact, since this wall was a single story wall, it carried approximately half of the inertial mass of the other two-story walls and hence the seismic demand on this wall during all tests was significantly less than the other two-story walls and consequently did not cause damage.

3.3.1.4 Wall 4

No noticeable damage occurred in this wall during the L0 and L1 level tests during which the wall remained fairly elastic. Significant sliding was observed during the L2 level test. A horizontal crack developed at the at the wall/base interface and the West toe of the wall crushed half a block in length and half a course in height after the L2 level test. The crushing of the West toe extended to the second course in height and the East wall toe crushed within half a block in length and half a course in height after the L3 level test. The horizontal crack at the wall base widened and a narrow crack started to develop at the wall/slab interface of the second story after the L3 level test. The vertical bars at the East and West wall toes buckled at the 2.43 and 3.77 sec respectively during the L3 level test. No signs of diagonal cracking were observed even after the L3 level test for this wall as well.

3.3.1.5 Wall 5

Horizontal cracks and mortar spalling were observed at the wall/base interface after the L0 and L1 level tests for this wall. Both wall toes were crushed

and subsequently both vertical bars buckled during the L2 level test. The damage to the toes extended up to the second course for the West toe and up to the first course for the East toe. The East vertical bar buckled at 3.31 sec and both wall toes crushed during the L3 level test, after which the wall exhibited more sliding and rocking. The damage to the West and East toes extended to the third course and second course respectively but was limited to a half block in length. A wide diagonal crack also appeared in the middle of the wall on the face shell of the masonry extending from the base to the top of the first course. A small crack was also observed at the wall/slab interface of the second story after the L3 level test.

3.3.1.6 Wall 6

During the installation of this wall, some cracks developed along the wall/base interface and above the second course due to a minor accidental out-of-plane loading on the wall. The base crack at the first story became wider and a narrow crack started to develop at the second story accompanied by some mortar spalling at the base of the wall after the L0 and L1 level tests. The wall also exhibited some rocking and sliding along the horizontal cracks during the L1 level test. The horizontal cracks became wider and extensive vertical cracks started to appear in the toes after the L2 level test. The damage to the toes extended up to the second course for the East toe and up to the first course for the West toe. During the L3 level test the East and West vertical bars buckled at 3.32 and 3.78 sec, respectively and both toes crushed completely and then the wall started to

exhibit extensive rocking and sliding on its base. The damage to the wall toes did not exceed the second course of the wall in height and half a block in length. Two minor diagonal cracks were visible after the L3 level test for this wall in the first and second courses.

3.3.2 Floor Displacements and Accelerations

Figure 3.6 shows the relative lateral displacement, drift ratio, and acceleration histories for the top story of Wall 6 for the L1, L2, and L3 level earthquakes as a representative sample of the wall responses. As can be observed from the Fig. 3.6-a, the drift ratio during the L1 level earthquake does not exceed 0.5 % while it reaches 2% during the L2 level earthquake. The consistently high and low peaks of displacements (or drifts) and acceleration responses, respectively, during the L3 level earthquake after 3.32 seconds shown in the Fig. 3.6-a and 3.6-b, respectively, are attributed to the buckling of the vertical bars and the subsequent rocking of the wall, which resulted in almost 4% drift. The decrease in the frequency of the displacement and acceleration histories after 3.32 seconds for the L3 level curves is also due to the wall stiffness degradation due to masonry crushing and the subsequent vertical bar buckling at the wall toes.

The displacement, drift ratio, and acceleration time histories for the rest of the walls which are provided in Appendix A also exhibited similar trends as Wall 6 except for Wall 3 which remained elastic during the L0, L1, and L2 level tests

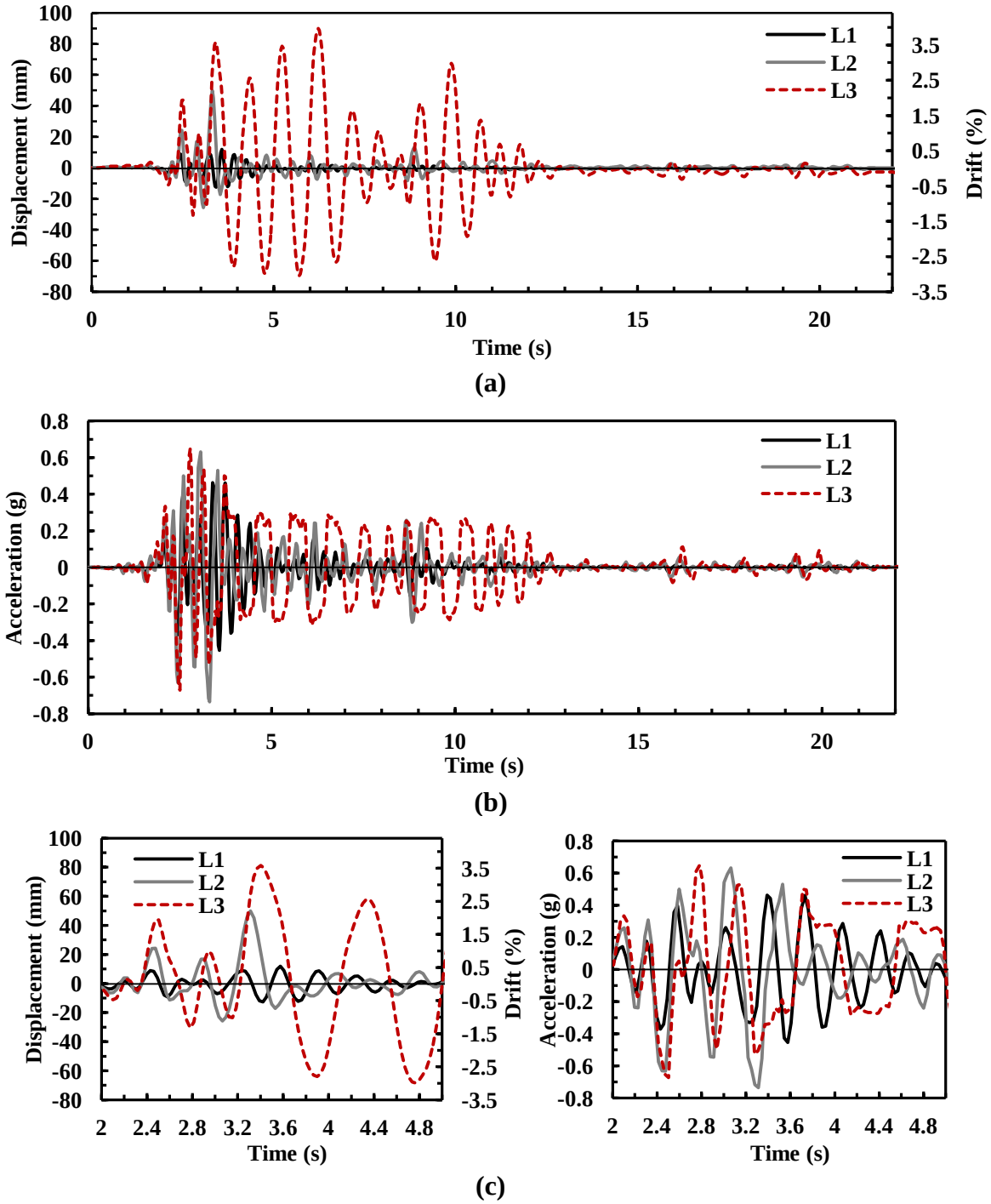

Figure 3.6: Responses history of top story of Wall 6 under the L0, L1, and L2 level records: **a)** Relative lateral displacement and drift, **b**) Acceleration, **c)** Responses between 2-5 seconds

and experienced slight yielding during the L3 level tests without major damage to the wall.

3.3.3 Hysteretic Response

3.3.3.1 Base Shear-Top Wall Displacement Relationships

The base shear-top wall displacement relationships of the walls for L1 and L2 levels are shown in Fig. 3.7. The base shear values are computed by multiplying the story masses by the corresponding acceleration measured during the tests. As Fig. 3.7 shows, all walls experienced extensive nonlinear response with drift levels typically exceeding 2% during the L2 level test except for Walls 3 and 4. Wall 3 remained almost elastic even during the L2 level test with drift levels less than 0.2% and the drift levels for Wall 4 exceeded 1% in the positive region (West direction) and 0.5% in the negative region (East direction) but did not reach the drift ratios of Walls 1,2, 5, and 6. It is also observed that Walls 1, 2, 4, 5, and 6 experienced pinched force-displacement responses during the L1 level tests and loss of strength and increase in the energy dissipation resulting from the increase in the wall damage during the L2 level tests.

3.3.3.2 Moment-Curvature Relationships

Figure 3.8 shows the moment-curvature relationships at the base of the walls during the L1 and L2 level tests. The values of the moment at the base of the walls are computed from the values of the lateral forces (masses multiplied by their corresponding acceleration) at each story multiplied by their corresponding height from the wall bases.

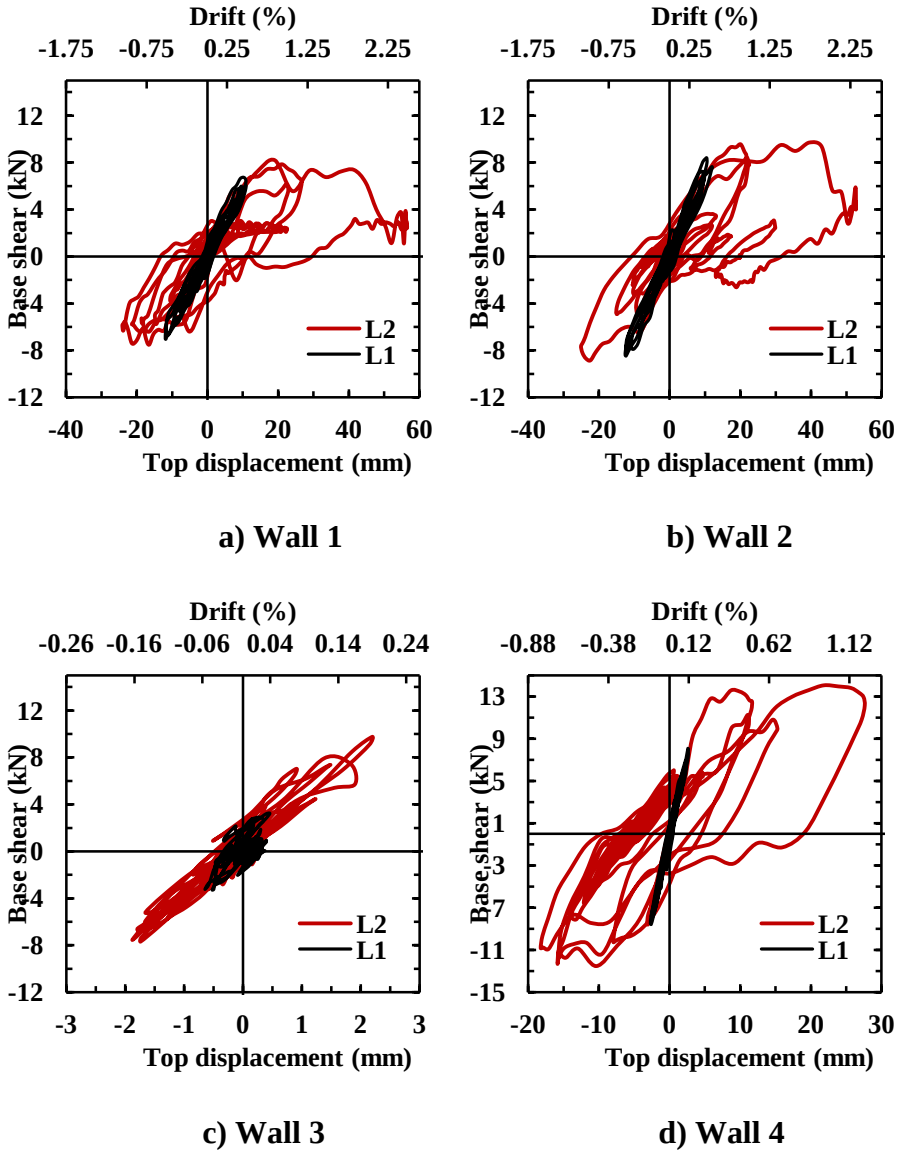

Figure 3.7: Base shear-top floor displacement curves for walls under L1 and L2 level earthquakes

The curvature at the wall base is calculated from the vertical wall displacements measured using the string potentiometers installed above the wall bases (See Fig 3.3-a) as will be explained later in the paper under the Analysis of Experimental Results section. All walls, except Wall 3, experienced extensive

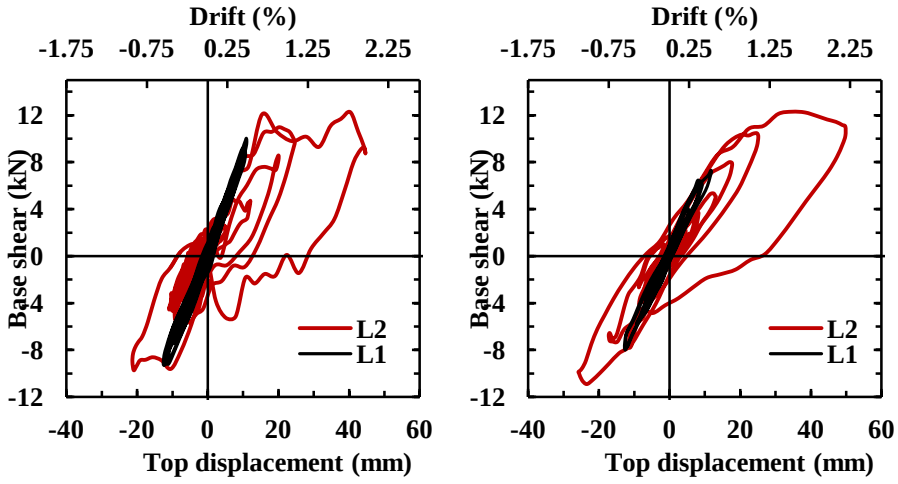

Figure 3.7 (contd): Base shear-top floor displacement curves for walls under L1 and L2 level earthquakes

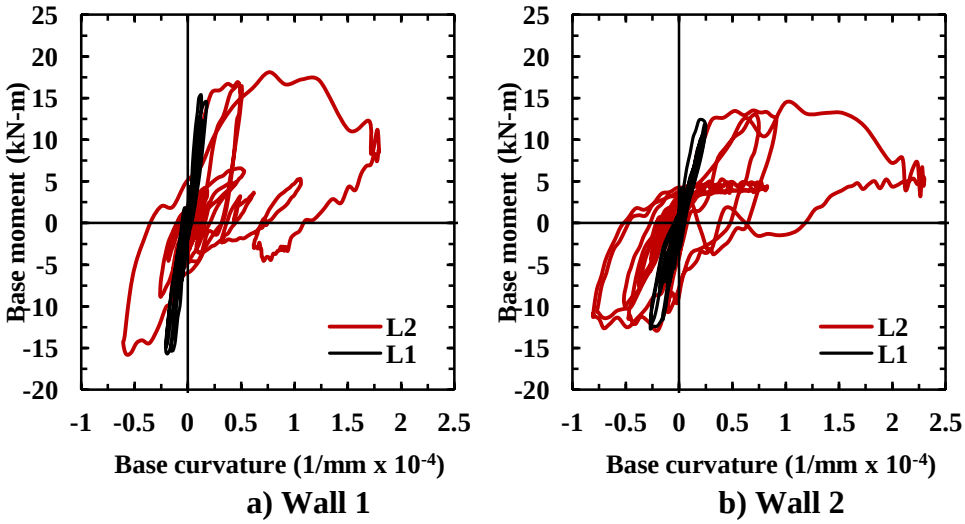

Figure 3.8: Base moment-curvature curves for walls under L1 and L2 level earthquakes

nonlinear flexural response during the L2 level tests but responded in almost a linear elastic manner during the L1 level tests. The stiffness degradation and the

increased energy dissipation, indicated by the area enclosed by the hysteresis loops, recorded during the L2 level tests also correspond to the increased wall damage during the L2 compared to the L1 level tests.

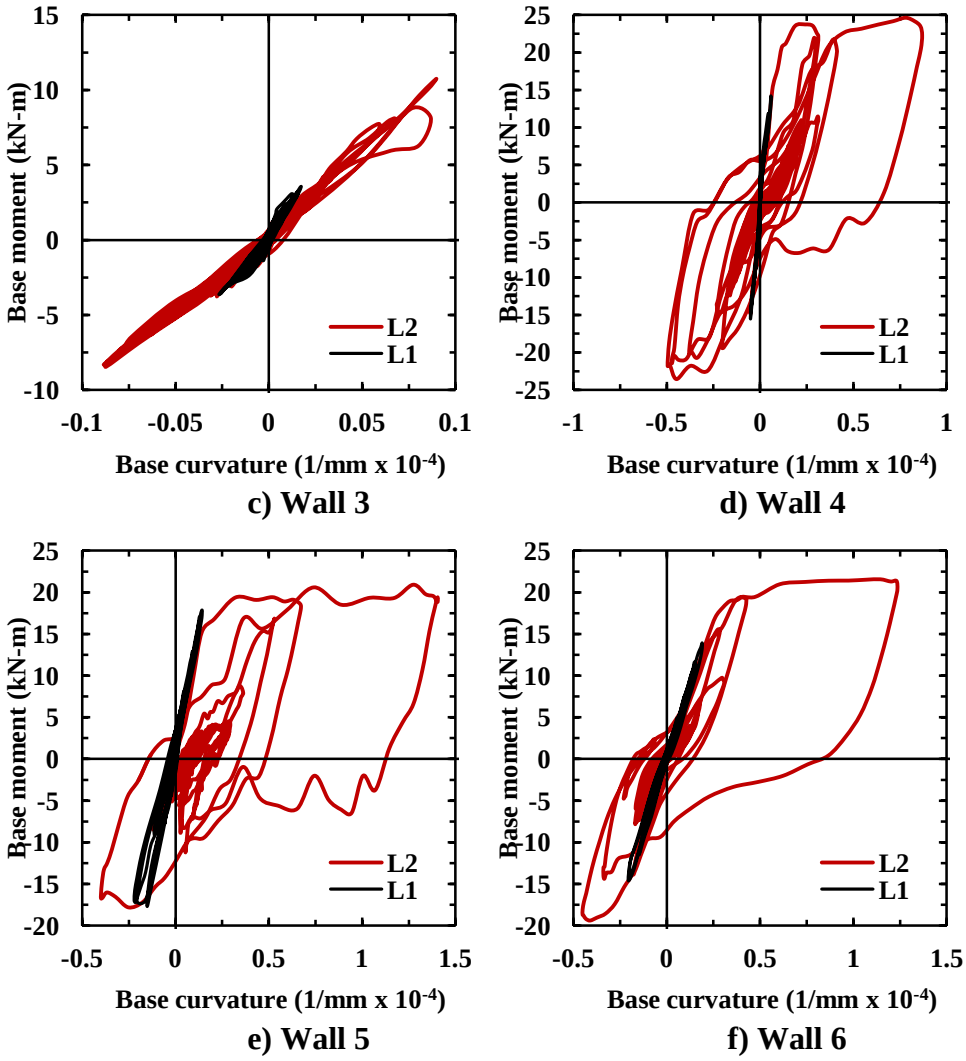

Figure 3.8 (contd): Base moment-curvature curves for walls under L1 and L2 level earthquakes

3.4 Analysis of Experimental Results

3.4.1 Wall Base Moment, Curvature, and Shear

The experimental yield moments and ultimate moment capacities ($M_{yr,e}$ and $M_{ur,e}$)and corresponding curvatures ($\varphi_{yr,e}$ and $\varphi_{ur,e}$) of the model walls are presented in Table 3.4. Wall yielding is identified when either one of the end vertical bars reaches the yield strain at the wall/base interface. This was determined from the measurements of the strain gauges installed on the same location (see Fig. 3.3-b).The experimental ultimate moment capacity of the walls)and corresponding curvatures are identified as the maximum moment carried by the wall prior to toe crushing and/or vertical bar buckling and the corresponding curvature, respectively. Table 3.4 also gives the predicted analytical yield moments and ultimate moment capacities ($M_{yr,a}$ and $M_{ur,a}$) and corresponding curvatures ($\varphi_{yr,a}$ and $\varphi_{ur,a}$) of the model walls. The ultimate values are obtained based on the provisions of CSA-S304.1 (2004) while the yield values are evaluated at the onset of yielding of the end vertical bar based on the beam theory. The experimentally obtained mechanical properties of the materials were used in the computation of the nominal flexural capacity of the walls and subsequently the material strength reduction factors for masonry and steel ($\emptyset_m$ and $\emptyset_s$) were set to unity in the calculations of the values in Table 3.4.

The variations in the ratios (P/P_i) of the axial load values, at the time where the yield and ultimate moments are reached, to the initial applied axial load are also presented in Table 3.4.

Table 3.4: Wall Characteristics

Wall	1	2	3	4	5	6
At Yield						
$M_{yr,e}\ (kN-m)$	11.25	11.06	11.10	16.60	13.06	10.90
$M_{yr,a}\ (kN-m)$	11.85	10.63	11.85	17.66	15.32	15.28
$M_{yr,e}/M_{yr,a}$	0.95	1.04	0.94	0.94	0.85	0.71
$\varphi_{yr,e}(mm^{-1}) \times 10^{-6}$	6.75	11.9	9.75	8.38	9.41	14.4
$\varphi_{yr,a}(mm^{-1}) \times 10^{-6}$	5.74	5.62	5.74	3.73	5.56	6.05
$\varphi_{yr,e}/\varphi_{yr,a}$	1.18	2.12	1.7	2.24	1.69	2.37
P_y/P_i	1.03	1.04	1.05	1.02	1.02	1.03
Yielding record level	L0	L0	L3	L2	L0	L1
At Ultimate Strength						
$M_{ur,e}\ (kN-m)$	18.21	14.78	*14.46	25.79	21.16	21.71
$M_{ur,a}\ (kN-m)$	14.64	11.26	14.64	21.74	16.15	18.49
$M_{ur,e}/M_{u,a}$	1.24	1.31	0.99	1.19	1.31	1.17
$\varphi_{ur,e}(mm^{-1}) \times 10^{-5}$	11.75	10.70	*1.43	9.25	12.98	11.22
$\varphi_{ur,a}(mm^{-1}) \times 10^{-5}$	6.28	8.40	6.28	6.28	7.19	4.68
$\varphi_{ur,e}/\varphi_{ur,a}$	1.87	1.27	0.23	1.47	1.81	2.40
P_u/P_i	1.10	1.09	*1.00	1.09	1.09	1.07
V_u/V_{rd}	0.81	0.54	*0.72	0.79	0.92	0.81
V_u/V_{rs}	0.52	0.64	*0.35	0.70	1.09	0.39
Ultimate record level	L2	L2	*L3	L3	L2	L2

*** The wall did not reach its ultimate capacity. Maximum loads are reported**

As mentioned previously, a soft spring was used to minimize the variations in the axial load levels, caused by the stretching of the threaded bars during wall movement, during the tests. The values show that the maximum variation of the axial load did not exceed 5% and 10% at the yield and ultimate moments, respectively.

The ratios between the experimentally obtained yield moment capacities to their predicted analytical values in Table 3.4 reflect general close predictions with a maximum difference of 6% for Walls 1, 2, 3, and 4 and 15% and 29% for Walls 5 and 6. The corresponding ratios at the ultimate levels are within 31% difference. On the other hand, the much higher variation between the experimentally-obtained and the analytically predicted curvatures, especially at ultimate level, reflects the conservatism in the ultimate strain value specified by the current North American masonry deign codes.

The nominal sliding (V_{rs}) and diagonal (V_{rd}) shear strengths of the model walls are obtained based on the equations proposed by CSA-S304.1 (2004) for RM shear walls using the material properties obtained in the laboratory ($i.e. \emptyset_m$=$\emptyset_s = 1.0$).The ratio of the base shear of the walls at yield and at ultimate moments to the nominal sliding and diagonal shear capacities of the walls are presented in Table 3.4. These values show that except for Wall 5, the base shear demand has been well below the shear capacity of the walls at yield and ultimate moment levels confirming the fact that the responses of the walls were dominated by the flexural response as designed. The slight deviation of Wall 5 is within the typical level of conservatism pertaining to shear capacity expressions in design codes.

3.4.2 Dynamic Wall Properties

The dynamic properties of the model walls were obtained before and after each test using static pull-back tests and also during each test using the acceleration transmissibility plots.

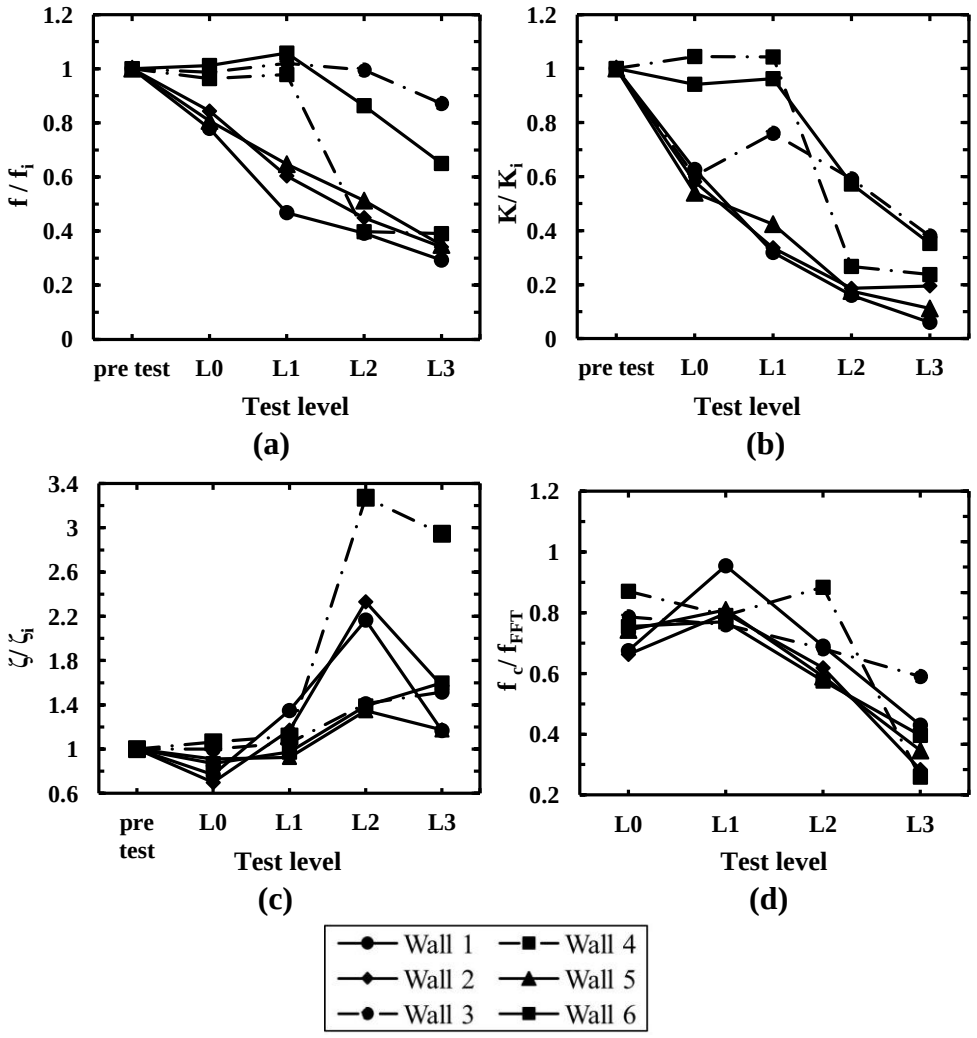

Figure 3.9: The variation of Different Dynamic Properties of the Wall with the Level of Earthquake: **a)** Undamped fundamental frequency; **b)** Lateral stiffness; **c)** Equivalent modal viscous damping; **d)** Normalized damped frequency of the walls obtained from transmissibility functions.

3.4.2.1 Static Pull-Back Tests

These tests were conducted before and after each test by pulling and rapidly releasing the top story mass to allow the wall to vibrate freely. The damped fundamental frequency of the walls (f_d) were obtained by performing a Fast Fourier Transformation (FFT) algorithm on the top story acceleration response history. The logarithmic decay method was used to obtain the equivalent modal viscous damping of the walls. The damping values (ξ) were used to obtain the undamped fundamental frequency (f) of the walls based on the following equation:

$$f = f_d/\sqrt{1-\xi^2} \tag{3.1}$$

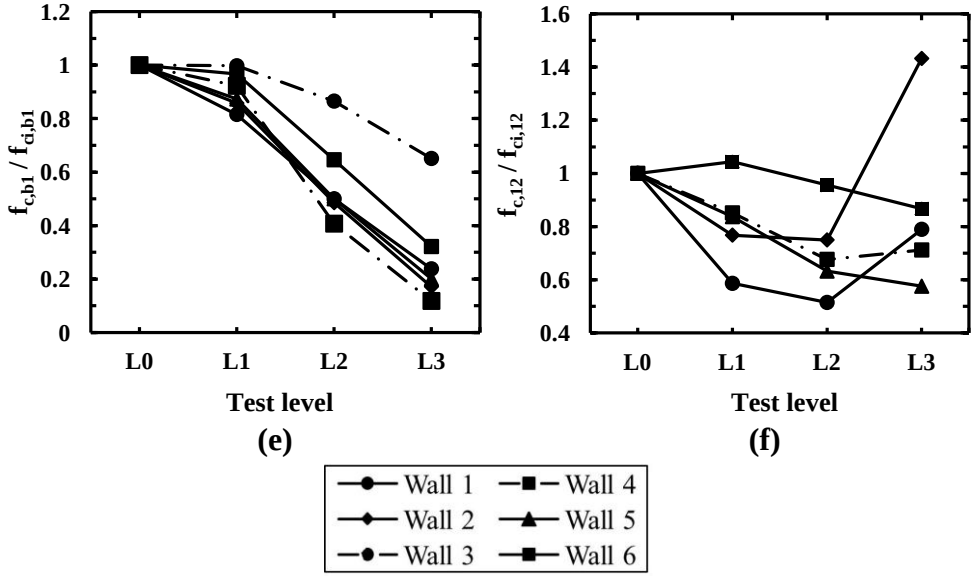

Figure 3.9 (contd): The variation of Different Dynamic Properties of the Wall with the Level of Earthquake: ; **e**) Normalized damped frequency of the walls obtained from transmissibility functions between the base and top of first story; and **f)** Normalized damped frequency of the walls obtained from transmissibility functions between the first and second stories

Figure 3.9-a shows the variation of the undamped fundamental frequency of the walls obtained after the shake table tests at different levels normalized to their corresponding initial values. These curves show a continuous reduction in the fundamental frequency of the walls with increased earthquakes intensity as a result of the damage accumulation and the subsequent lateral stiffness degradation. The exceptions are Walls 3, 4, and 6, which show almost no variation for the first three levels. This observation is consistent with the fact that Walls 3 and 4 did not reach yield until the L3 and L2 level respectively and hence no considerable damage occurred during these first two levels. The behaviour of Wall 6 can be explained based on the fact that the initial fundamental frequency of this wall increased prior to the tests due to the damage that occurred to this wall before testing as explained earlier. A similar trend is observed for the variation of lateral stiffness of the walls measured based on the static pull-back test results as shown inFig. 3.9-b. Table 3.5 lists the aforementioned dynamic properties of the walls.

Table 3.5: Dynamic properties and lateral stiffness of the walls

Wall	**1**	**2**	**3**	**4**	**5**	**6**
$\boldsymbol{f_i\ (HZ)}$	7.14	6.17	13.93	8.94	6.61	3.65
$\boldsymbol{\xi_i}$ (%)	11.41	9.62	6.05	7.62	12.63	19.89
$\boldsymbol{K_i(kN/m) \times 10^3}$	1.67	1.38	15.61	3.19	1.88	0.63

Figure 3.9-c shows the variation of equivalent viscous damping of the walls obtained after the tests at different record intensities normalized to their corresponding initial values. The increase in the damping ratio up to the L2 level observed in this figure is consistent with the increase in the nonlinear response of the walls at higher record intensities. As can be observed from Fig. 3.9-c, this increase is more pronounced in the case of Walls 1, 2, and 4 as a result of the larger damage experienced by these walls during the L2 level test compared to other walls. The reduction observed in the values of damping ratio at the L3 level compared to the L2 level tests for Walls 1, 2, 4, and 5 is also justified by the reduction of energy dissipation due to the vertical bar buckling and the rocking response of these walls at the L3 level tests.

3.4.2.2 Acceleration Transmissibility Evaluation

The damped fundamental frequency of the walls was also quantified based on the acceleration transmissibility plots between the acceleration response of the table and the top wall stories. Figure 3.9-d shows the variation of the damped fundamental frequency of the walls at different record levels normalized to their corresponding values obtained based on the static pull-back tests after each level test. These plots show that the values obtained from transmissibility analysis are generally less than the values obtained from the static pull-back tests. This is consistent with the fact that the values of the fundamental frequency of the walls are reduced as a result of the nonlinear response and the corresponding damping

and the stiffness degradation of the walls during the tests. This reduction is also observed during the static pull-back tests, but are more pronounced during the shake table tests, which generate larger displacement amplitudes. In addition, the walls experienced significant nonlinear response during the shake table tests while they remained within the elastic limit during the static pull-back tests. As expected, the increased wall nonlinearity during higher intensity level tests reduced the wall fundamental frequencies, compared to their initial values, as confirmed by Fig. 3.9-d.

Figures 3.9-e and 3.9-f show the variation of the damped fundamental frequency of the walls obtained from the acceleration transmissibility between the shake table and the top of the first story and between top of the first and the second stories, respectively. The values are normalized to the L0 level tests. The steeper negative slope of the curves in Fig. 3.9-e compared to Fig. 3.9-f confirms that most of the damage to the walls is concentrated in the first story.

3.4.3 Curvatures along Wall Heights

In order to compute the average curvature response histories of the walls along the wall height, the average vertical strain in the walls over three height segments are obtained based on the vertical displacements at both wall ends measured at three different heights. The method is depicted for a general wall in Fig. 3.10 where the average curvature at time *t* over the i^{th} height segment ($\varphi_i(t)$) can be obtained based on the following equation:

$$\varphi_i(t) = \frac{\varepsilon_{Ti}(t)+\varepsilon_{Ci}(t)}{l_w} = \frac{\Delta_{Ti}(t)/h_{segment,i}+\Delta_{Ci}(t)/h_{segment,i}}{l_w} = \frac{\Delta_{Ti}(t)+\Delta_{Ci}(t)}{l_w h_{segment,i}} \qquad (3.2)$$

where, $\varepsilon_{Ti}(t)$ and $\varepsilon_{Ci}(t)$ are the *absolute* tensile and compressive strain at the ends of the wall at time *t* over the i^{th} height segment.

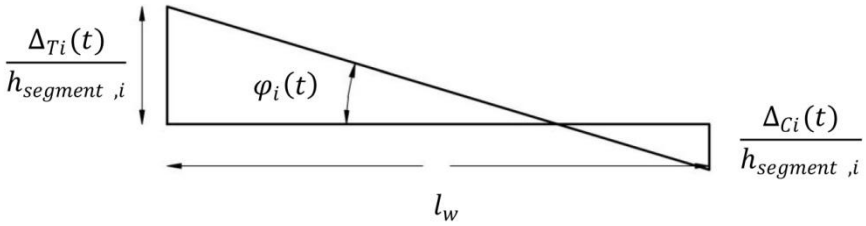

a) Computation of curvature from strain

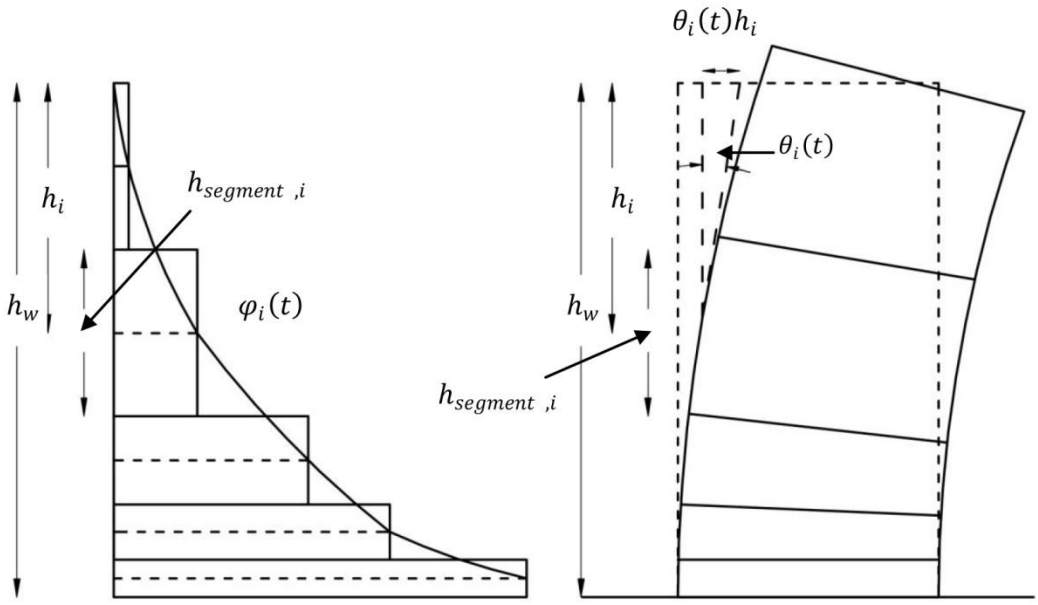

b) Computation of flexural lateral displacement

Figure 3.10: Curvatures and rotations of a shear wall

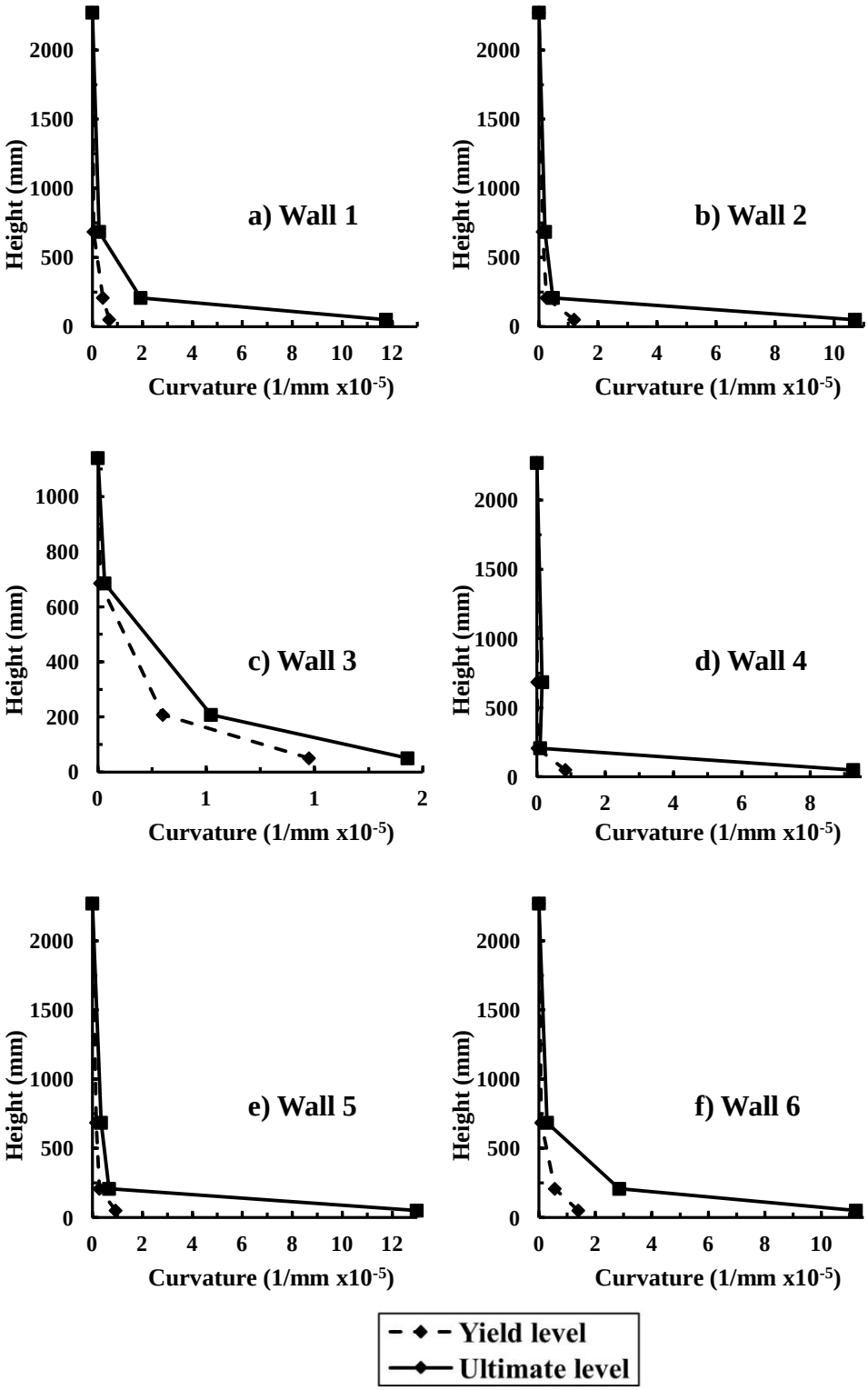

Figure 3.11: The average curvature profile of the walls at the yield and ultimate levels

Figure 3.11 shows the average curvature profiles of the walls obtained from the experimental data at the times the yield moment and ultimate moment capacity of the walls are reached. Note that the results shown for the ultimate level for Wall 3 correspond to the maximum load attained by this wall as it did not reach its ultimate flexural capacity during the tests as explained earlier. The curvature profiles typically show significant higher nonlinearity in the first compared to the second stories and at the ultimate level compared to the yield level, which are both attributed to the observed concentration of wall damage at their base regions.

3.4.4 Displacement Components

There are typically three different sources of the lateral displacement of a wall; namely: the flexural displacement, the base sliding and the shear deformations. The flexural contribution to the lateral displacement of the walls at time *t* can be computed form the curvature profile based on the following equation (see Fig. 3.10):

$$\Delta_{f,e}(t) = \sum_{i=1}^{n} \theta_i(t) h_i = \sum_{i=1}^{n} \varphi_i(t)\, h_{segment,i} h_i \qquad (3.3)$$

where, $\theta_i(t)$ is the average rotation of the wall at time *t* over the i^{th} height segment, h_i is the distance from the center of the i^{th} height segment to the point where the

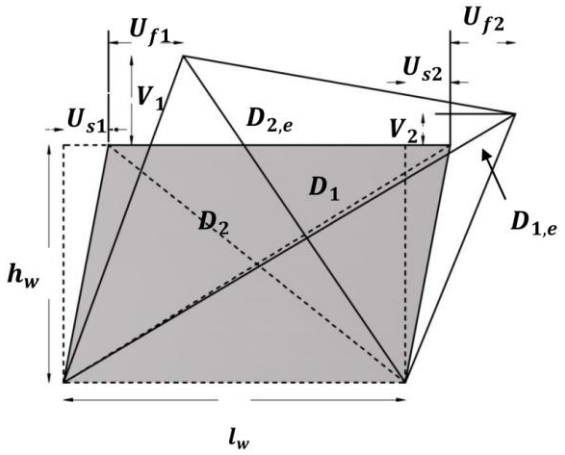

(a)

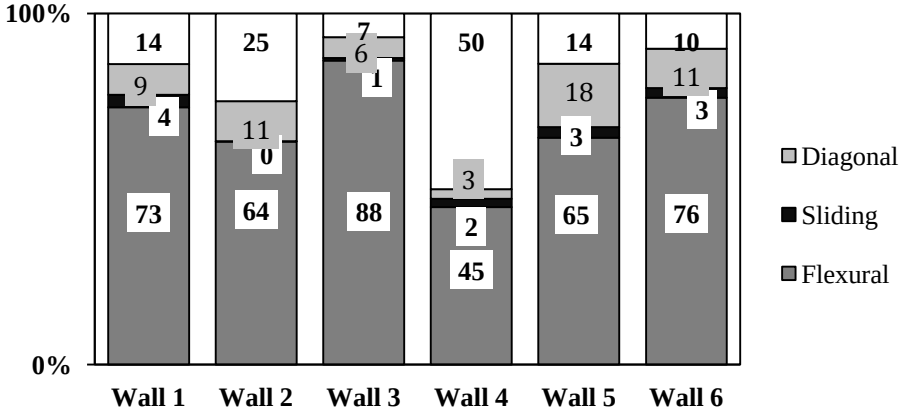

(b)

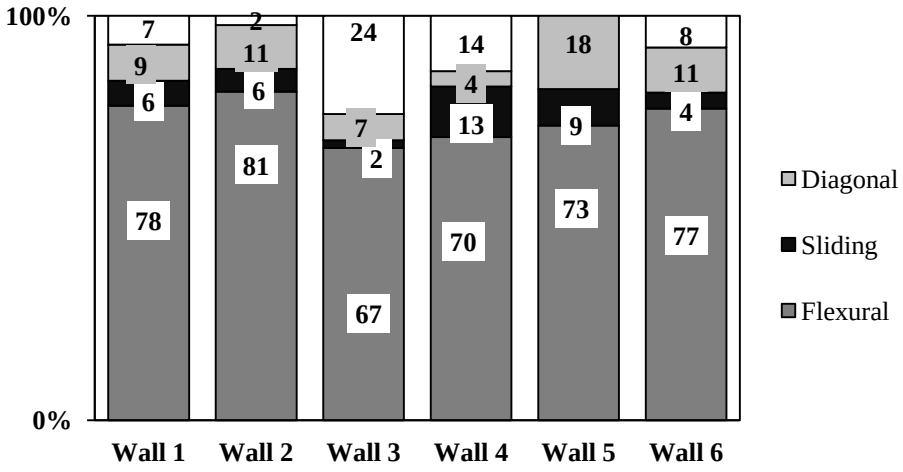

(c)

Figure 3.12: Lateral Wall displacement: **a)** Computation Model; **b)** Contribution of different deformation components in the first storey at yield and **c)** Contribution of different deformation components in the first story at ultimate

lateral flexural displacement is to be computed and n is number of height segments between the base of the wall and this point.

The sliding contribution to the lateral displacement was isolated utilizing the direct measurements of the wall base sliding. The sum of the diagonal and flexural displacement at the top of the first story of the walls can be computed based on the diagonal and vertical deformations at this level obtained from the direct measurements of the instrumentation during the tests. For this purpose the approach proposed by Massone and Wallace (2004) was adopted in the current study. Considering the deformed wall shape shown in Fig. 3.12-a, the average shear deformation of the wall at the first story can be obtained from the following equation:

$$\overline{U}_d = \frac{\sqrt{D_1^2-h^2}-\sqrt{D_2^2-h^2}}{2} = \frac{\sqrt{D_{1.e}^2-(h+V_2)^2}-\sqrt{D_{2.e}^2-(h+V_1)^2}-U_{f1}-U_{f2}}{2} \quad (3.4)$$

where D_1 and D_2 are the diagonal length of the wall at the first story without considering the vertical deformations while $D_{1,e}$ and $D_{2,e}$ are the diagonal length of the wall at the first story directly measured by the displacement transducers during the test which include the effect of the vertical deformations of the wall. Based on the above equation and assuming that the flexural deformations U_{f1} and U_{f2} are equal on each side of the wall, the sum of the shear and flexural displacement at the top of the first story of the walls can be computed using:

$$\overline{U}_d + U_f = \frac{\sqrt{D_{1.e}^2-(h+V_2)^2}-\sqrt{D_{2.e}^2-(h+V_1)^2}}{2} \quad (3.5)$$

The percentage contribution of flexural, sliding, and shear lateral displacement at the first story of the walls when the yield moment and ultimate moment capacity of the walls are reached are computed and are shown in Figs. 3.12-b and 3.12-c, respectively. Based on the values shown in the figure, the walls primarily responded in flexure as flexural deformations dominated the lateral deformation for all of the walls causing more than 64% of the lateral deformations in most walls at both the yield and ultimate moment while sliding takes the minimum contribution of the lateral deformation at the first story of the walls. The percentage contributions of the three sources of the lateral deformation are almost the same at both the yield and ultimate levels. It is also observed from these graphs that the sum of the isolated displacement components averaged 86% at yield (without considering Wall 4), and 94% at ultimate (without considering Wall 3) of the total measured lateral displacement of the wall at the first story, which confirms the applicability of the adopted displacement component isolation technique. Wall 4 was not considered in the above calculations at yield as one of the vertical string potentiometers malfunctioned. In addition, as noted earlier, Wall 3 did not reach its ultimate flexural capacity during the tests, and subsequently it was not considered in the above calculations at ultimate.

3.5 Conclusions

There is an urgent need for a fundamental understanding of the seismic performance of RM wall SFRS in order to facilitate their adoption in the next generation of PBSD codes in North America. In order to respond to this need, shake table tests were performed on scaled model fully grouted RM shear walls. This paper reports on the main experimental results and observations from the tests and analyses of the dynamic properties, lateral strength of the walls and displacement components. The following are the main conclusions based on the current study:

The failure mode of the walls was mainly in the form of masonry crushing at the wall toes and buckling of the end vertical bars followed by sliding and rocking of the walls. In general, all the damage was concentrated at the wall bases. The amount of damage to the walls was minor for all walls during the L1 level tests and was considerable but repairable under the L2 level tests. Nevertheless, all walls maintained their integrity during the L3 level tests and no signs of diagonal cracking were observed in the walls, which demonstrated the effectiveness of the horizontal reinforcements in eliminating shear failure of the walls at ultimate levels.

Increased energy dissipation was observed for the walls corresponding to increase in the excitation amplitude during different test levels. This observation was based on the base-shear-top floor displacement and base moment-curvature curves and also based on the change of natural frequency and equivalent modal

damping of the walls obtained from the dynamic characteristics identification tests. The curvature profiles along the wall heights show an increase in the nonlinear flexural response of the walls with increased excitation amplitude and a concentration of nonlinear deformations at the base of the wall.

The contributions of different displacement sources to the total displacement of the first story indicated that the wall responded mainly in flexure. In addition, the technique adopted for the flexure and shear displacement component isolation yielded acceptable results when compared to the total measured wall displacements.

The test results confirmed the adequate seismic performance of lightly RM shear walls even for high level of seismic demands. It can be inferred that the widely-spaced reinforcement can be very cost-effective in RM wall construction in areas with low to moderate seismicity. In general, the test results contribute to the RM SPD and can facilitate further seismic performance analyses and calibration of numerical models towards better quantification of the seismic performance of RM SFRS.

3.6 Notations for Chapter 3

A_g = Gross cross-sectional area of the wall
D_1, D_2 = Diagonal length of the wall
$D_{1,e}$, $D_{2,e}$ = Experimentally measure deformed diagonal length of the wall
E = Energy
E_s = Young's modulus
$E_{prototype}$ = Modulus of elasticity of prototype structure
E_{model} = Modulus of elasticity of model structure
F = Force
K = Lateral stiffness
K_i = Initial lateral stiffness before test
L = Length
$L_{prototype}$ = Length of prototype
L_{model} = Length of model structure
$M_{yr,e}$ = Experimental yield moment capacity
$M_{ur,e}$ = Experimental ultimate moment capacity
$M_{ya,e}$ = Analytical yield moment capacity
$M_{ua,e}$ = Analytical ultimate moment capacity
P_i = Initial actual axial load on the walls
P_y = Actual axial load at yield moment capacity
P_u = Actual axial load at ultimate moment capacity
S_a = Spectral acceleration
S_v = Longitudinal reinforcement spacing
S_L = Length scale factor
S_E = Modulus of elasticity scale factor
T = Time
U_{f1}, U_{f2} = Flexural lateral deformation
V_u = Base shear at ultimate moment capacity
V_{rs} = Nominal sliding shear strength
V_{rd} = Nominal diagonal shear strength
V_1, V_2 = Vertical deformations of story
EI_c = Cracked flexural stiffness
a = Acceleration
f =Frequency, Undamped fundamental frequency
f_d = Damped fundamental frequency
f_s = Sampling frequency

f'_m = Compressive strength of masonry
f_i = Initial undamped fundamental frequency before test
f_c = Damped fundamental frequency from the acceleration transmissibility plots
f_{FFT} = Damped fundamental frequency from FFT analysis
$f_{c,b1}$ = Damped fundamental frequency from the acceleration transmissibility plots between the the table and top of the first story
$f_{c,12}$ = Damped fundamental frequency from the acceleration transmissibility plots between top of the first and second story
g = Gravitational acceleration
h = Height of story
h_i = Distance of the centre of the i^{th} height segment from the point where the lateral flexural displacement is to be computed
$h_{segment,i}$ = Height of i^{th} vertical segment along the wall height
l_w = Wall length
m_p = Mass of prototype structure
v = Velocity
Δm = Added lumped mass required for dynamic similitude
$\varphi_i(t)$ = Average curvature at time *t* over the i^{th} height segment
$\varphi_{yr,e}$ = Experimental yield curvature capacity
$\varphi_{ur,e}$ = Experimental ultimate curvature capacity
$\emptyset_s$ = Resistance factor for reinforcing bars
$\emptyset_m$ = Resistance factor for masonry
$\varepsilon_{m,ult}$ = Compressive strain of the masonry at ultimate stress
ρ = Material density
ρ_v = Longitudinal reinforcement ratio
δ = Displacement
ξ = Equivalent modal viscous damping
ξ_i = Initial equivalent modal viscous damping before test
σ = Stress
ϵ = Strain
$\varepsilon_{Ci}(t)$ = Compressive strain at the corners of the wall at time *t* over thei^{th} height segment
$\varepsilon_{Ti}(t)$ = Tensile strain at the corners of the wall at time *t* over thei^{th} height segment
ν = Poisson ratio

$\Delta_{Ti}(t)$ = Tensile deformation at the corners of the wall at time *t* over the i^{th} height segment

$\Delta_{Ti}(t)$ = Compressive deformation at the corners of the wall at time *t* over the i^{th} height segment

$\Delta_{f,e}$ = Experimentally obtained flexural deformation

$\theta_i(t)$ = Average rotation of the wall at time *t* over the i^{th} height segment

3.7 References for Chapter 3

American Society for Testing and Materials, (2012-a). "Standard specification for deformed and plain carbon-steel bars for concrete reinforcement (A615/A615M-12)." West Conshohocken, Pa: ASTM International.

American Society for Testing and Materials, (2010-a). "Standard specification for grout for masonry (C476-10 ed.)." West Conshohocken, Pa.: ASTM International.

American Society for Testing and Materials, (2007). "Standard test method for flow of hydraulic cement mortar (C1437-07 ed.)." West Conshohocken, Pa: ASTM International.

American Society for Testing and Materials, (2012-b). "Standard test method for reconstruction and construction evaluation of mortars for plain and reinforced unit masonry (C780-12)." West Conshohocken, Pa.: ASTM International.

American Society for Testing and Materials, (2004). "Standard test method for Young's modulus, tangent modulus, and chord modulus (E111-04 ed.)." West Conshohocken, Pa: ASTM International.

American Society for Testing and Materials, (2012-c). "Standard test methods for sampling and testing concrete masonry units and related units (C140-12)." West Conshohocken, Pa.: ASTM International.

ATC. (2007). "Interim Testing Protocols for Determining the Seismic Performance Characteristics of Structural and Nonstructural Components (FEMA-461)." Applied Technology Council. Federal Emergency Management Agency, Washington D.C., USA.

ATC. (2009). "Quantification of building seismic performance factors (FEMA-P695)." Applied Technology Council. Federal Emergency Management agency, Washington D.C., USA.

Caccese, V., and Harris, H. G. (1990). "Earthquake Simulation Testing of Small-Scale reinforced Concrete Structures." ACI Structural Journal , 87 (1), 72-80.

Canadian Standard Association, S304.1 (2004). “Design of Masonry Structures”. Mississuaga, ON: CSA.

Canadian Standards Association, A179 (2004). “Mortar and grout for unit masonry”. Mississauga, ON.: CSA.

Carrillo, J., and Alcocer, S. (2011). “Improved External Device for a Mass-Carrying Sliding System for Shaking Table Testing.” Journal of Earthquake Engineering and Structural Dynamics, 40, 393-411.

Drysdale, R., and Hamid, A. (2005). “Masonry Structures- Behavior and Design.” 3rd ed., Canada Masonry Design Centre, Mississauga, Canada.

Ghorbanirenani, I., Tremblay, R., Léger, P., and Leclerc, M. (2012). “Shake Table Testing of Slender RC Shear Walls Subjected to Eastern North America Seismic Ground Motions.” Journal of Structural Engineering, 138(12), 1515–1529.

Harris, H. G., and Sabnis, G. (1999). “Structural Modeling and Experimental Techniques.” Second ed., CRC Press.

Lestuzzi, P., and Bachmann, H. (2007). “Displacement Ductility and Energy Assessment from Shaking Table Tests on RC Structural Walls.” Engineering Structures, 29, 1708-1721.

Massone, L. M., Wallace, J. W. (2004). “Load-Deformation Responses of Slender Reinforced Concrete Walls.” ACI Structural Journal, 101(1).

Mojiri, S., Tait, M. J., and El-Dakhakhni, W. W. (2012). “Shake table testing and analytical modeling of fully-grouted reinforced concrete block masonry shear walls.” 15th International Brick and block Masonry Conference, Florianopolis, Brazil.

National Research Council of Canada (NRCC) (2010). “National Building Code of Canada (NBCC) .” Institute for Research in Construction, Ottawa, Canada.

National Institute of Standards and Technology (NIST). (2010). "Evaluation of the P-695 methodology for quantification of building seismic performance factors." NIST GCR 10-917-8, NIST, Gaithersburg, MD, USA.

Pacific Earthquake Engineering Research Center: NGA Database. (Accessed September, 2011). http://peer.berkeley.edu/nga/

CHAPTER 4: SEISMIC RESPONSE ANALYSIS OF FULLY GROUTED LIGHTLY REINFORCED CONCRETE BLOCK MASONRY SHEAR WALLS BASED ON SHAKE TABLE TESTS

4.1 Introduction

This chapter includes detailed analyses of the experimental results reported in chapter three based on which the performance of the tested RM shear walls are investigated in terms of their inelastic behaviour characteristics, various energy components, and the effective dynamic properties of the walls including the effective secant stiffness, period, and equivalent viscous damping.

This chapter contains the work in the following article:

Mojiri, S., Tait, M. J., El-Dakhakhni, W. W. (2013). "Seismic Response Analysis of Fully Grouted Lightly Reinforced Concrete Block Masonry Shear Walls Based on Shake Table Tests." *ASCE Journal of Structural Engineering*, Under Review.

4.2 Summary of the Test Program

Figure 4.1 shows the cross section and reinforcement details of the six third-scale model shear walls investigated. Details of the reduced-scale and the full-scale design parameters are presented in Table 4.1.

The design parameters for the six shear walls are chosen to represent those found in typical low-rise commercial buildings and meeting the requirements of the conventional construction category based on the Canadian masonry design code (CSA S304.1, 2004).

Table 4.1: Details of the prototype and model walls

Wall	Number of Stories	Length P/M[1](mm)	Aspect ratio	Ver. Reinf. P/M[1]	ρ_v P/M[1](%)	S_v P/M[1](mm)	Hor. Reinf. (First floor)	Axial stress
1	2	1,800/598	3.77	3M15/3-D4*	0.18/0.20	798/266	M10 @ 390 mm/ W1.7 @ 130 mm	$0.02f'_m$
2				2M15/2-D4	0.12/0.13	1596/532		
3	1		1.88	3M15/3-D4*	0.18/0.20	798/266		
4	2	2,600/865	2.62		0.12/0.14	1197/399		
5		1,800/598	3.77	2M25/2-D7**	0.29/0.24	1596/532		
6				3M15/3-D4*	0.18/0.20	798/266		0.05 f'_m

1-Prototype/Model
***D4=26 mm^2**
****D7=45 mm^2**

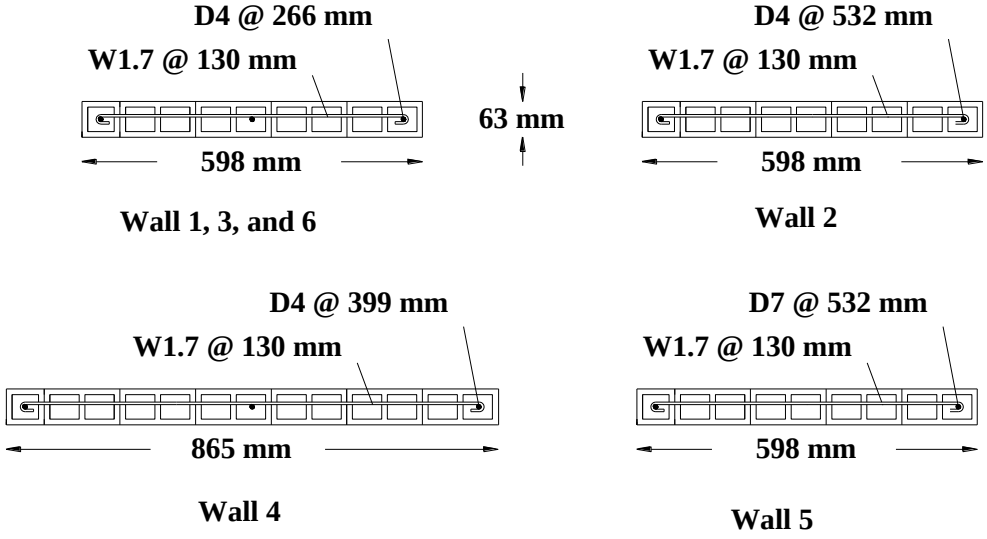

Figure 4.1: Cross section of the model walls

The model walls were constructed from fully grouted 63 x 63 x 130 mm third-scale concrete masonry units and were reinforced vertically with D4 and D7 deformed bars with diameters of 5.75 mm and 7.6 mm, respectively. Smooth W1.7 wires with a 3.8 mm diameter were used to provide the horizontal (shear) reinforcement in the walls. The experimental evaluated average compressive strength of the masonry (f'_m), based on four course masonry prisms, was 17.7 MPa (c.o.v. = 13.6%) (CSA S304.1, 2004). The average yield strength of the D4, the D7, and the W1.7 steel reinforcement was 490 MPa (c.o.v. = 1%), 487 MPa (c.o.v. = 3.2%), and 281 MPa (c.o.v. = 0.4%), respectively (ASTM A615-09, 2009).

The test setup shown in Fig. 4.2 includes a uniaxial shake table, the external mass support system (EMSS), which includes the frame, masses, linear bearings and links, the lateral (out-of-plane) support system (LSS), and an axial loading system (ALS). The EMSS was designed to carry the majority of the weight of the inertial mass and was used to facilitate situations where RM walls, acting as the main SFRS, would be required to carry seismic masses that are not consistent with the gravitational loads (e.g. in the common case of RC columns carrying a significant portion of gravity loads).

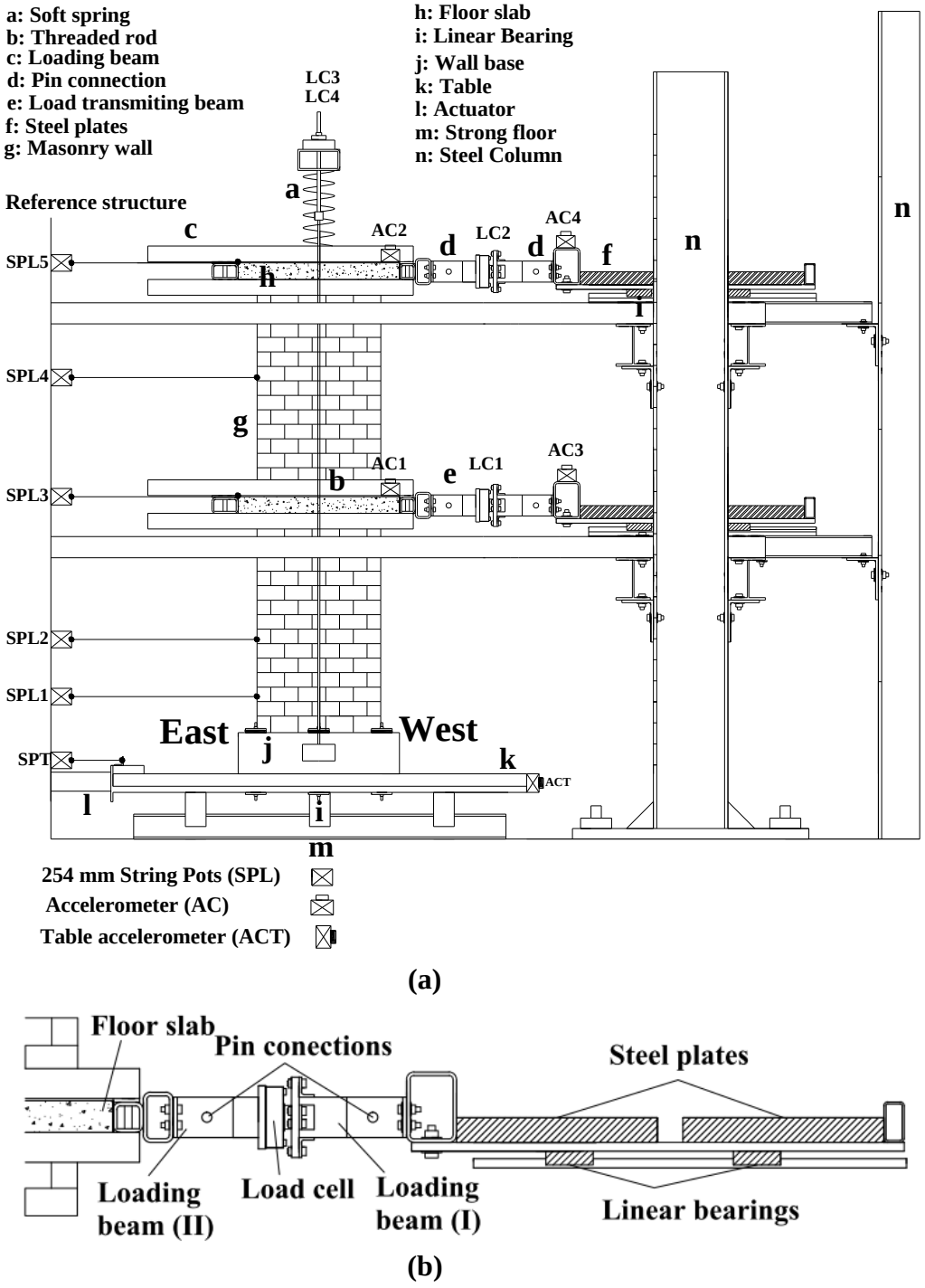

Figure 4.2.: a) Test setup and instrumentation; **b)** Details of the loading beam and mass trolley at each floor level

Figures 4.2 and 4.3 show the instrumentation that was utilized. Displacement transducers were used to measure the absolute displacement of the shake table as well as the displacements of the walls at various locations along their heights including possible wall sliding at the base, first story and second story lateral displacements, vertical deformations of the walls along their heights and the diagonal deformations within the first story. In addition, the acceleration of the shake table and at the floor and roof levels, as well as the lateral and axial forces applied on the walls, were recorded using accelerometers and load cells, respectively. Finally, strain gauges were installed at four different locations along the end vertical reinforcement bars to evaluate the extent of plasticity following bar yielding.

For this study, the Loma Prieta 1989 earthquake record from PEER NGA strong motion database (PEER NGA Database, 2011) was selected. The third-scale model record was obtained following the dynamic similitude requirements (Harris and Sabnis, 1999). The original record was selected and scaled to four different intensity levels, L0, L1, L2, and L3, covering a wide range of seismic hazard levels in high seismic zones across Canada (NRCC 2010). The resulting values of the peak ground acceleration (PGA) of the table response were 0.19g, 0.24g, 0.61g, and 0.84g for the L0, L1, L2, and L3 levels, respectively. Full details of the test program and experimental results can be found elsewhere (Mojiri et al., 2013).

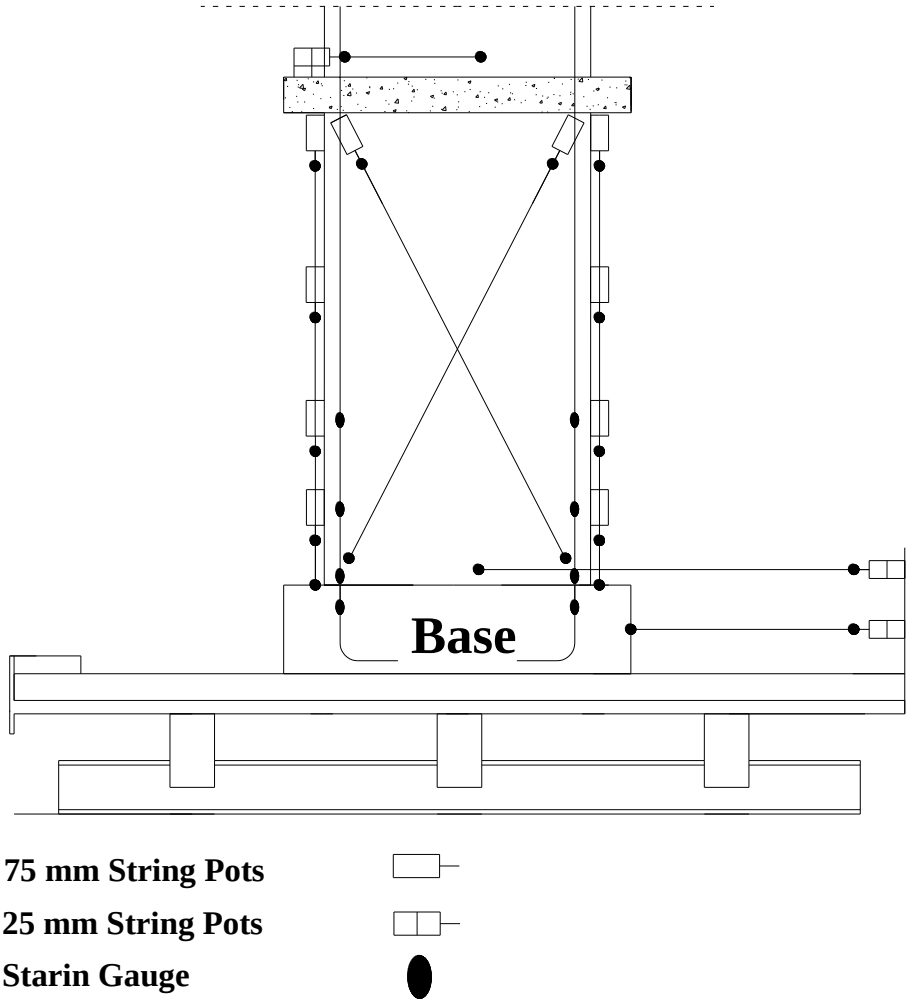

Figure 4.3: External and internal instrumentation in the first floor

4.3 Analysis of Wall Inelastic Deformations

4.3.1 Displacement Ductility

As a first step towards quantifying the seismic performance of the test walls, their displacement ductility levels are evaluated based on shake table test results. The displacement ductility levels of the walls are computed at 0.5% and

1% drift ratios of both the first story and top of the walls as well as at the maximum lateral load and are presented in Table 4.2.

Table 4.2: Displacement ductility and response modification factors of walls

Wall	1	2	3	4	5	6
$\mu_{\Delta,0.5\%,1}$	2.6	2	N.R.	5.0	2.2	1.9
$\mu_{\Delta,0.5\%,1}^{id}$	1.5	1.3	N.R.	2.8	1.2	N.Y.
$\mu_{\Delta,0.5\%,2}$	2.2	1.6	N.R.	4.2	1.8	1.8
$\mu_{\Delta,0.5\%,2}^{id}$	1.3	1.0	N.R.	2.3	N.Y.	N.Y.
$\mu_{\Delta,1\%,1}$	5.3	3.4	N.R.	9.4	4.2	3.8
$\mu_{\Delta,1\%,1}^{id}$	3.1	2.2	N.R.	5.1	2.2	1.7
$\mu_{\Delta,1\%,2}$	4.6	3.2	N.R.	9.4	3.6	3.5
$\mu_{\Delta,1\%,2}^{id}$	2.7	2.0	N.R.	5.1	1.9	1.6
$\mu_{\Delta,u}$	8.0	4.2	2.3	7.7	6.3	6.8
$\mu_{\Delta,u}^{id}$	4.6	2.7	1.5	4.2	3.3	3.1
R_u	4.6	2.7	1.5	4.2	3.3	3.1

N.Y.: No yielding N. R.: Not reached

The displacement ductility levels in Table 4.2 are computed based on two approaches. In the first approach, the levels of the (experimental) displacement ductility (μ_{Δ}) are computed as the ratio of the top floor total lateral deformation at a certain limit to the top floor total lateral deformation at the yield level. The latter is defined as the onset of the yielding of the wall end vertical bars (referred to as *experimental* yield point). In the second approach, the *idealized* displacement ductility (μ_{Δ}^{id}) levels are computed based on assuming an idealized elastic-perfect plastic top floor displacement-base shear response as suggested by Priestly et al.

(2007). In this more conservative approach, the idealized yield displacement is defined as the point of intersection of the line connecting the origin to the point of the experimental yield load and corresponding displacement, and extending up to the level of the nominal strength, where the latter is taken as the maximum lateral load attained by the walls. From Table 4.2, it can be inferred that the minimum displacement ductility level computed based on the first approach (i.e. the experimental ductility values) for the two story walls (Walls 1, 2, 4, 5, and 6), which reached their maximum capacity during the tests, is 1.6 and 3.2 at 0.5% and 1% drift levels respectively. This minimum increases to 4.2 at the maximum load. Following the more conservative second approach, the idealized ductility has minimum values of 1.0, 1.6 and 2.7 at the 0.5%, 1% drift and maximum load levels, respectively. The ductility values of Wall 3 reported at maximum load as presented in Table 4.2 are considerably lower than those for other walls as this wall neither experienced significant inelastic deformations nor reached its maximum capacity during the tests (Mojiri et al., 2013). As can be observed from Table 4.2, the maximum idealized ductility values reached by the walls during the tests is as high as 4.6. This shows that, similar to recent test observations by Kasparik et al. (2012), RM shear walls, including those with minimal reinforcement, such as the walls tested, can still reach considerable ductility levels, which can be relied upon in seismic design. The values of the ductility-related seismic response modification factor (R_d) employed in force-based seismic design approaches are also presented in Table 4.2 for the maximum load level. Such

values are taken as equal to the corresponding idealized displacement ductility levels based on the equal-displacement approach (NRCC, 2010). The values range from 1.5 to 4.6, which suggest a considerable variation between the response modification factors for the walls. It should be noted that, based on the NBCC (2010), the reinforcement scheme of the tested walls designate them under the *conventional construction category*, which is not permitted as a SFRS in seismic zones.

Figure 4.4 shows the variation of displacement ductility levels of the walls at the maximum load for each level computed based on the yield displacement of the walls. From the results presented in Table 4.2 and Fig. 4.4 it can be observed that the displacement ductility demand of the walls varies for different walls at the same excitation level (see Fig. 4.4). In addition, the displacement ductility demand also varies for the same wall at different excitation levels (see Fig. 4.4). Moreover, the displacement ductility demand varies for different walls at the same displacement demand (particularly for Wall 4, see Table 4.2). These observations support the notion proposed by Priestley et al. (2007) that, instead of using fixed values, the displacement ductility demand should be obtained based on the predicted level of seismic demand and a realistic quantification of the SFRS response during earthquakes. In addition, different values of displacement ductility levels might be necessary for the same SFRS with different design and geometrical parameters. This indicates that force-based design approaches, which are adopted by most current seismic design codes, may need to be revisited.

Although simple to employ, prescribing a single fixed value of the seismic force modification factors (R_d in NBCC 2010 and R in ASCE 7-10, 2010) for each SFRS type could lead to non-uniform risk of failure during seismic events. The latter is against the current code philosophies, which adopt uniform hazard spectra to estimate the seismic loading levels on the SFRS. Similar recommendations were also recently put forward based on a study commissioned by the National Institute of Standards and Technology (NIST, 2010).

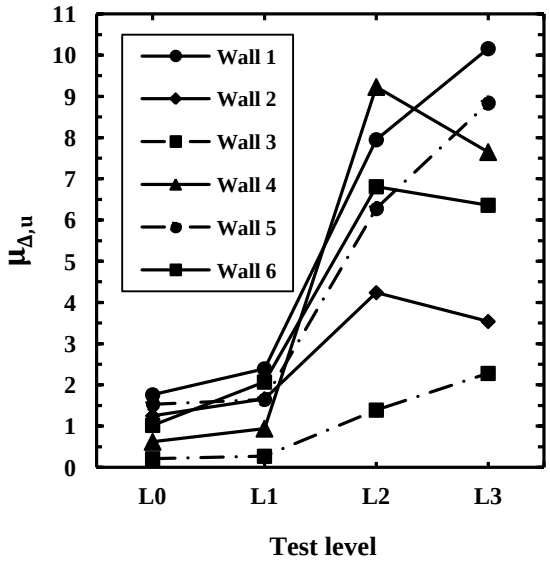

Figure 4.4: Variation of the displacement ductility of walls at maximum load of each test level

4.3.2 Extent of Plasticity

The inelastic deformations of flexurally-dominated shear walls are concentrated in the regions close to the wall bases. These regions are referred to as the plastic hinge zones where most of the energy dissipation process takes

place. Therefore, both the seismic performance and the displacement response of RM shear walls that are expected to fail in flexure are highly affected by the level of inelastic deformations at this region. An approximation of the extent of plasticity (L_p) can be obtained either from the lateral deformation profile, the extent of yielding in the end vertical bars, or the average curvature profiles of the walls based on the experimental data. The following paragraphs discuss the application of the three approaches on all walls excluding Wall 3, which experienced negligible inelastic behavior during the shake table tests (Mojiri et al., 2013).

Figure 4.5 shows the lateral deformation profiles of two story walls at yield and at top floor drift ratios of 0.5% and 1%. The rapid change in slope (kink) in the deformation profiles observed in the curves at the height of 270 mm may approximately represents the center of the plastic hinge zone over which the walls are experiencing essentially rigid body rotations. As can be observed from Fig. 4.5, the kink in the curve is more pronounced at a top drift of 1% compared to that at a top drift of 0.5%, indicating the significant plastic deformations occurring at 1% drift.

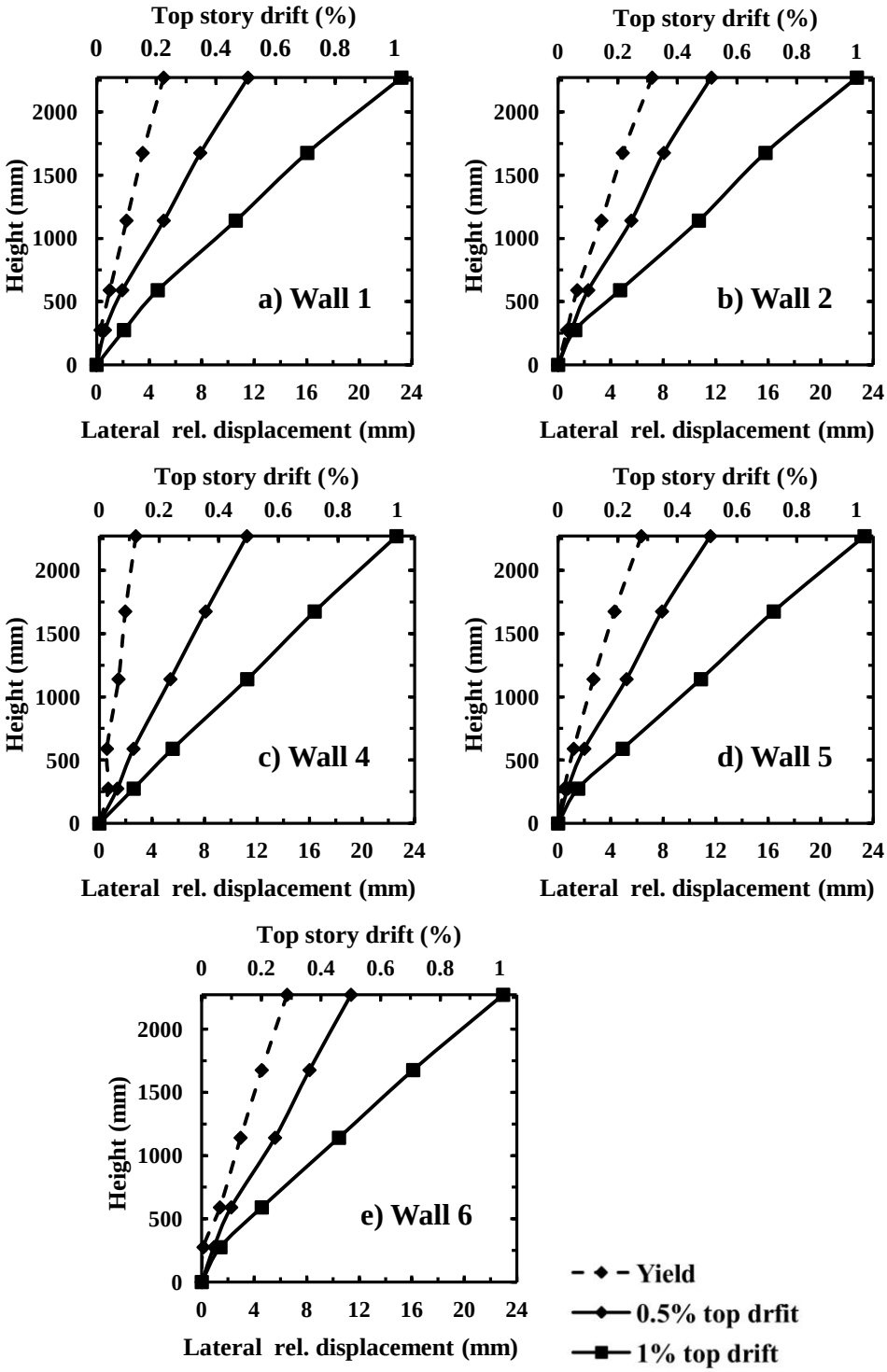

Figure 4.5: Lateral deformation profile of walls at yield and top drift ratios of 0.5% and 1%

Table 4.3: Bounds of extent of plasticity ($L_{p,1\%,2}$) (mm from wall base) (lower bound, upper bound) and equivalent plastic hinge length ($l_{p,1\%,2}$) at 1% top floor drift

Wall No.	1	2	4	5	6
Lateral deformation profile	(-, 550)	(-, 550)	(-, 550)	(-, 550)	(-, 550)
Strain of end vertical bar profile	(170, 370)	(20, 170)	(20, 170)	(370, -)*	(370, -)
Average curvature profile	(200, 700)	(50, 200)	(50, 200)	(50, 200)	(200, 700)
$L_{p,1\%,2}$	(200, 370)	(50, 170)	(50, 170)	(50, 200)	(370, 550)
$L_{p,1\%,2}/l_w$	(0.35, 0.62)	(0.08, 0.28)	(0.06, 0.20)	(0.08, 0.35)	(0.62, 0.92)
$l_{p,1\%,2}$	122	100	102	107	225
$l_{p,1\%,2}/l_w$	0.20	0.17	0.12	0.18	0.38

* Erroneous data due to malfunction of the instrumentation were not considered in determination of the final bounds

The bounds of the extent of plasticity (L_p) at 1% top floor drift obtained based on the lateral deformation profiles are presented in Table 4.3, showing that, for all walls, the maximum L_p value does not exceed 550 mm or 38% of the wall length.

Figure 4.6 shows the tensile strain profile of the wall end vertical bars at yield and at top drift ratios of 0.5% and 1% normalized to the end bar (0.00245 mm/mm) yield strain. The strain value at 1% drift at the base of Wall 4 is not shown in the curves as the strain gauges malfunctioned in this wall.

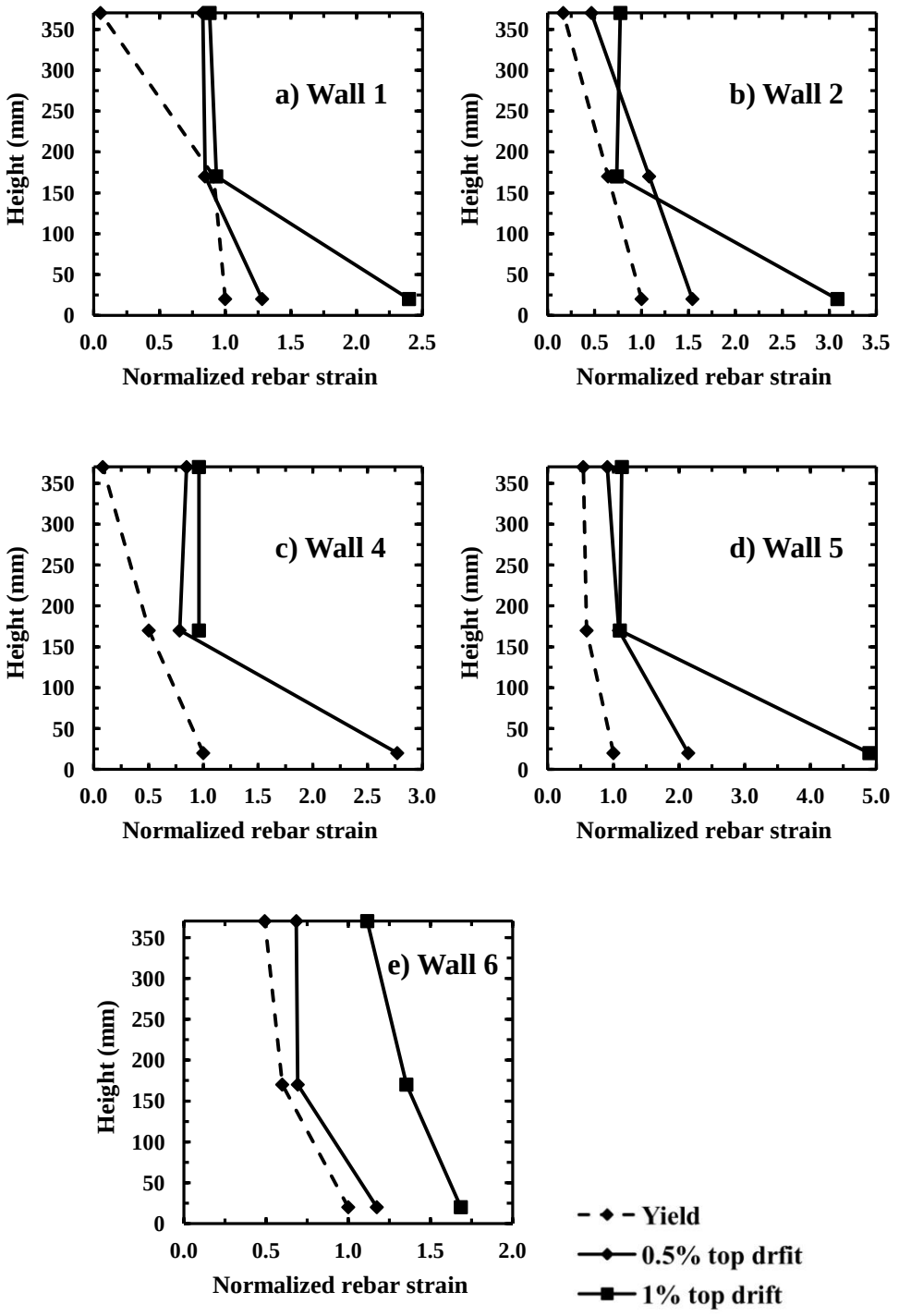

Figure 4.6: End bar strain profile of walls at yield and top drift ratios of 0.5% and 1% normalized to the bar yield strain

Comparing the profiles at 1% drift to those at 0.5% drift in Fig. 4.6, it can be observed that increased strains in the vertical bars are primarily concentrated at the base of the walls while the strains at the higher wall levels do not show significant variation following yielding of the vertical bars at the base. This shows that the inelastic wall deformations are concentrated at the areas closer to the base within the plastic hinging zone. The bounds of L_p obtained based on the extent of yielding of the vertical bars from the base of the walls at top drift of 1% are presented in Table 4.3. The values show that the maximum plasticity height from the wall bases does not exceed 170 mm for Walls 2 and 4while it falls in the range of 170 mm to 370 mm for Wall 1 and is at least 370 mm for Walls 5 and 6.

The average curvature profiles at the yield and at top drift ratios of 0.5% and 1%, which are normalized to the base yield curvature (defined as the curvature of the wall bases when the first vertical bar yields), are shown in Fig. 4.7. The average curvature value at time t_i over the k^{th} height segment $\varphi_{k,i}$ is computed experimentally using the following equation:

$$\varphi_{k,i} = \frac{\varepsilon_{T,k,i}+\varepsilon_{C,k,i}}{l_w} = \frac{\Delta_{T,k,i}/h_{segment,k}+\Delta_{C,k,i}/h_{segment,k}}{l_w} = \frac{\Delta_{T,k,i}+\Delta_{C,k,i}}{l_w h_{segment,k}} \quad (4.1)$$

where $\varepsilon_{T,k,i}$ and $\varepsilon_{C,k,i}$ are the tensile and compressive strain at the corners of the wall at time t_i over the k^{th} height segment ($h_{segment,k}$) obtained using the values of the vertical deformation of the wall over the k^{th} height segment measured by the string potentiometers (see Fig. 4.3).

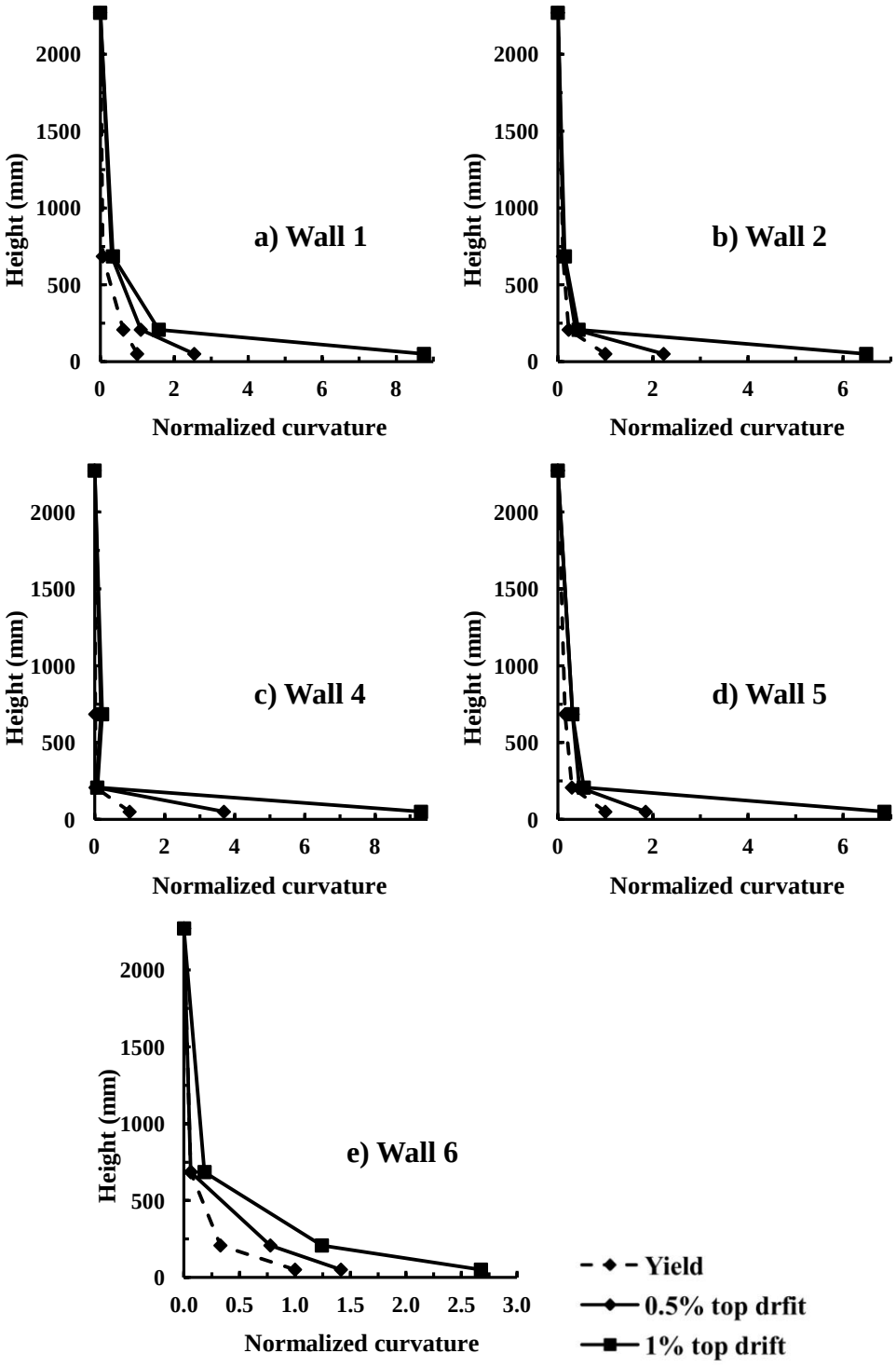

Figure 4.7: Average curvature profiles at yield and at top drift ratios of 0.5% and 1% normalized to the base yield curvature

The bounds of the extent of plasticity (L_p) can also be approximated based on the height of the curvature profiles wherein the average recorded curvatures are above the recorded base yield curvature. The bounds are obtained at top drift ratio of 1% and are presented in Table 4.3. The results show that the maximum extent of the plasticity height from the base of the walls falls in the range of 50 mm and 200 mm for Walls 2, 4, and 5 while it falls in the range of 200 mm to 700 mm for Walls 1 and 6.

4.3.3 Curvature Ductility and Equivalent Plastic Hinge Length

The average curvature profiles shown in Fig. 4.7 show a range of curvature ductility ($\mu_\varphi = \varphi/\varphi_y$) at the base of the walls between 2.7 for Wall 6 and 9.3 for Wall 4 at the top drift ratio of 1% showing extensive inelastic deformation of the walls at their bases at this deformation level. Moreover, these curves generally show an increase in the curvature profile nonlinearity in the first story at top drift ratio of 1% compared to the top drift ratio of 0.5% and yield level due to formation and development of the plastic hinge zone.

The upper bound values of L_p (both absolute and normalized to the wall lengths) from the three values obtained based on the lateral deformation profile, the extent of yielding in the end vertical bar, and the average curvature profiles of the walls, are presented in Table 4.3. Based on these values, the plasticity zone is extended from the base of the wall to a height equal to 35% of the wall length for

Walls 2, 4, and 5. It is extended at least up to 35% and 62% of wall length from the wall base over the height of the wall for Walls 1 and 6.

In order to assess the displacement demand and capacity of RM walls, the effect of inelastic deformations will be represented by an equivalent plastic hinge length (l_p) as suggested by Paulay and Priestley (1992). In this approach the inelastic displacements of the wall can be approximated assuming rigid body rotation of the wall around the center of its plastic hinge region and assuming constant plastic curvature within this region. This model, which is applied to the first story of the walls, can be expressed as:

$$\Delta_p = \theta_p(h_w - \frac{l_p}{2}) \tag{4.2}$$

where $\Delta_p = \Delta_{flex} - \Delta_{y,flex}$ is the plastic flexural lateral displacement and $\theta_p = \varphi_p l_p$ is the plastic rotation of the wall around the mid length of the plastic hinge zone.

The equivalent plastic hinge length values at a top drift of 1% are computed experimentally for the model walls based on the above equation and are presented in Table 4.3. The ratio of the experimentally obtained equivalent plastic hinge length to the wall length presented in Table 4.3 ranges from 0.12 for Wall 4 to 0.38 for Wall 6. Again, it should be noted that the design of such walls falls under the conventional construction category of the National Building Code of

Canada (NRCC 2010), which is not permitted in seismic zones. As such, no specific plastic hinge value is provided in the CSA S304.1 (2004).

4.4 Wall Input Energy Distribution and Characteristics

SFRS absorb and dissipate seismic energy in different ways during an earthquake event depending on their type (e.g. frame versus shear wall system) and material properties (e.g. concrete versus steel). Investigation of the seismic response of SFRS through their energy dissipation and absorption mechanisms is essential to understanding their seismic performance. In addition, the level of energy dissipated through inelastic response of the SFRS is an indication of the amount of induced damage and can also be used to quantify its seismic performance. Subsequently, quantifying the input seismic energy distribution within a SFRS permits a better understanding of its seismic performance. Such an approach was employed by Lestuzzi and Bachmann (2007), in which they investigated the seismic performance of six reduced-scale Reinforced Concrete (RC) shear walls tested on a shake table. In their study, they focused on quantifying the level of input energy, the ratio of the hysteretic energy to the input energy, and distribution of the hysteretic energy dissipation along the height of the wall and within the plastic hinge region. Various methods to compute the seismic energy components are discussed by Uang and Bertero (1990) and Christopoulos and Filiatrault (2006).

4.4.1 Quantification of Energy Components

As stated previously, studying the energy dissipation and absorption mechanisms of SFRS permits a better understanding and evaluation of their seismic performance capabilities. Considering the test setup shown in Fig. 4.2, the energy balance of the test setup-model wall system can be represented by the following equation:

$$E_{in}^{a} = E_{k}^{a} + E_{d} + E_{a} + E_{f} \tag{4.3}$$

where E_{in}^{a} is the absolute input energy into the system from the shaking table, which based on Eq. 4.3 will be transformed to absolute kinetic energy (E_{k}^{a}), energy that is damped through viscous damping mechanism (E_{d}), energy that is absorbed through the elastic and inelastic actions of the structural members (E_{a}), and energy that is dissipated by the friction in the system (E_{f}).

The values of different energy components mentioned above can be calculated through the integration of their corresponding resisting/input forces over their corresponding relative/absolute displacements. The absolute input energy (E_{in}^{a}) results from the total force exerted by the shake table into the shear wall-EMSS acting through the shake table absolute displacements. The absolute kinetic energy (E_{k}^{a}) is related to the absolute velocity of the system and the viscously damped energy (E_{d}) and absorbed energy (E_{a}) result from viscous damping forces and restoring forces respectively in the walls acting through the

floor relative displacements. The absorbed energy contains a recoverable part, which is the strain energy stored in the system through elastic deformations of the structural members, and a non-recoverable part, which is the hysteretic energy dissipated in the system through inelastic deformations in the structural members. However, the cumulative absorbed energy computed at the end of the earthquake when there is no motion only includes the total hysteretic energy dissipated during the earthquake. The total resisting force at each floor level is comprised of the sum of the viscous damping forces and restoring forces at each floor. As such, the total resisting force can be used to compute the sum of the viscously damped and absorbed energies. In the following sections details of the quantification of friction forces, friction energy, and flexural strain energy are presented. Details of quantification of other forces and energy components are presented in Appendix B. Note that i and n indexes in the following equations refer to the values at time t_i and t_n(end of the record) respectively and j index refers to the j^{th} story. The positive direction of the forces, accelerations, and displacements is taken to be in the west direction as indicated in Fig. 4.2. The readings of the load cells mounted in the loading beams are also considered positive and negative, respectively, when they are in tension and compression.

4.4.1.1 Friction energy

Energy is continuously dissipated via friction in the system i.e. in the LSS, in the real hinges of the loading beams, and by the linear bearings in the EMSS.

Assuming that the two first sources of friction are negligible compared to the friction forces developed in the linear bearings, the energy dissipated by the coulomb friction action in the system ($E_{f,n}$) can be computed as:

$$E_{f,n} = \sum_{j=1}^{m} \sum_{i=1}^{n} f_{cfj,i} \, \Delta u_{j,i} \tag{4.4}$$

where $f_{cfj,i}$ and $\Delta u_{j,i}$ are the coulomb friction force and absolute lateral displacement increment at the j^{th} story, respectively.

The friction force can be calculated from the measured total lateral force by recognizing that this force is the sum of the inertial force of the external mass and the friction force. Therefore the coulomb friction forces ($f_{cfj,i}$) can be obtained by:

$$f_{cfj,i} = F_{LCj,i} + m_{j2} \ddot{u}_{j,i,2} \tag{4.5}$$

In Eq. 4.5, m_{j2} is part of the inertial mass supported externally at the j^{th} story composed of the mass of the mass trolley (which includes the steel plates) and the portion of the loading beams between the load cells and the EMSS at the corresponding story (loading beam (I) in Fig. 4.2-b**)**. Also, $\ddot{u}_{j,i,2}$ is the absolute acceleration measured by the accelerometers attached on the external masses (AC3 and AC4 in Fig. 4.2-a).

4.4.1.2 Total flexural energy

The total energy absorbed by the walls through flexural actions $E_{F,n}$ can be obtained by computing the work done by the moment acting along the height of the walls as:

$$E_{F,n} = \sum_{k=1}^{p} E_{F,k,n} = \sum_{k=1}^{p} \sum_{i=1}^{n} M_{k,i}\theta_{k,i} =$$

$$\sum_{k=1}^{p} \sum_{j=1}^{m} \sum_{i=1}^{n} F_{s,j,i} h_{k,j} \theta_{k,i} = \sum_{j=1}^{m} \sum_{i=1}^{n} F_{s,j,i} \ \Delta u_{F,j,i} \quad (4.6)$$

In Eq. 4.6, $E_{F,k,n}$ is the flexural energy absorbed in the k^{th} height segment, $M_{k,i}$ is the moment at the centre of the k^{th} segment in the wall height, $F_{s,j,i}$ is the total lateral story force defined in Appendix A (available online under Supplemental Material), $\Delta u_{F,j,i}$ is the relative flexural lateral deformation increment of j^{th} floor, and $h_{k,j}$ is the distance of the j^{th} floor from the centre of k^{th} height segment. It can also be inferred that the flexural energy absorbed is the work performed by the total story lateral forces over their corresponding lateral flexural deformations. In Eq. 4.6, $\theta_{k,i}$ is the average rotation in the k^{th} segment of the wall height and can be obtained from:

$$\theta_{k,i} = \varphi_{k,i} h_{segment,k} \quad (4.7)$$

where the average curvature over the k^{th} height segment ($\varphi_{k,i}$) can be obtained from Eq. 4.1.

4.4.2 Energy Component Response Histories

The response histories of the energy components are computed experimentally based on the formulations discussed above and are presented in Fig. 4.8 for Wall 1 at L1 and L2 levels. It can be observed from Fig. 4.8 that more than 80% of the flow of the total seismic energy to the system occurs within the first 3 seconds of the records when the absolute kinetic energies are maxima. The input energy response histories show a general increase in the input energy to the system beyond this initial time. The response histories of the absorbed and viscously damped energy also show the same general trend, with observed reductions in the energy indicating a restoring of the strain energy. The response histories of the coulomb friction energy also show a continuous increase in the frictionally damped energy component. It is also observed that the amount of cumulative energy dissipated by coulomb friction is less than 20% at the L2 level and less than 30% at the L1 level. Similar trends for the energy response histories of other walls were observed as can be seen in Appendix C.

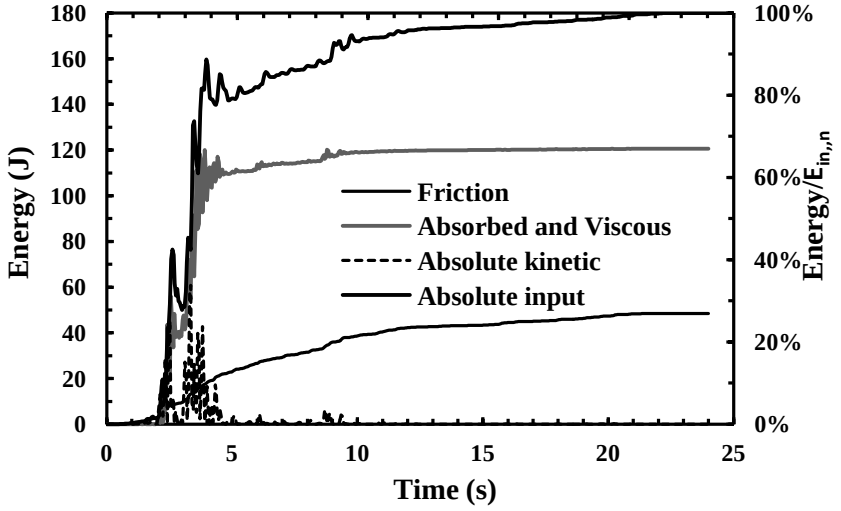

(a)

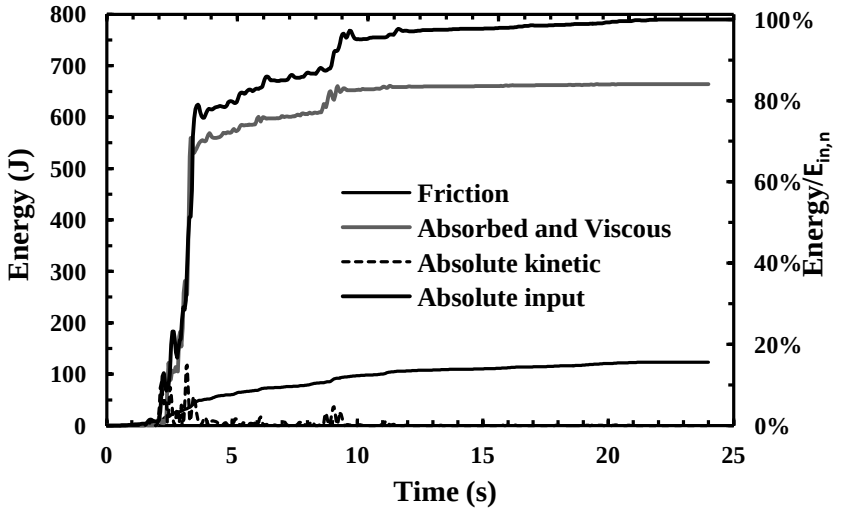

(b)

Figure 4.8: Response history of different energy components for Wall 1: **a)** During the L1 level test, **b)** During the L2 level test

4.4.3 Variation in the Total Input Energy

The cumulative energy component values for each of the walls at the end of the L1 and L2 level tests are presented in Table 4.4. The values show significant increase in the input energy for most of the walls at the L2 level compared to the L1 level. Moreover, it can be seen that there is considerable variation in the amount of input energy for different walls for the same excitation level. The amount of input energy is primarily attributed to the value of the fundamental frequency of the wall during the tests in relation to the frequencies at which the seismic energy is concentrated at for a specific earthquake record. Based on a Fast Fourier Transform (FFT) analysis of the shake table acceleration response at the L2 level, it was observed that most of the excitation energy is concentrated at frequencies in the range of 0.2 Hz to 5 Hz, referred to as the bulk energy frequency range hereafter. The values of the damped fundamental frequencies of the walls during L1 and L2 level tests evaluated from acceleration transmissibility plots between the acceleration response of the table and the top wall stories (f_c) are also presented in Table 4.4. As can be observed from the energy values in this table, the walls with fundamental frequencies in the bulk energy frequency range mentioned above absorbed a significant amount of energy during the tests. For example, Wall 3 with a fundamental frequency outside of the bulk energy frequency range has absorbed a minimal amount of energy at both L1 and L2 levels while Wall 5 with fundamental frequencies within the bulk energy frequency range absorbed a significant amount of energy at both L1 and L2 levels.

Table 4.4: Values of energy components for the walls at L1 and L2 levels

Wall	1	2	3	4	5	6
L1 level						
$E^{a}_{in,n}\ (J)$	175	173	27	66	192	156
$E_{f,n}(J)$	49	55	20	39	47	56
$E_{a,d,n}(J)$	121	114	7	29	155	101
$f_c(Hz)$	3.3	3.7	14.18	8.71	4.25	3.79
L2 level						
$E^{a}_{in,n}(J)$	780	832	85	955	848	817
$E_{f,n}(J)$	123	154	56	116	150	131
$E_{a,d,n}(J)$	664	698	34	851	744	690
$f_c(Hz)$	2.71	2.7	13.8	3.44	3.34	3.03

The behaviour of Wall 4 is of particular interest as, based on the results presented in Table 4.4, it absorbed a small amount of energy at the L1 level but absorbed a significant amount of energy at the L2 level compared to the other walls. The increased level of energy absorbed occurred as a result of the change in the fundamental frequency of this wall, which was originally outside the bulk energy frequency range during the L1 level test, but shifted into the bulk energy frequency range during the L2 level due to increased wall damage and consequent reduction in stiffness. This illustrates that using the initial elastic structural properties for seismic design, as suggested by current force-based seismic design codes, may result in an inaccurate evaluation of the seismic demand on the SFRS leading to non-uniform risk due to the scattered levels of damage following an earthquake event. This issue is more critical for earthquakes having an uneven distribution of energy over the excitation frequency range, which is the case for

the earthquake record used in this study. A more uniform level of risk may be achieved by utilizing displacement-based design techniques where the actual effective dynamic properties of structures at expected levels of response during seismic events, expressed in terms of parameters like effective period and effective stiffness, are utilized as suggested by Priestley et al (2007).

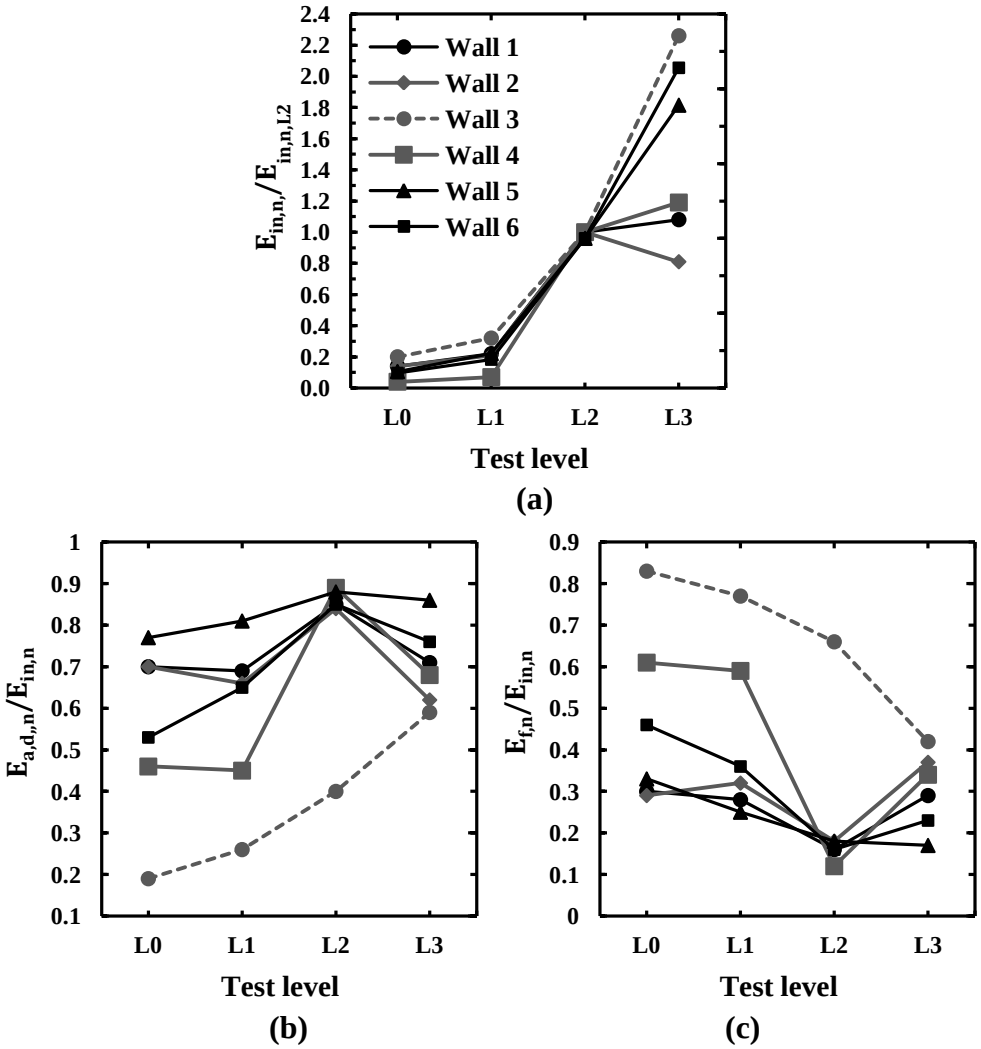

Figure 4.9: Variation of normalized cumulative energy values of the walls at the end of different test levels: **a)** The input energy normalized to the input energy at L2 level, **b)** The sum of the absorbed and viscously damped energies normalized to the input energy of the same test level, **c)** Coulomb friction energy normalized to the input energy of the same test level

Variations in the normalized cumulative energy values at the end of the four test levels are shown in Fig. 4.9. Figure 4.9-a show the variation in total input energy at the end of each test level normalized by the L2 level value. The curves show that the input energy was less than 50% of the L2 level at the L1 level for all walls and increased for all walls except Wall 2 at the L3 level. The increase in normalized cumulative energy at the L3 level was less for Walls 1 and 4 e than Walls 3, 5 and 6 mainly as a result of greater damage and early failure of end vertical bars and the corresponding loss of stiffness during the L3 level tests.

4.4.4 Variation in the Total Dissipated Energy

Variations of the total dissipated energy in the walls, i.e. sum of the viscously damped energy and the energy absorbed by the walls, at the end of different test levels normalized by their corresponding input energy values are shown in Fig. 4.9-b. The same energy values for L1 and L2 levels are presented in Table 4.4. The curves show the general trend of increased normalized energy dissipation with increased excitation levels up to L2 level. The increase in the ratio of the dissipated energy at higher levels is attributed to increased nonlinear flexural wall deformations occurring in the plastic hinge zone. The dissipated energy is approximately 85% to 90% of the total input energy at the L2 level for Walls 1, 2, 4, 5,and 6 as a result of development of a plastic hinging mechanism for these walls, however, it is only 40% of the total input energy for Wall 3 due to the significantly lower nonlinear response experienced by this wall. The reduction

in the ratio of the dissipated energy at the L3 level test for Walls 1, 2, 4, 5, and 6 is due to vertical bar buckling resulting in a rocking type response and reduced energy dissipation.

4.4.5 Distribution of Flexural Energy Dissipation

The distribution of flexural energy dissipation over the height of the first story is obtained by computing the contribution of each height segment in the first story based on Eq. 4.6. The contributions are computed as a percentage of the total energy dissipated in the walls i.e. sum of viscously damped and absorbed energy, and are presented in Fig. 4.10. It can be seen from Fig. 4.10-a that 51% or more of the total energy dissipated by the walls during the L1 level tests is due to flexural action in the segments of the first story. This increases for the L2 level tests, reaching a minimum of 74% for Walls 1, 2, 4, 5, and 6 and 69% for Wall 3. The difference between the flexural energy dissipated in the first story and the total energy dissipated in the walls is predominantly due to other sources of energy dissipation, including the flexural energy dissipated in the second story of the walls (in the case of two story walls), viscous damping, and nonlinear sliding and diagonal shear deformations in the walls. It can also be observed from Fig. 4.10 that the flexural energy dissipation between the height segments in the first story is more evenly distributed for the L1 level tests than the L2 level tests. Figure 4.10-b shows that the energy dissipated in the first segment of the first

story during the L2 level test ranges between 56% to 82% for Walls 1, 2, 4, 5, and 6 and is 42% for Wall 3.

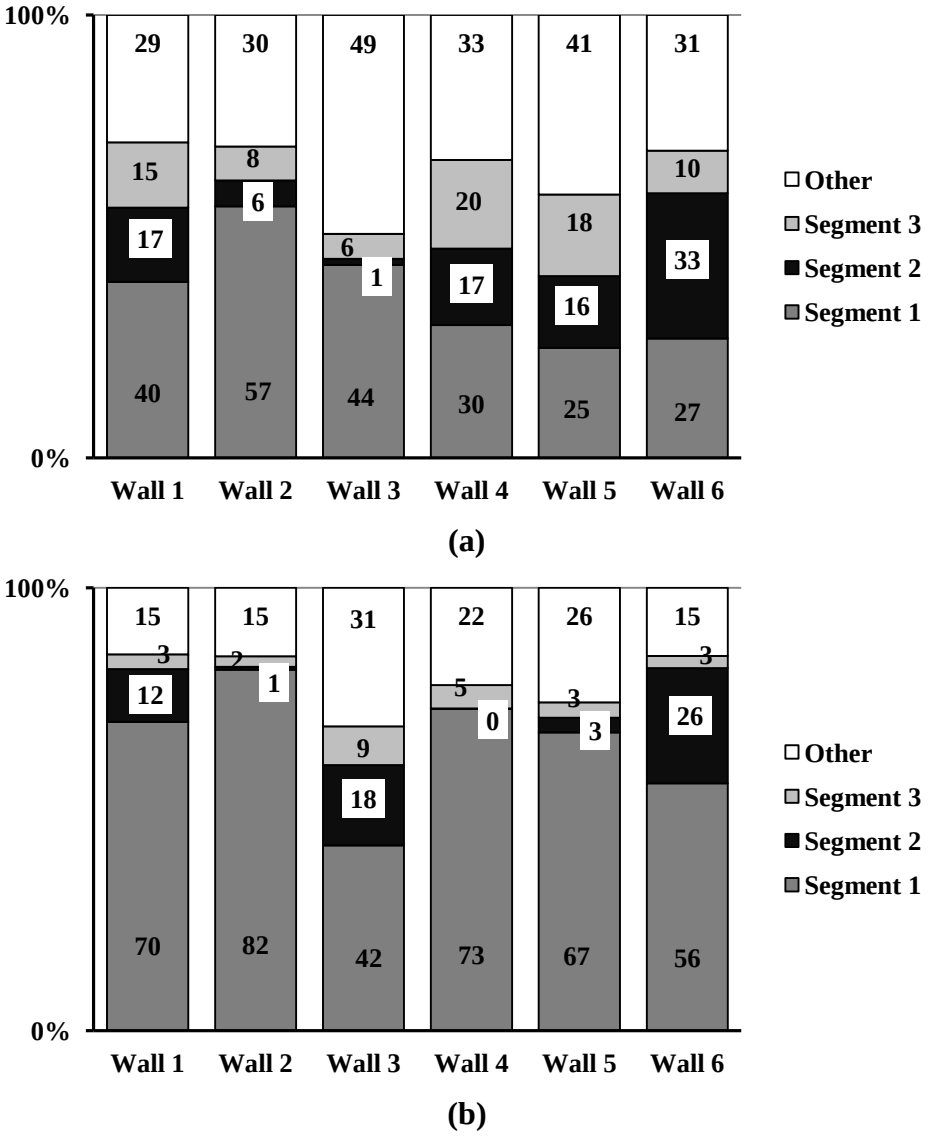

Figure 4.10: Distribution of flexural energy dissipation in the first story of walls: **a)** at L1 level, **b)** at L2 level

The above observations confirm that most of the energy dissipation in the walls occurs in the first story and is concentrated in an area close to the base i.e.

plastic hinge region. Therefore, in order to assure safe dissipation of energy without extensive loss of strength and failure, special seismic design provisions should be provided in this region as prescribed by design codes.

4.4.6 Variation of Coulomb Friction Energy

The energy dissipated by coulomb friction in the EMSS was experimentally calculated based on Eq. 4.8. The corresponding values are presented for L1 and L2 test levels in Table 4.4. Figure 4.9-c shows the variations of the coulomb friction energy normalized by the corresponding total input energy. The values in Table 4.4 show a low variation between the values of dissipated friction energy for different walls tested at the same excitation level. However, the curves in Fig. 4.9-c show that the ratio of the friction energy to the total input energy for a given test level can vary significantly, particularly at the L0 and L1 test levels. The curves show that a maximum of 46% of the total input energy was dissipated by friction in the external mass system for Walls 1, 2, 5, and 6, which increased to 83% and 61% of the total energy for Walls 3, and 4, respectively. As can be observed from Fig. 4.9-c, friction dissipates a significant portion of input energy at the L0 and L1 level tests. This is mainly due to the walls experiencing small relative inter-story lateral deformations, resulting in low energy dissipation, while the energy dissipated by friction is a function of the nearly constant friction forces and significantly larger absolute displacements. The increase in normalized energy dissipation observed for Walls 1, 2, 4, 5, and 6 for the L3 level test is

attributed to the large absolute lateral displacements due to the rocking response of the walls following the failure of the wall end bars.

In order to obtain the dynamic friction coefficient of the EMSS, the response history of the friction forces were computed from Eq. 4.9 during the shake table tests. The displacement response history of the friction forces for the first story of the EMSS obtained for low velocity sinusoidal excitation of the system with 12.7 mm displacement amplitude at 0.70 Hz (V_{max}= 55.86 mm/s) are presented in Fig. 4.11-a. It can be observed from this figure that the absolute values of friction forces are almost constant during the motions. However, the values are slightly affected by variations in the velocity during the motions. The peaks at the four corners of the loops in this figure correspond to the static friction forces, which are greater than dynamic friction forces and are developed at the end of the cycles at zero velocity.

The equivalent friction forces ($f_{cf,eq}$) were obtained by equating the friction energy measured during the motions to the energy dissipated by an equivalent constant friction force. The corresponding equivalent dynamic coefficients of friction ($\mu_{eq,d}$) are then obtained by dividing the values of the equivalent friction forces by the weight of the external masses. Figure 4.11-b shows the variations of the equivalent dynamic coefficients of friction of the system for the different walls at all four test levels. The equivalent dynamic coefficient of friction obtained from the application of a sinusoidal displacement to Wall 1 is 1.19% and is also shown in the same figure.

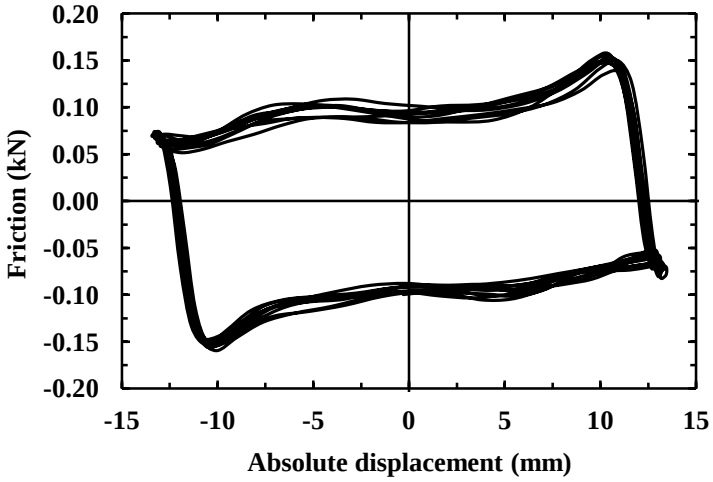

(a)

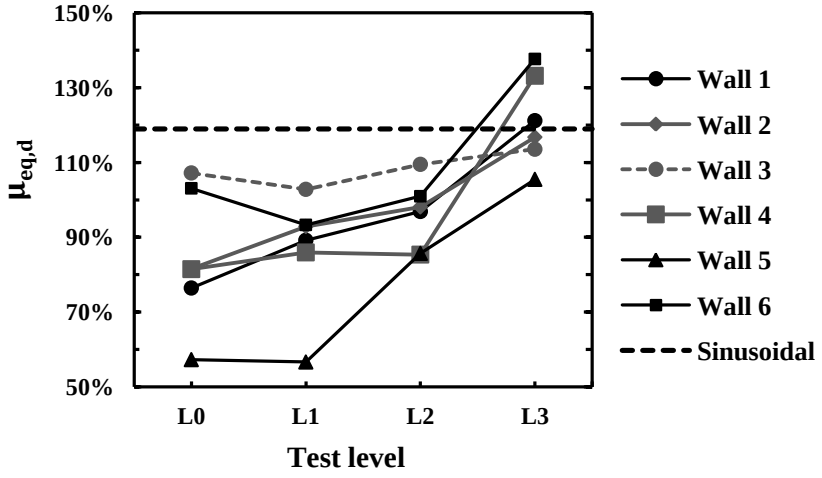

(b)

Figure 4.11: Variations of coulomb friction forces: **a)** The hysteresis of the friction forces from sinusoidal motions, **b)** The variation of the average dynamic friction coefficient

Figure 4.11-b shows a general increase in the values of $\mu_{eq,d}$ at higher earthquake levels. Similar to the observations made by Carrillo and Alcocer (2011), the variations are generally attributed to the variations in the maximum

absolute velocity of the motions. Based on the results presented in Fig. 4.11-b, the values of $\mu_{eq,d}$ vary in the range of 0.57% to 1.03% for the L1 level and 0.85% to 1.38% for the L2 level tests.

4.5 SDOF Model with Effective Wall Dynamic Properties

The procedure recommended by most current force-based seismic design codes (e.g. NRCC 2010) involves determination of seismic demands based on the initial elastic dynamic properties (stiffness, period, and damping) of the structure using elastic acceleration response spectra. These elastic properties are typically evaluated at the yield level (Paulay and Priestley, 1992, and Priestley et al., 2007). However, as mentioned previously, the response of SFRS may better be quantified through the use of their (effective) dynamic properties at their target or maximum response (i.e. following a displacement-based approach) rather than the corresponding elastic values and a fixed ductility value (i.e. following force-based approaches). To apply the displacement-based approach, and in order to account for the inelastic response of the SFRS but still utilize the elastic response spectra, the substitute structure method (Gulkan and Sozen 1974, Shibata and Sozen 1976) is adopted. In this approach the inelastic SDOF system can be modeled with a linear elastic system with effective dynamic properties, which include the secant stiffness, the period, and the damping ratio.

4.5.1 Effective mass

In order to determine the effective dynamic properties for the RM shear walls discussed in the current study, the first step is to determine the properties of equivalent SDOF system for the two story walls. The effective mass and displacement of the latter can be obtained assuming that the walls deform only in their first mode of vibration using the following two equations (Calvi and Kingsley 1995), respectively:

$$u_e^r = \frac{\sum_{j=1}^{m} m_j (u_j^r)^2}{\sum_{j=1}^{m} m_j u_j^r} \tag{4.8}$$

$$m_e = \frac{\sum_{j=1}^{m} m_j u_j^r}{u_e^r} \tag{4.9}$$

where u_e^r and m_e are the effective displacement and mass of the equivalent SDOF system when the j^{th} floor is experiencing u_j^r relative displacement.

4.5.2 Effective secant stiffness and period

The effective secant stiffness (K_e) and period (T_e) can be expressed as:

$$K_e = \frac{V_b}{u_e^r} \tag{4.10}$$

and

$$T_e = \sqrt{\frac{4\pi^2 m_e}{K_e}} \tag{4.11}$$

where V_b is the base shear of the MDOF system at the desired excitation level.

Table 4.5: Effective stiffness and period of walls

Wall	1	2	3	4	5	6
At yield level						
$K_{e,y}(kN/m) \times 10^3$	1.39	0.90	5.12	3.34	1.35	1.01
$T_{e,y}(s)$	0.24	0.29	0.09	0.16	0.24	0.28
At 0.5% top drift ratio						
$K_e/K_{e,y}$	0.58	0.80	N.A.	0.40	0.68	0.66
$T_e/T_{e,y}$	1.31	1.13	N.A.	1.57	1.22	1.23
At 1% top drift ratio						
$K_e/K_{e,y}$	0.28	0.40	N.A.	0.18	0.36	0.52
$T_e/T_{e,y}$	1.92	1.59	N.A.	2.35	1.69	1.38
At maximum load						
$K_e/K_{e,y}$	0.22	0.27	0.72	0.23	0.33	0.44
$T_e/T_{e,y}$	2.14	1.95	1.18	2.10	1.78	1.52

The effective secant stiffness and period of the RM shear walls at the yield and maximum load and at the top drift ratio of 0.5% and 1% are computed based on Eqs. 4.10 and 4.11 and the results are presented in Table 4.5. It can be observed that the secant stiffness of the walls reduces significantly and the effective period increases correspondingly at higher levels of response compared to the yield level. Based on the results presented in Table 4.5, the reduction of effective secant stiffness and the elongation of effective period at the maximum

lateral load are up to 78% and 214% of their corresponding values at the yield level. The same trends are observed in Fig. 4.12, which shows the variations of the secant effective stiffness and period at maximum load for each test level normalized to their corresponding values at the L0 level.

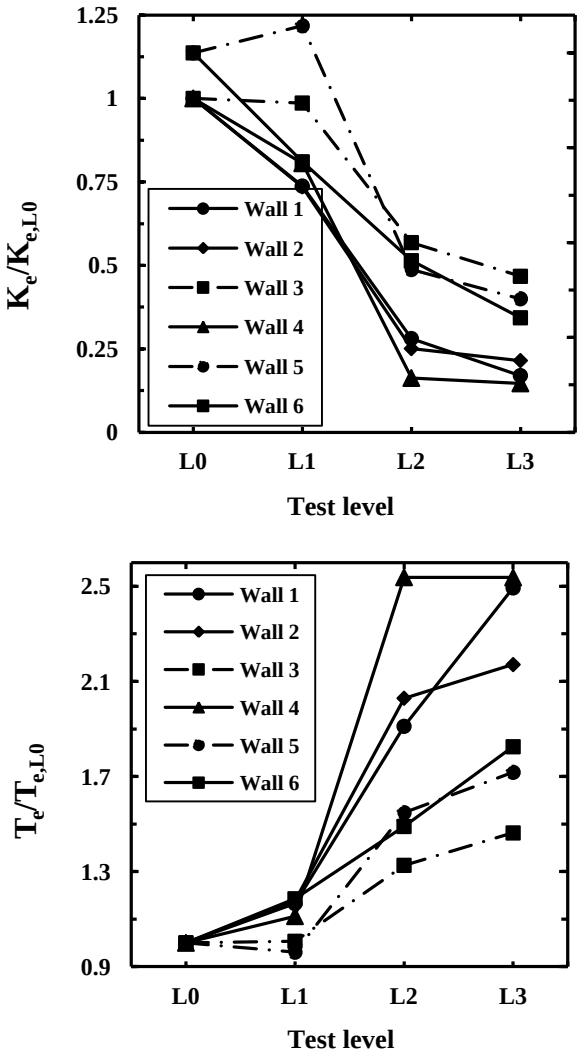

Figure 4.12: Variations of the secant effective stiffness and period at maximum load for each test level normalized to their corresponding values at the L0 level

4.5.3 Equivalent viscous damping ratio

In the substitute structure approach, the effect of the inelastic response of the SFRS is taken into account through consideration of equivalent hysteretic viscous damping ratio (ξ_{hyst}). The latter can be evaluated by equating the energy absorbed by hysteretic steady-state cyclic response to given displacement level to the equivalent viscous damping of the substitute structure (Jacobsen, 1960). The above approach adapted to the equivalent SDOF representation of the walls can be expressed by:

$$\xi_{hyst} = \frac{E_{a1}}{2\pi V_b u_e^r} \tag{4.12}$$

where E_{a1} is the energy absorbed by the equivalent SDOF representation of walls in the cycle corresponding to u_e^r. The equivalent viscous damping ratio (ξ_{eq}) is defined as the sum of the equivalent viscous damping ratio in the elastic range (hereafter referred to as elastic viscous damping ratio (ξ_{el})) and the equivalent hysteretic damping ratio (ξ_{hyst}). The equivalent viscous damping ratio can be obtained from Eq. 4.12 by setting the value of E_{a1} to the sum of the viscously damped and absorbed energies ($E_{a,d}$) as defined in Eq. 4.6.

The equivalent viscous damping ratio (ξ_{eq}) values of the walls are computed at the maximum loads of each test level and are presented in Fig. 4.13. As can be observed from the figure, the equivalent viscous damping ratios

increase at higher levels for all walls, particularly at L2 and L3 levels for Walls 1, 2, 4, 5, and 6, due to the increase in the inelastic deformations and damage to the walls. The values of equivalent viscous damping ratios of Walls 1, 2, 4, 5, and 6 range between 4% and 7% at L0 and L1 levels and between 16% and 24% at L2 and L3 levels. The values of equivalent viscous damping ratio at L2 and L3 levels for Wall 3 are 3% and 8%, respectively. The values are significantly less than the other two story walls due to the limited inelastic deformations experienced by Walls 3, even at the L3 level test.

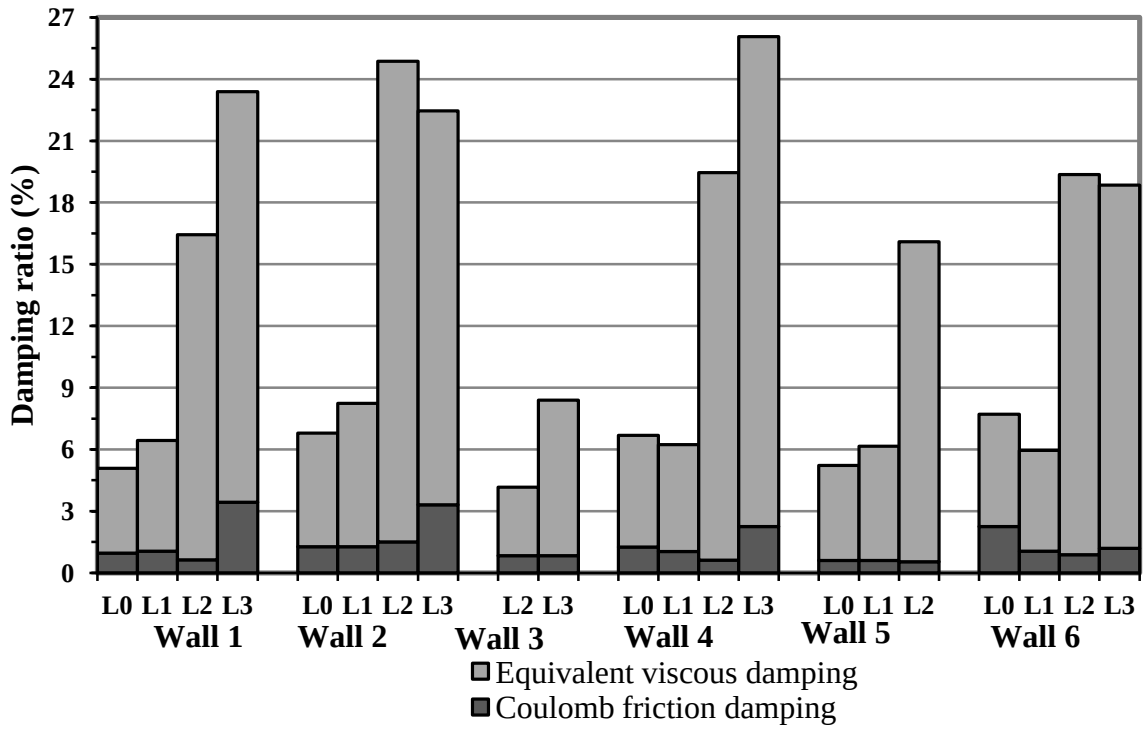

* Values are not presented for L0 and L1 levels for Wall 3 and L3 level for Wall 5 due to instrumentation malfunction.

Figure 4.13: Variations of equivalent viscous damping ratios and equivalent coulomb friction damping ratios of the walls

4.5.4 Equivalent coulomb friction damping ratio

The equivalent coulomb friction damping imposed by the coulomb friction forces in the external mass supporting system are computed using Eq. 4.12 and by substituting E_{a1} by the friction energy dissipated in a cycle (E_{f1}). This energy is computed considering constant friction forces equal to the equivalent friction forces ($f_{cf,eq}$) during the cycle. Although friction forces act through the absolute lateral displacement of the mass trolley, in computation of E_{f1} it is assumed that only the energy dissipated by the friction forces over the relative displacements influence the wall response. In other words, the remaining friction energy, which is in fact dissipated over the shake table displacement, is considered to not affect the energy absorbed by the walls. The values of the equivalent coulomb friction damping ratios ($\xi_{\mu,eq}$) are computed as explained above at the maximum loads of each test level and are presented in Fig. 4.13. It is observed from the figure that in general the values of $\xi_{\mu,eq}$ do not vary considerably and, in most of the cases, are in the range of 0.5% to 1.5%.

It can be shown that the coulomb friction damping does not affect the natural period of a structure (Chopra, 2001). However, in order to evaluate the effect of the added coulomb friction damping on the response of the walls, the spectral response accelerations of the SDOF system corresponding to the effective period of the walls at the maximum load for each test level are computed. The values of the spectral response accelerations are computed twice, once based on equivalent viscous damping ($S_{a,eq}$) and once based on total equivalent viscous

damping including the coulomb friction damping ($S_{a,T}$). The values of $S_{a,T}/S_{a,eq}$ presented in Fig. 4.14 show that the added friction damping has led to only a small reduction in the spectral response acceleration, with the exception of Wall 6 at the L0 level, which shows 13% reduction in the spectral response acceleration, respectively. Based on the above results, energy dissipation by the coulomb friction forces during the tests has only a minor influence on the response of the walls.

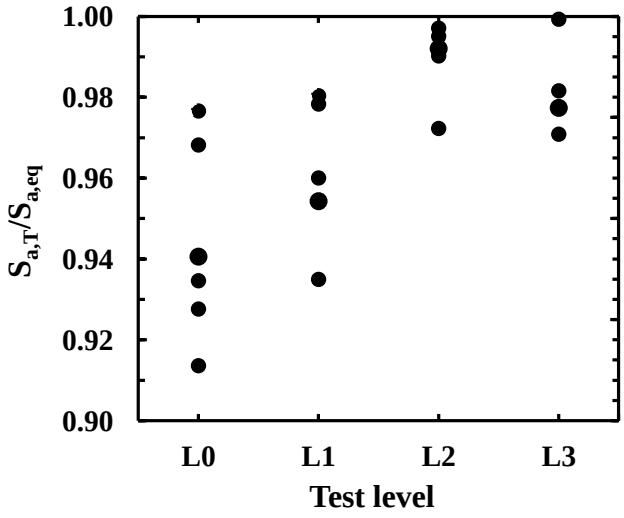

Figure 4.14: The variations of the normalized spectral acceleration response affected by the coulomb friction damping

4.5.5 Base Shear Prediction

In order to show the importance of consideration of effective properties of the walls and the efficiency of the substitute SDOF model in predicting the seismic demand, the maximum base shear of the walls at the L2 test level is first estimated based on the effective properties approach and subsequently based on

the elastic properties approach. In the substitute SDOF approach (i.e. using the effective properties), the base shear of the walls is computed by multiplying the effective mass (m_e) of the walls to the elastic spectral response acceleration (S_a) corresponding to the effective period (T_e) and total equivalent viscous damping ($\xi_{eq,T}$), including the coulomb friction damping. The effective parameters in the substitute SDOF approach are obtained at the maximum load during the L2 level test. Conversely, for the force-based approach, the base shear is computed by multiplying the total mass of the system (m) to the elastic spectral response acceleration (S_a) corresponding to the initial elastic period ($T_{i,el}$) and 3% of assumed elastic viscous damping (ξ_{el} = 3%). An elastic damping ratio of 5% is usually prescribed for RM and RC structures considering the damping effect of non-structural elements. However, selection of a lower and more conservative value of 3% elastic viscous damping is mainly due to the absence of secondary structures in the model walls.. The base shear values based on the elastic properties are then divided by the response modification factors corresponding to the idealized displacement ductility level of the walls at the maximum load at L2 level ($R_{u,L2}$).

The relevant parameters used in both substitute structure and force-based methods are presented in Table 4.6. The ratios of the estimated maximum base shear to the experimental maximum base shear of the walls during the L2 level tests for both methods are also presented in Table 4.6. The values show that the base shear values estimated by the substitute SDOF approach are generally in

good agreement with the experimental values with a maximum variation of 10% occurring in Wall 1 and Wall 2. The ratios of the estimated maximum base shear based on the force-based method show that the maximum base shear is consistently underestimated by up to 60%. This is attributed to the fact that the force-based method is based on initial properties of the walls, where as can be observed from the values presented in Table 4.6, the effective period of the system varies considerably during the tests. In addition, as discussed in the energy distribution section, using the initial period can result in possible errors in evaluating the seismic demands.

Table 4.6: Computation of maximum base shear at L2 level test based on effective and initial elastic properties of the walls

Wall	**1**	**2**	**3**	**4**	**5**	**6**
Based on effective properties						
$T_e(s)$	0.50	0.57	0.10	0.33	0.42	0.42
$m_e(kg)$	1,993	2,004	1,120	2,159	2,012	1,975
$\xi_{eq,T}$ (%)	16	25	4	19	16	19
$S_a\,(g)$	0.483	0.375	0.926	0.648	0.730	0.676
$V_{u,L2}/V_{e,u,L2}$	0.90	0.90	0.96	0.96	1.04	1.07
Based on initial elastic properties						
$T_{i,el}(s)$	0.14	0.16	0.07	0.11	0.15	0.27
$m\,(kg)$	2,218	2,218	1,120	2,320	2,218	2,218
ξ_{el} (%)	3	3	3	3	3	3
$S_a\,(g)$	1.148	0.929	0.685	1.264	0.979	1.267
$R_{u,L2}$	4.61	2.67	1	5.05	3.27	3.09
$V_{u,L2}/V_{e,u,L2}$	0.51	0.88	0.71	0.40	0.47	0.73

4.6 Conclusions

The current study presented detailed analyses of the seismic response of fully-grouted RM shear walls based on shake table tests. The following conclusions are drawn from the results and discussion presented in this paper:

The experimental displacement ductility levels of the two story walls were at least 1.6 and 3.3 at 0.5% and 1% drift levels, respectively. These values were at least 4.3 at the maximum load. The idealized ductility values were at least 1.5 and 2.7 at 1% drift level and maximum load, respectively. The maximum idealized ductility values reached by the walls during the tests was as high as 4.6. This shows that RM shear walls, even with minimal reinforcement such as the walls tested, can develop considerable nonlinear deformation capacity that can be relied on for seismic design. The values of the ductility related response modification factors (R_d) ranged between 1.5 and 4.5, which suggests a considerable variation in the wall seismic responses.

A range of displacement ductility levels were obtained for RM shear walls depending on their geometry, design, and seismic demands. It is observed that variable displacement ductility levels are obtained for shear walls belonging to the same category of SFRS, however, current seismic design codes like National Building Code of Canada (NBCC)(NRCC 2010) prescribe a single R_d value for each type of SFRS. It also draws attentions to the fact that force-based approaches may lead to SFRS designed with a non-uniform risk of failure. The findings, however, support the notion that displacement ductility demands considered for

computation of design seismic forces for the walls and generally any SFRS, should be obtained based on the actual level of seismic demand and realistic estimations of response of structures during earthquakes. This results in different levels of displacement ductility for the same SFRS with different design and geometry parameters and level of seismic hazards.

Investigations on the extent of plasticity based on the lateral deformation profile, extent of yielding in the wall end bars, and the average curvature profiles of the walls, revealed that for top drift ratio of 1%, the plasticity zone is extended within the base of the wall and a height equal to 35% of the wall length for Walls 2, 4, and 5 and is extended at least up to 35% and 62% of wall length from the wall base over the height of the wall for Walls 1 and 6. Equivalent plastic hinge lengths of the walls at top drift ratio of 1% were found to be in the range of $0.12l_w$ for Wall 4 to $0.38l_w$ for Wall 6. These observations confirm that lightly RM shear walls can develop plastic hinging mechanisms and reliably dissipate energy in the plastic hinge zone.

The investigations on the input seismic energy revealed that the amount of absorbed energy by an SFRS during an earthquake might vary considerably based on the variations of its dynamic properties as a result of damage. Findings from this study also showed the applicability of using the effective dynamic properties of RM shear walls during an earthquake event to determine the seismic demands.

Evaluating energy distribution showed that up to 74% of the energy dissipation in the walls occurred in the first story and was concentrated at the base

of the wall in the plastic hinge zone. This reaffirms that, as prescribed by masonry design codes, special seismic design provisions should be employed in this region to facilitate reliable energy dissipation without extensive loss of wall strength.

Investigations on the effective dynamic properties of the walls based on substitute SDOF representation of the walls showed the significant variation of effective secant stiffness, period and equivalent viscous damping at different response levels. The results revealed that the reduction of effective secant stiffness and the elongation of effective period at the maximum lateral load are up to 78% and 214% of their corresponding values at the yield level. The values of effective equivalent viscous damping of two story walls are in the range of 4% to 7% at L0 and L1 levels while they range between 16% and 24% at L2 and L3 test levels. The maximum base shear values, estimated based on effective dynamic properties of the walls, were close to the experimental values with errors in the range of 10% while estimated values based on the initial elastic dynamic properties underestimate the actual values up to 60%. Findings revealed that the added friction damping has decreased the spectral response acceleration by 7% or less for Walls 1, 3, 4, 5 and 9% and 11% for Walls 2 and 6, respectively, confirming that the external mass supporting system does not alter the seismic response of the walls significantly.

4.7 Notation for Chapter 4

C = Damping coefficient
E_{in}^{a} = Absolute input energy
E_{k}^{a} = Absolute kinetic energy
E_f = Friction energy
E_d = Viscous damping energy
E_a = Absorbed energy (by wall)
$E_{a,d}$ = Sum of the viscously damped and absorbed energies by the walls
E_s = Strain energyE_h = Hysteretic energy
E_F = Flexural energy (Energy dissipation through flexural actions)
F_{st} = Total force exerted by the shake table into the shear wall-mass supporting system
F_s = Total lateral story force acting on the wall at the corresponding level
F_{LC} = Lateral load measured by the floor load cells
F_d = Viscous damping forces
F_r = Restoring forces
K = Lateral stiffness at the top of the walls
K_e = Effective secant stiffness
T = Period
L_p = Extent of plasticity
M = Moment
R_d = Ductility-related response modification factor
R = Response modification factor
S_a = Spectral response acceleration
S_v = Longitudinal reinforcement spacing
V_b = Base shear
V_{max} = Maximum velocity
f'_m = Compressive strength of masonry
f_s = Sampling frequency
f_c = Damped fundamental frequency from the acceleration transmissibility plots
f_{cf} = Coulomb friction force developed in the external mass supporting system
f_d = Damped fundamental frequency
$h_{k,j}$ = Distance of the j^{th} floor from the centre of k^{th} height segment

$h_{segment}$ = Height of the vertical segment along the wall height
l_w = Wall length
l_p = Equivalent plastic hinge length
m_e = Effective mass
m_1 = Mass of the system moving rigidly with the shake table (lower half part the model walls)
m_j = Total inertial mass corresponding to the j^{th} floor
m_{j1} = Part of the inertial mass of the j^{th} floor supported by the walls
m_{j2} = Part of the inertial mass supported externally at the j^{th} story
u^r = Relative displacement$\dot{u}$ = Absolute velocity
$\dot{u}^r$ = Relative velocity
$\dot{u}_{st}$ = Absolute velocity of the shake table
$\ddot{u}_{st}$ = Acceleration of the shake table
$\ddot{u}_1$ = Absolute acceleration recorded by the accelerometers attached to the RC slabs
$\ddot{u}_2$ = Absolute acceleration recorded by the accelerometers attached to the external masses
Δu_{st} = Shake table displacements increment
Δu = Absolute lateral displacement increment
Δu^r = Relative lateral displacement increment
Δu_F = Relative flexural lateral deformation increment
ρ_v = Longitudinal reinforcement ratio
ξ = Viscous damping ratio
ξ_{hyst} = Hysteretic viscous damping
ξ_μ = Coulomb friction damping ratio
ε_T = Tensile strain at the corners of the wall
ε_C = Compressive strain at the corners of the wall
Δ_T = Tensile deformation at the corners of the wall
Δ_C = Compressive deformation at the corners of the wall
Δ_p = Plastic flexural lateral displacement
Δ_{flex} = Total flexural lateral displacement
$\Delta_{y,flex}$ = Flexural lateral displacement at yield
μ_φ = Curvature ductility

μ_{Δ} = Displacement ductility level based on displacement at top of the wall
$\mu_{eq,d}$ = Equivalent dynamic coefficients of friction
φ = Average curvature
φ_y = Wall yield curvature
φ_p = Wall plastic curvature
θ = Rotation of the wall
θ_p = Plastic rotation of the wall

SUBSCRIPTS

i = Value at time t_i, initial
n = Value at time t_n (end of the time history)
j = Value related to j^{th} story
k = Value related to k^{th} height segment
0.5%,1 = Obtained at 0.5% drift ratio at the first story
$0.5\%, 2$ = Obtained at 0.5% drift ratio at the top of the wall
$1\%, 1$ = Obtained at 1% drift ratio at the first story
$1\%, 2$ = Obtained at 1% drift ratio at the top of the wall
u = Obtained at maximum load
y = Obtained at the yield level
1 = Computed in one complete cycle
eq = Equivalent
e = Effective, Experimental
el = Elastic
T = Total

SUPERSCRIPTS

id = Idealized

4.8 References for Chapter 4

American Society for Testing and Materials, (2009). "Standard specification for deformed and plain carbon-steel bars for concrete reinforcement (A615/A615M-09b ed.)." West Conshohocken, Pa: ASTM International.

ASCE7, (2010). "Minimum design loads for buildings and other structures." Structural Engineering Institute, American Society of Civil engineers, Reston, Va, USA.

Calvi, G. M., and Kingsley, G. R. (1995). "Displacement-based seismic design of multi-degree-of-freedom bridge structures." *Earthquake engineering & structural dynamics*,24(9),1247-1266.

Canadian Standard Association, (CSA S304.1). Design of Masonry Structures. S304.1. Mississauga, ON: CSA, 2004.

Carrillo, J., Alcocer, S. (2011). "Improved External Device for a Mass-Carrying Sliding System for Shaking Table Testing." *Journal of Earthquake Engineering and Structural Dynamics*, 40, 393-411.

Chopra, Anil K. Dynamics of structures: Theory and applications to earthquake engineering. Vol. 2. Upper Saddle River, NJ: Prentice Hall, 2001.

Christopoulos, C. Filiatrault, A. (2006). "Principles of supplemental damping and base isolation", IUSS Press, Milan, Italy.

Gulkan, P., Sozen, M. A. (1974). "Inelastic responses of reinforced concrete structure to earthquake motions." In ACI Journal Proceedings, 71(12). ACI.

Harris, H. G., Sabnis, G. (1999). "Structural Modeling and Experimental Techniques", Second ed., CRC Press.

Jacobsen, L. S. (1960). "Damping in Composite Structures." *In Proceedings of the 2nd World Conference on Earthquake Engineering*, Japan, vol. 2, pp. 1029-1044.

Kasparik, T., Tait M. J., and El-Dakhakhni W. W. (2012).”Seismic Performance Assessment of Partially-Grouted Nominally-Reinforced Concrete Masonry Structural Walls Using Shake Table Testing.” *Journal of Performance of Constructed Facilities*, Accepted for publication.

Lestuzzi, P., and Bachmann, H. (2007). “Displacement Ductility and Energy Assessment from Shaking Table Tests on RC Structural Walls.” *Engineering Structures*, 29, 1708-1721.

Mojiri, S., El-Dakhakhni, W. W., Tait, M. J. (2013). “Shake Table Seismic Performance Assessment of Fully Grouted Lightly Reinforced Concrete Block Shear Walls “. *Journal of Structural Engineering*, Submitted for publication.

National Research Council of Canada (NRCC) (2010). “National Building Code of Canada (NBCC),” Institute for Research in Construction, Ottawa, Canada.

National Institute of Standards and Technology (NIST). (2010). “Evaluation of the P-695 methodology for quantification of building seismic performance factors.” NIST GCR 10-917-8., NIST, Gaithersburg, MD, USA.

Pacific Earthquake Engineering Research Center: NGA Database. (Accessed September, 2011). http://peer.berkeley.edu/nga/

Paulay, T., Priestley, M., J., N. (1992). “Seismic Design of Reinforced Concrete and Masonry Buildings.” John Wiley & Sons, Inc., New York and Toronto, 139-142.

Priestley, M.J.N., G.M. Calvi, and M.J. Kowalsky. “Displacement-Based Seismic Design of Structures.” Pavia: IUSS Press, 2007.

Shibata, A., and Sozen, M. A. (1976). “Substitute-structure method for seismic design in R/C.” *Journal of the Structural Division*,102(1), 1-18.

Uang, C., Bertero, V. V. (1990). “Evaluation of seismic energy in structures.” *Earthquake Engineering & Structural Dynamics*, 19(1), 77-90.

CHAPTER 5: SEISMIC FRAGILITY ASSESSMENT OF LIGHTLY-REINFORCED CONCRETE BLOCK MASONRY SHEAR WALLS

5.1 Introduction

This chapter focuses on development of analytical fragility curves based on the performance of RM walls tested under shake table excitations, reported in previous chapters. The chapter has two phases. In the first phase the seismic response of the shear walls is modeled by a simplified analytical model that was calibrated based on the shake table test results and the predicted response history of the walls using the developed models were verified against the experimental test results. In the second phase of study the experimental results and the analytical model developed in the previous chapters are employed towards fragility assessment of the two story walls.

This chapter contains the work in the following article:

Mojiri, S., Tait, M. J., El-Dakhakhni, W. W. (2013). "Seismic Fragility Assessment of Lightly-Reinforced Concrete Block Masonry Shear Walls." ASCE Journal of Structural Engineering, Submitted.

5.2 Summary of the Experimental Program and Test Results

The experimental program involved shake table testing of six third-scale RM shear walls. Scaling followed the laws of dynamic similitude (Harris and Sabnis 1999) and the RM shear walls were selected to represent different design parameters in low-rise buildings satisfying the *RM Conventional Construction*

category based on the Canadian masonry design code (CSA S304.1, 2004) and the NBCC (NRCC 2010).

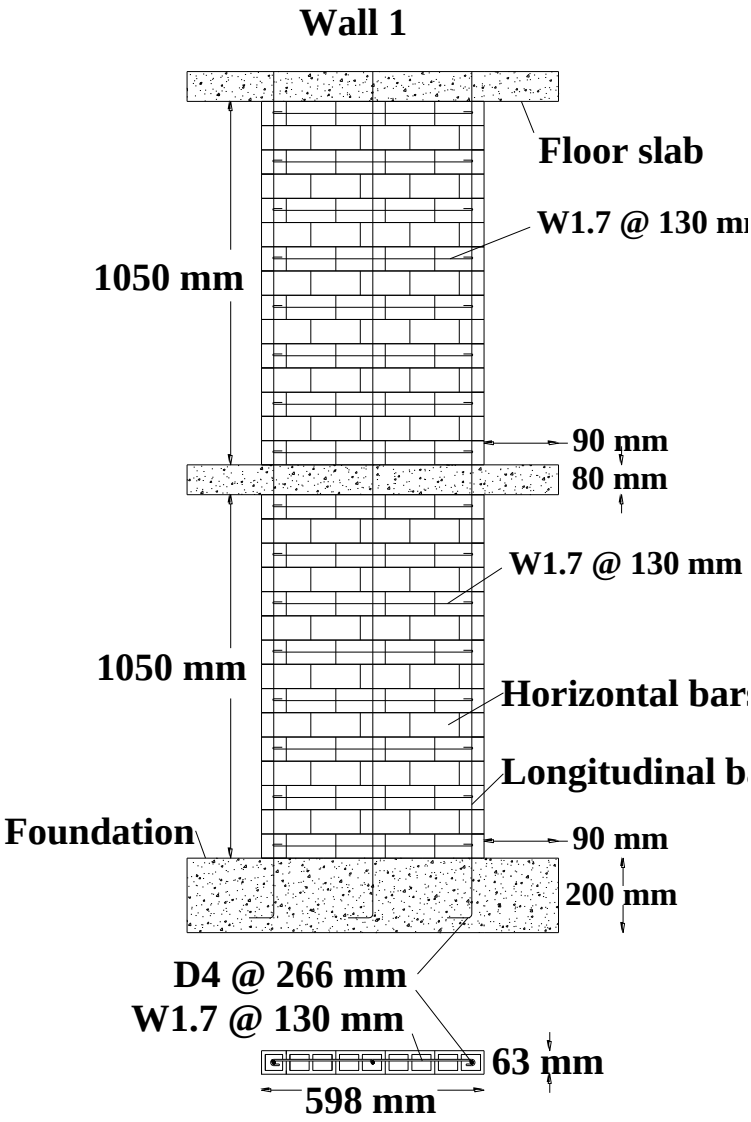

Figure 5.1: Elevation and cross section of the experimental third-scale model of Wall 1

The design details of the reduced- and full-scale walls are presented in Table 5.1. Figure 5.1 shows the elevation of the one of the tested walls (Wall 1)

together with its cross section and reinforcement details in plan. The walls were tested on a shake table with an external mass supporting system that carries the majority of the inertial mass. This approach was adopted to enhance the shake table performance and to facilitate decoupling the gravity loads and the inertial masses. Such situation typically arises in low-rise construction where gravity-loaded RC or steel columns would carry a significant portion of the gravity loads, while RM walls are required to carry the majority of the lateral inertial masses which are not consistent with the gravitational loads. The required additional axial load was applied at the top of the walls by post-tensioned threaded rods built in series with a soft spring to reduce axial load fluctuations. The out-of-plane movements of the walls were restrained using a lateral support system (Mojiri et al. 2013-a).

The Loma Prieta 1989 earthquake record used for the shake table tests was scaled to four different intensity levels, L0, L1, L2, and L3, covering a wide range of seismic hazard levels specified for high seismic zones across Canada (NRCC 2010). The Peak Ground Acceleration (PGA) of L0, L1, L2, and L3 intensity levels were 0.19g, 0.24g, 0.61g, and 0.84g, respectively. The original full-scale record was obtained from PEER NGA strong motion database (PEER NGA Database 2011) and the third-scale model record was generated based on dynamic similitude requirements (Harris and Sabnis 1999).

Table 5.1: Details of the full scale and reduced-scale walls and experimental evaluation of the parameters used in the analytical models

Wall	1	2	3	4	5	6
Details of the full scale and reduced-scale walls						
Number of Stories	2		1	2		
Story Height P/M[1](mm)	3,390 / 1,130					
Length P/M (mm)	1,600 / 598			2,600/865	1,600 / 598	
Aspect ratio	3.68		1.84	2.54	3.68	
Ver. Reinf. P/M	3M15 / 3- D4*	2M15 / 2-D4	3M15 / 3-D4		2M25 / 2-D7**	3M15 / 3-D4
ρ_v P/M (%)	0.18/0.20	0.12/0.13	0.18/0.20	0.12/0.14	0.29/0.24	0.18/0.20
S_v P/M (mm)	798/266	1596/532	798/266	1197/399	1596/532	798/266
Hor. Reinf. P/M (mm)	M10 @ 390 mm / W1.7 @ 130 mm					
Axial stress	0.02 f'_m					0.05 f'_m
Experimental evaluation of the parameters used in the analytical models						
A_{se} (mm^2)	6,246	3,877	22,072	45,136	3,681	3,662
$M_y(kN.m)$	11.25	11.06	11.1	16.6	13.06	10.9
$M_u(kN.m)$	18.21	14.78	18.21	25.79	21.16	21.71
$l_p(mm)$	122	100	122	102	107	225
$\mu_{\varphi,u}$	17	9	17	12	18	8
Added inertial mass, 1st floor (kg)	1,016	1,016	1,080	1,040	1,016	1,016
Added inertial mass, 2nd floor (kg)	1,080	1,080	N.A.	1,103	1,080	1,080
Axial load, 1st floor (kN)	2.93	2.93	15	2.93	2.93	2.93
Axial load, 2ndfloor (kN)	12.07	12.07	N.A.	12.07	12.07	27.07

1-Prototype/Model *D4=26 mm^2 **D7=45 mm^2 N.A.: Not Applicable

The failure modes of the walls were mainly dominated by flexural response in the form of steel yielding followed by crushing of the masonry and subsequent buckling of the vertical bars located at the wall toes. The cracking pattern was primarily horizontal flexure and shear cracks along the wall/base interface and vertical cracks in the wall toes. Initiation of yielding in Walls 1, 2, and 5 occurred at the L0 level while Walls 3, 4, and 6 started to yield at the L3, L2, and L1 level tests, respectively. Both vertical end bars failed subsequently after buckling in Walls 1, 2, 4, and 6 at either the L2 or L3 level tests. However, in Wall 5 only one of the vertical bars failed at the L3 level and none of the vertical bars of Wall 3 failed during the tests. All two-story walls exhibited extensive base sliding and rocking after failure of their end vertical bars but maintained their overall integrity even after the L3 level tests. Wall 3 did not experience significant damage during the tests since the seismic demand on this wall during all tests was significantly less than the other two-story walls. Other walls, however, experienced extensive damage that was predominantly localized within the first and second courses at the wall toe regions.

Analysis of the test results revealed that flexural deformations dominated the lateral deformation for all of the walls contributing to more than 65% of the total lateral deformations in most walls at both the yield and ultimate moment. Base sliding had the minimum contribution of the lateral deformations causing less than 10% of the lateral deformations of the first story in most of the walls at both yield and ultimate moment. The extent of the plastic hinge zone was up to

62% of the wall length from the base of the walls. The energy investigations also revealed that up to 74% of the energy dissipation in the walls occurred in the first story and was mainly concentrated at the base of the wall in the plastic hinge zone. Complete details of the experimental results and their analyses can be found elsewhere (Mojiri et al. 2013-a, and 2013-b).

5.3 Analytical Model

5.3.1 Model Development

As the response of the walls was dominated by flexural behaviour, each story of the walls is modeled with a two dimensional one-component Giberson beam element (Giberson 1969). In this lumped plasticity model, linear elastic behaviour is considered throughout the element and the nonlinear inelastic behaviour is concentrated at the element ends, in the plastic hinge region, (Paulay and Priestley 1992). For this study, both flexural and shear deformations are considered to be linear elastic throughout the elements. As sliding deformations were only a minor contribution to the overall response of most of the walls they were not considered in the model.

Several bi-linear and tri-linear hysteretic models are proposed in the literature for modeling the nonlinear hysteretic behaviour of RC and RM elements (Fukada 1969, Takeda et al. 1970, and Otani 1974). In this study, the nonlinear moment-curvature hysteretic behaviour of the elements within the plastic hinge

zone is modeled using the *Fukada* tri-linear degrading stiffness model (Fukada 1969).

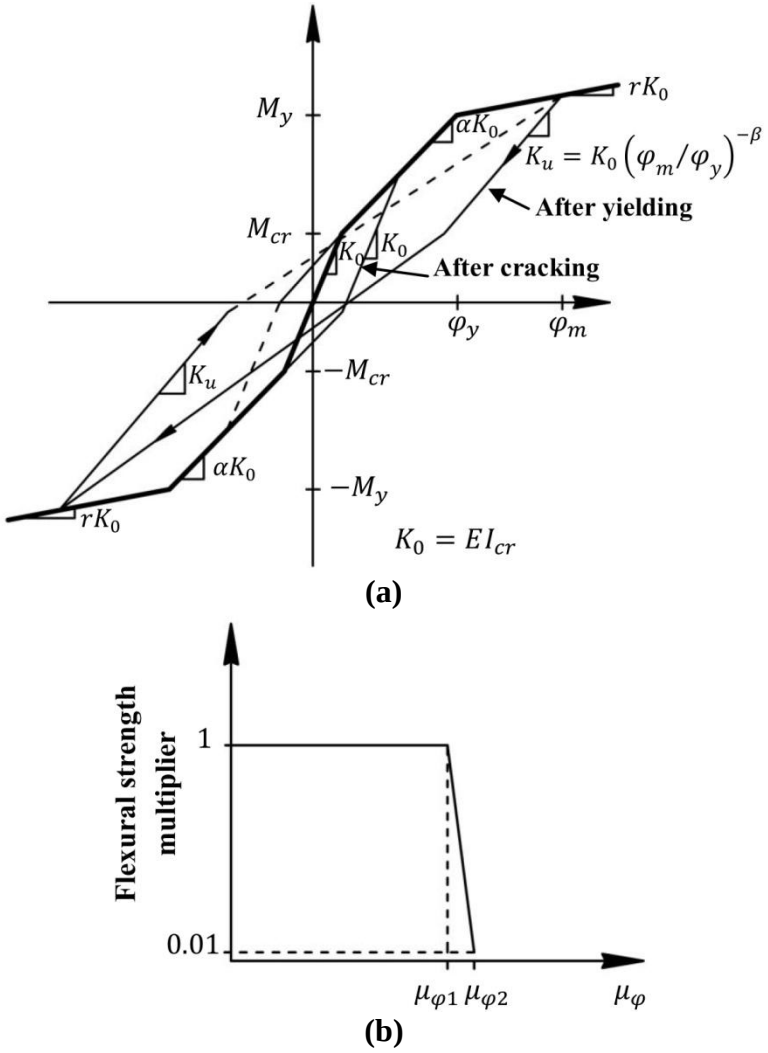

Figure 5.2: Stiffness and strength degradation models. **a)** Fukada flexural hysteresis model with stiffness degradation, **b)** Flexural strength degradation model

In this model the unloading and reloading stiffness values are significantly lower than the initial elastic stiffness. As indicated in Fig. 5.2-a, the nonlinear

moment-curvature behaviour is simulated using a tri-linear model. The first segment simulates the essentially elastic response and is designated as the model up to the cracking moment (M_{cr})), It is followed by second segment up to a level that is designated as the yield moment (M_y), after which is the last segment that simulates the post-yield behavior. In this model, the flexural stiffness of the first segment is considered as $K_0 = EI_{cr}$ and the flexural stiffness of the second and third segments are represented by αK_0 and rK_0, respectively. As indicated in Fig. 5.2-a, the post-yield unloading stiffness is a function of the curvature ductility and in subsequent cycles the model reloads to the maximum moment-curvature point in the previous cycle.

As mentioned in the previous section, the experimental results confirmed that the tested shear walls failed in flexural mode. Based on this, a flexural strength degradation model was used to model their flexural failure. In this model, the flexural strength of the walls at the base drops to 1% of the ultimate capacity when the maximum curvature ductility capacity is reached as shown in Fig. 5.2-b. Damping in the system is modeled following a Rayleigh damping model for each degree of freedom. A portion of the seismic energy in the experimental test system was dissipated through coulomb friction forces that developed in the linear bearings of the external mass supporting system. To simulate this horizontal nonlinear springs with elastic-perfect plastic hysteretic behaviour are introduced in the model. One end of each of these springs is connected to the wall at each floor level and the other end is fixed to the ground at the same height level.

Each story of the walls was modeled by a beam element with a length equal to the story height (1,100 mm). Table 5.1 shows the values of applied compressive axial load and inertial mass at each floor level used in the analytical models. The inertial mass at each floor level was computed from the mass of the RC floor slabs, loading beams, a portion of the out-of-plane supporting system supported by the walls, mass trolleys, and external added mass (steel plates) (Mojiri et al. 2013-a). The rest of the inertial mass was included in the model based on the unit mass of the masonry ($\rho = 2{,}040$ kg/m^3) measured in the laboratory and was also lumped at the floor levels within the model. The axial load consisted of the weight of the walls, part of the loading, beams the out-of-plane supporting system, and the axial loading system supported by the walls, and the axial load applied by the post-tensioned threaded rods at the top of the walls.

5.3.2 Model Parameters Evaluation

The elastic properties of the beam elements that required calibration were the Young's and shear modulus of the element material (E_s and G), gross area (A_g) and effective shear area (A_{se}) of the element cross section, as well as the moment of inertia of the element cross sections (I). The Young's and shear moduli of the element material were calculated based on the results of the compression tests on masonry prisms in the laboratory and utilizing a Poisson ratio (ν) of 0.2 (Drysdale and Hamid 2005). The resulting Young's and shear

moduli values used in the analytical model were 10.25 GPa and 4.27 GPa, respectively. The gross area of each wall was computed by multiplying the length and thickness of each wall. The effective shear area of a cantilever beam can be obtained from the following equation:

$$A_{se} = \frac{V_b h}{G \Delta_s} \quad (5.1)$$

where V_b is the base shear, h is the height of the wall, and Δ_s is the lateral shear deformation at the top of the wall (corresponding to a height h). The effective shear areas of the tested walls at the yield level, defined as the first yielding of the outermost vertical reinforcement bar were used in the analytical models. Such values were obtained by applying Eq. 5.1 to the first story of the walls and by substituting h and Δ_s parameters in Eq. 5.1 by the corresponding height and lateral shear deformations of the first story of each wall. The values of the experimental effective shear area of the tested shear walls at the yield level used in the analytical models are presented in Table 5.1. The results of the static pull-back tests performed on the walls prior to and after each shake table test (Mojiri et al. 2013-b) were used to quantify the initial elastic moment of inertia of the walls. For this purpose the following equation was employed:

$$EI = \frac{Ph^3}{3\Delta} \quad (5.2)$$

which is the relationship between the elastic flexural stiffness (EI), top lateral force (P), and top lateral elastic deformation (Δ) for an elastic cantilever wall. The resulting initial elastic moment of inertia of the walls prior to each test level are presented in Table 5.2.

Table 5.2: Experimental evaluations of the Fukada hysteresis model parameters for each earthquake level used in the analytical models of the walls

Wall	**1**	**2**	**3**	**4**	**5**	**6**
L0 level						
$\boldsymbol{I_{cr}(mm^4) \times 10^8}$	6.012	4.975	6.757	11.51	6.767	2.289
$\boldsymbol{\alpha}$	0.198	0.129	0.116	0.119	0.143	0.242
$\boldsymbol{r}$	0.01	0.008	0.01	0.009	0.01	0.047
L1 level						
$\boldsymbol{I_{cr}(mm^4) \times 10^8}$	3.765	2.891	4.07	12.022	3.654	2.155
$\boldsymbol{\alpha}$	0.336	0.233	0.2	0.113	0.282	0.259
$\boldsymbol{r}$	0.016	0.013	0.016	0.009	0.018	0.05
L2 level						
$\boldsymbol{I_{cr}(mm^4) \times 10^8}$	1.919	1.673	5.137	12.003	2.868	2.203
$\boldsymbol{\alpha}$	0.787	0.44	0.155	0.114	0.374	0.253
$\boldsymbol{r}$	0.032	0.023	0.013	0.009	0.023	0.049
L3 level						
$\boldsymbol{I_{cr}(mm^4) \times 10^8}$	N.A.	N.A.	3.996	3.076	2.868	1.31
$\boldsymbol{\alpha}$	N.A.	N.A.	0.204	0.53	0.374	0.465
$\boldsymbol{r}$	N.A.	N.A.	0.016	0.035	0.023	0.082

N.A.: Not applicable

5.3.3 Model Calibration

The NRHA was implemented using the Ruaumoko software (Carr 2004) with *P-Delta* effects. The properties of the plastic hinge at the base of the walls in

the models, including the equivalent plastic hinge length and the parameters of the Fukada hysteresis model, were calibrated using the experimental results. The corresponding values are presented in Tables 5.1 and 5.2. To extract these values, the yield level was considered as the first yielding of the outermost vertical reinforcement bar in the walls. The values of the plastic hinge length were evaluated at a top drift ratio of 1%. To calibrate the Fukada hysteresis model, the values of the experimental initial elastic moment of inertia obtained prior to each test level were used as the initial elastic stiffness (K_0) of the wall model for the NRHA at the same test level. For consistency, the cracking moment, or the moment at which the first kink in the tri-axial moment-curvature relationship occurs, was considered as one-third of the yield moment for each wall. It should be noted that the values of equivalent plastic hinge length and ultimate flexural strength of Wall 1 were used for Wall 3 as this wall did not reach 1% top drift ratio and its ultimate flexural capacity during the shake table tests. The Fukada stiffness parameters are not presented for Wall 1 and Wall 2 for L3 level as these walls failed during the L2 level test. The value of β in the Fukada hysteresis model was also taken as 0.5 for all of the walls, which is considered to be an appropriate value for RC and RM shear walls (Carr 2004).

The curvature ductility attained at the base of the walls at the maximum load ($\mu_{\phi,u}$) during the shake table tests was used as the wall model curvature ductility capacity (see Fig. 5.2-b). The strength degradation should occur gradually in order to avoid numerical instability issues in the numerical model. As

such, it was assumed that the flexural capacity at the base of the walls starts to degrades linearly with curvature ductility at $\mu_{\phi,u}$ ($\mu_{\phi 1} = \mu_{\phi,u}$) and reaches 1% of the flexural strength of the walls at a curvature ductility equal to $\mu_{\phi,u} + 1$ ($\mu_{\phi 2} = \mu_{\phi,u} + 1$). This is considered to be a conservative approach as RM walls have a lower rate of strength degradation after exceeding their ultimate capacities (Shedid et al. 2010-a and -b). However, this approach was employed solely to identify the initiation of the flexural failure of the walls during their response history and was not aimed to model the response of the walls after reaching their ultimate flexural capacity.

5.4 Analysis Results

5.4.1 Wall Dynamic Characteristics

As the values of elastic viscous damping ratio (ξ_{el}) of the walls were not measured experimentally, the NRHA was performed for a range of different values of elastic viscous damping ratio at each mode of vibration for the wall models in order to quantify representative values. This study revealed that a 1% elastic viscous damping ratio for each mode of vibration for all walls resulted in good agreement between predicted and measured response values. This value is much lower than the 5-7% range of elastic viscous damping ratios, which is typically prescribed for RM and RC shear walls (Chopra 2001, Priestley et al. 2007).

The values of undamped experimentally measured and analytically predicted initial elastic period (T_i) of the walls are presented in Fig. 5.3. The experimental values were obtained by performing static pull-back tests prior to the shake table tests. The values in Fig. 5.3 show that the analytical model yields periods that are generally in good agreement with experimental values. The errors are within the range of 1-5% for Walls 2, 3, 4, and 5 while it is 12% for Wall 1 and 24% for Wall 6. The higher level of error for Wall 6 can be attributed to the slight damage that occurred to this wall prior to the shake table test due to a minor accidental out-of-plane loading on the wall, which might have affected its in-plane response.

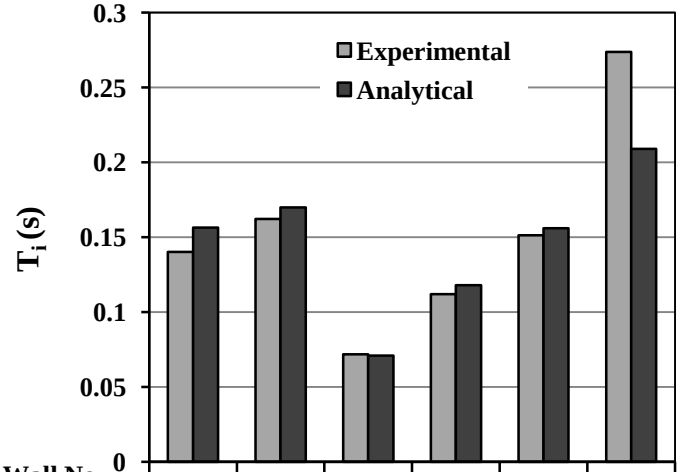

Wall No.	1	2	3	4	5	6
Experimental	0.14	0.16	0.07	0.11	0.15	0.27
Analytical	0.16	0.17	0.07	0.12	0.16	0.21

Figure 5.3: Experimental and analytical evaluation of initial period of the walls

5.4.2 Response Histories and Hysteretic Relationships

Experimental and analytical base moment-curvature hysteretic relationships of the walls are shown in Fig. 5.4. The results are shown up to the peak response of the walls. The curves show that generally, except for Walls 3 and 6, there is a good match between the hysteresis models employed and the actual wall responses and that the models were able to capture the general trend of the hysteresis behaviour of the walls. The deviations for Walls 3 and 6 can be attributed to the inherent errors in measurement of very small deflections of Wall 3 and to the damage incurred into Wall 6 prior to its testing.

Experimental and analytical response histories of top floor relative displacement and base shear of the walls during the L2 earthquake levels are shown in Figs. 5.5 and 5.6. Note that in the cases where the analytical results indicate failure of the walls (deterioration of flexural strength), the analytical results are not shown since the flexural strength degradation model was not calibrated for the response of the walls after reaching their ultimate flexural capacity. From Figs. 5.5 and 5.6, it is observed that, in all cases, the model was capable of capturing the response variation trends for both the displacement and base shear. However, some variations are observed in the response histories of the top relative displacement after reaching the peak values, which are mainly attributed to the approximations inherent in the hysteresis model used in the plastic hinge region.

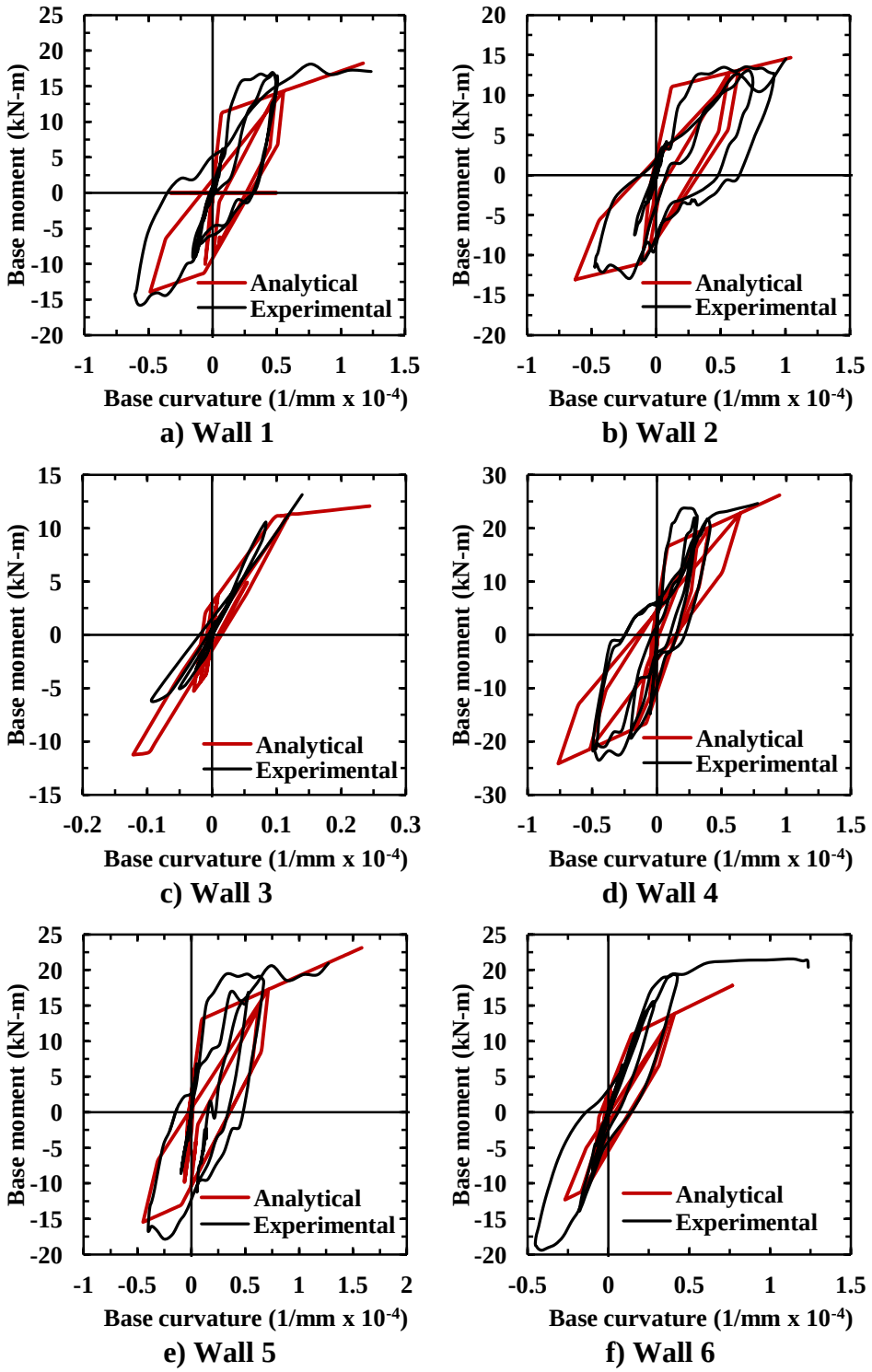

Figure 5.4: Experimental and analytical base moment - curvature hysteresis of walls during L2 earthquake (L3 earthquake for Wall 3)

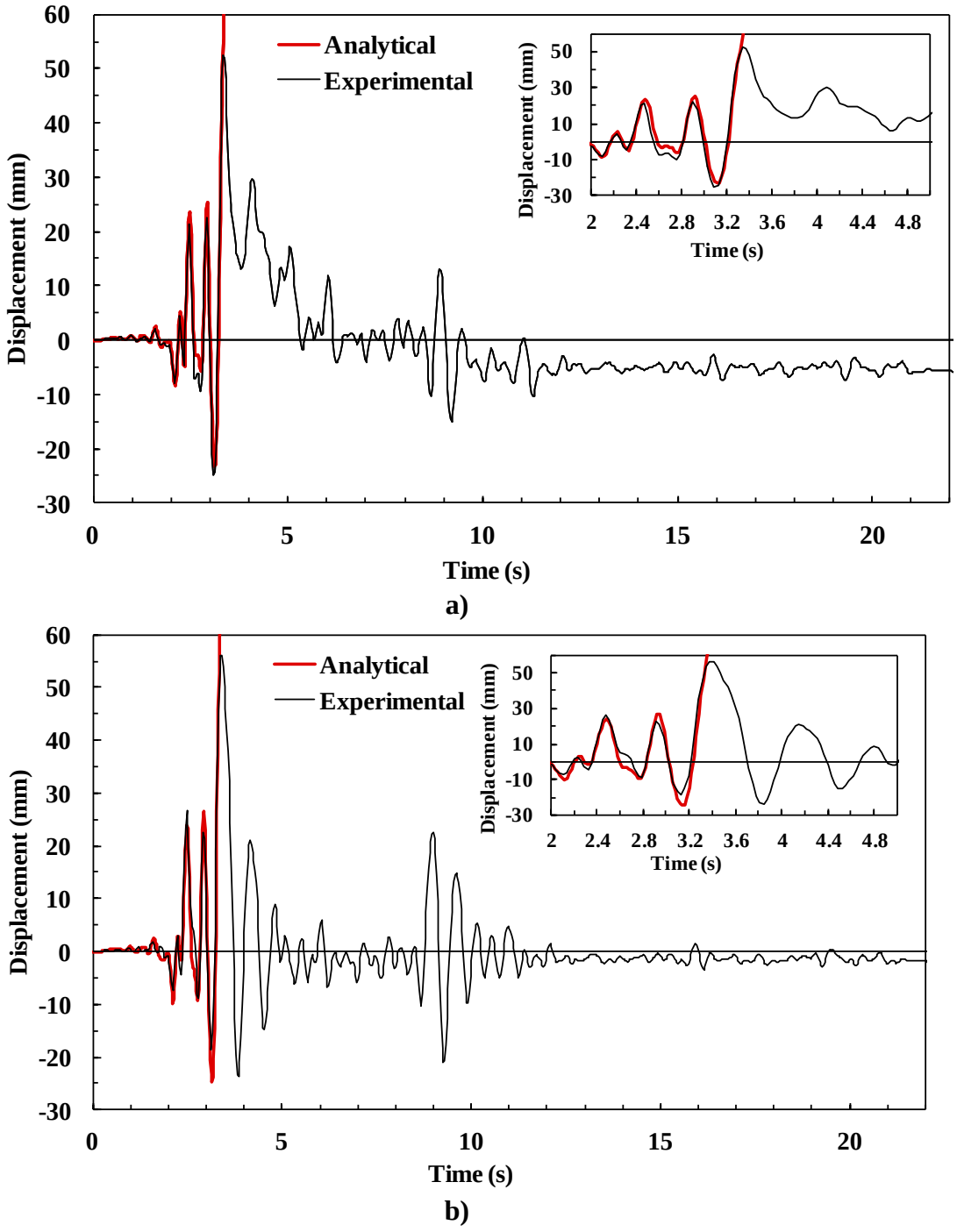

Figure 5.5: Experimental and analytical response histories of top floor relative displacement of walls during L2 earthquake. **a)** Wall 1, **b)** Wall 2

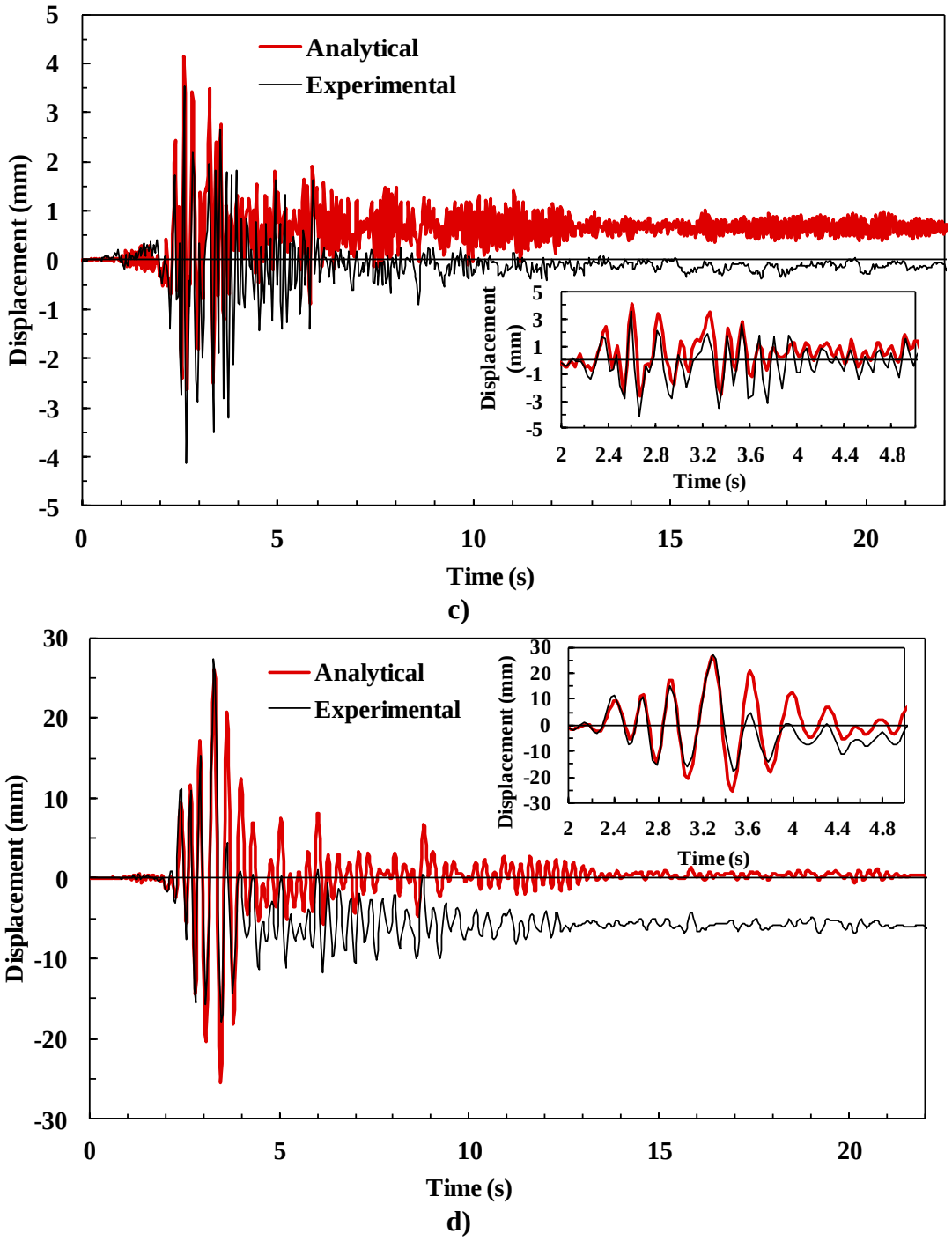

Figure 5.5 (cntd): Experimental and analytical response histories of top floor relative displacement of walls during L2 earthquake. **c)** Wall 3, **d)** Wall 4

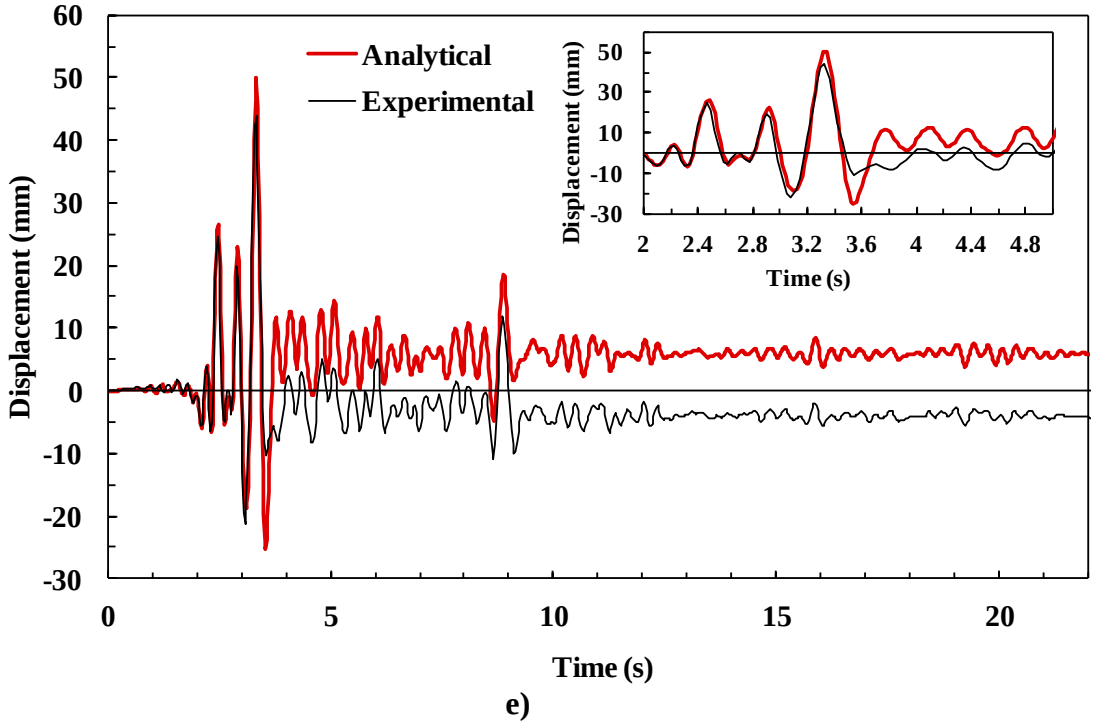

e)

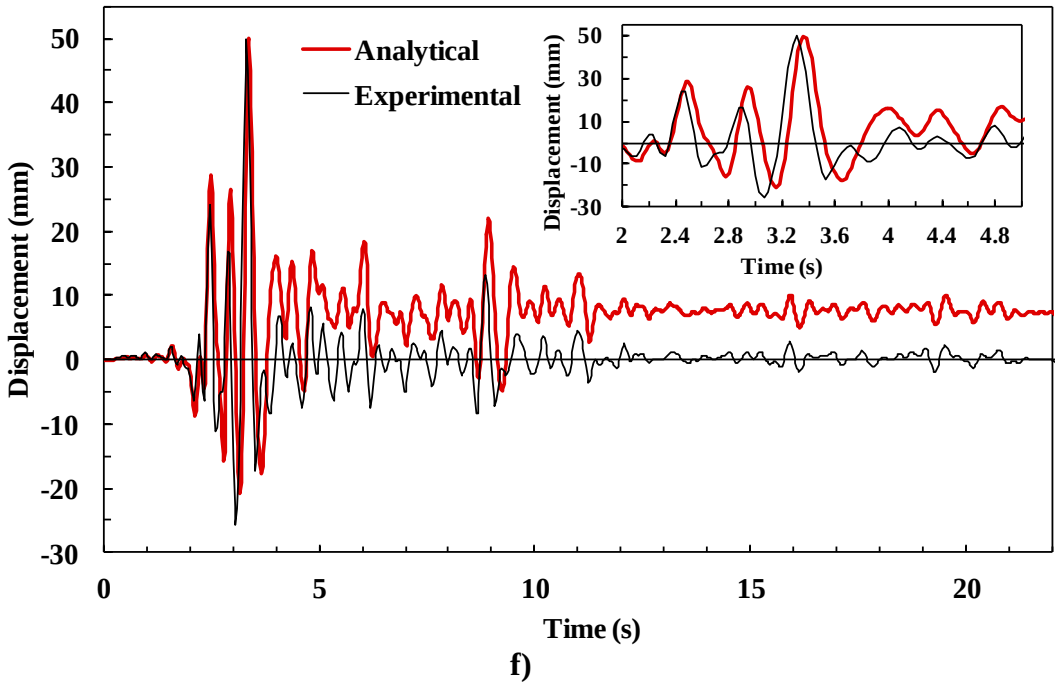

f)

Figure 5.5 (cntd): Experimental and analytical response histories of top floor relative displacement of walls during L2 earthquake. **e)** Wall 5, **f)** Wall 6

It is also observed that the model predicts failure for Walls 1 and 2 during the L2 level earthquake which is consistent with the experimental observations.

Table 5.3 shows the record level and time at which yield and failure were measured and predicted. As can be observed from the results in Table 5.3, the model was capable of predicting the earthquake level and time reasonably well relative to the experimental results for most of the walls. However, for Walls 2 and 5, the model predicts yielding at higher earthquake levels than what was observed experimentally and fails to predict the failure of Wall 6. Nevertheless, for these walls the model was still capable of predicting seismic demands close to the yield and failure capacity and at the correct yielding and failure record levels.

Table 5.3: Experimental and analytical evaluations of record level and time for yielding and failure of the walls

Wall	**1**	**2**	**3**	**4**	**5**	**6**
Time (s)						
Yield (E)	2.63	2.77	2.57	2.32	2.85	2.41
Yield (A)	2.86	2.42	2.36	2.34	2.4	2.41
Failure (E)	3.32	3.32	N.R.	2.433	3.31	3.32
Failure (A)	3.31	3.33	N.R.	2.44	3.32	N.F.
Level						
Yield (E)	L0	L0	L3	L2	L0	L1
Yield (A)	L0	L1	L3	L2	L1	L1
Failure (E)	L2	L2	N.R.	L3	L3	L3
Failure (A)	L2	L2	N.R.	L3	L3	N.R.

N.R.: Not reached, E: Experimental, A: Analytical

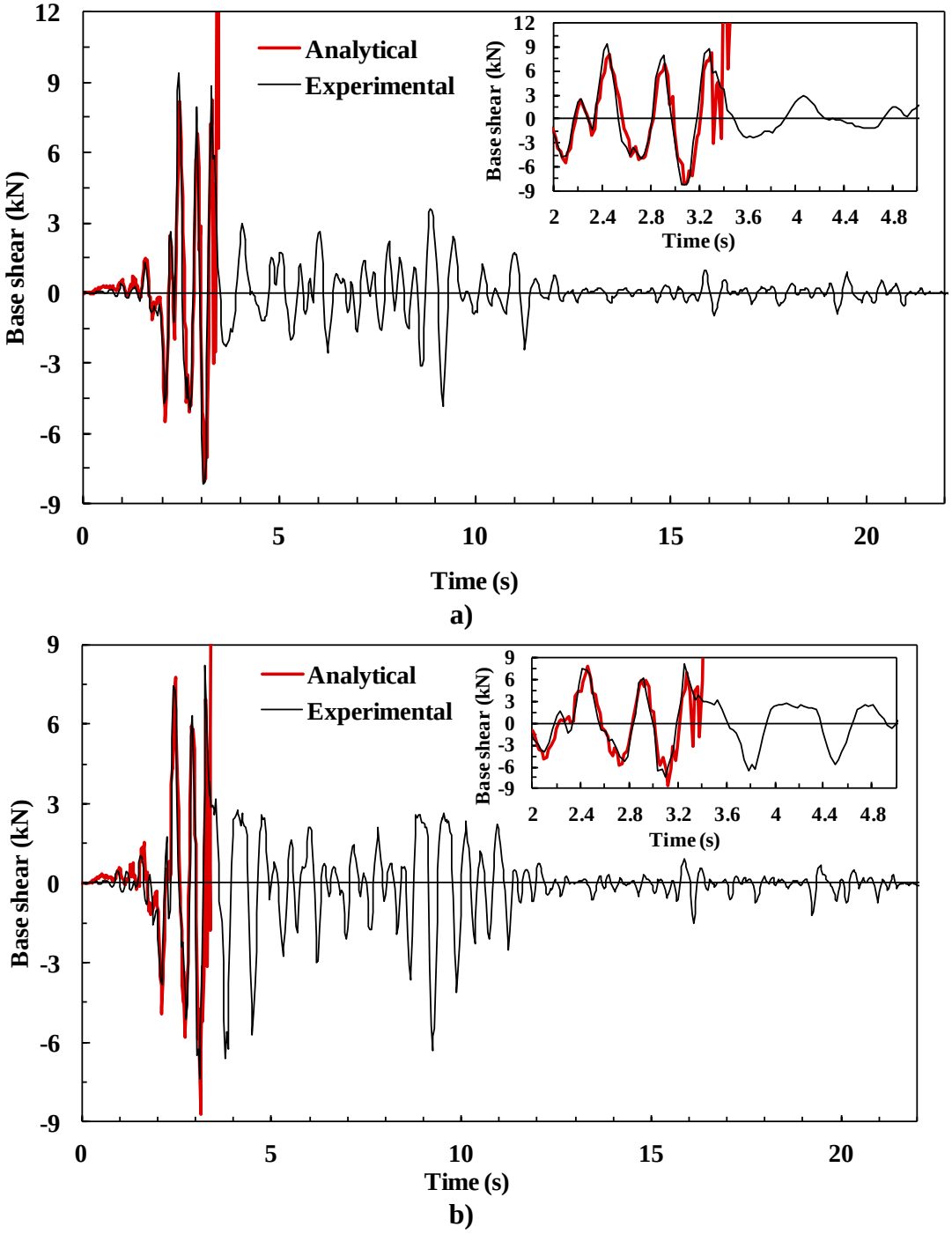

Figure 5.6: Experimental and analytical response histories of base shear of walls during L2 earthquake. **a)** Wall 1, **b)** Wall 2

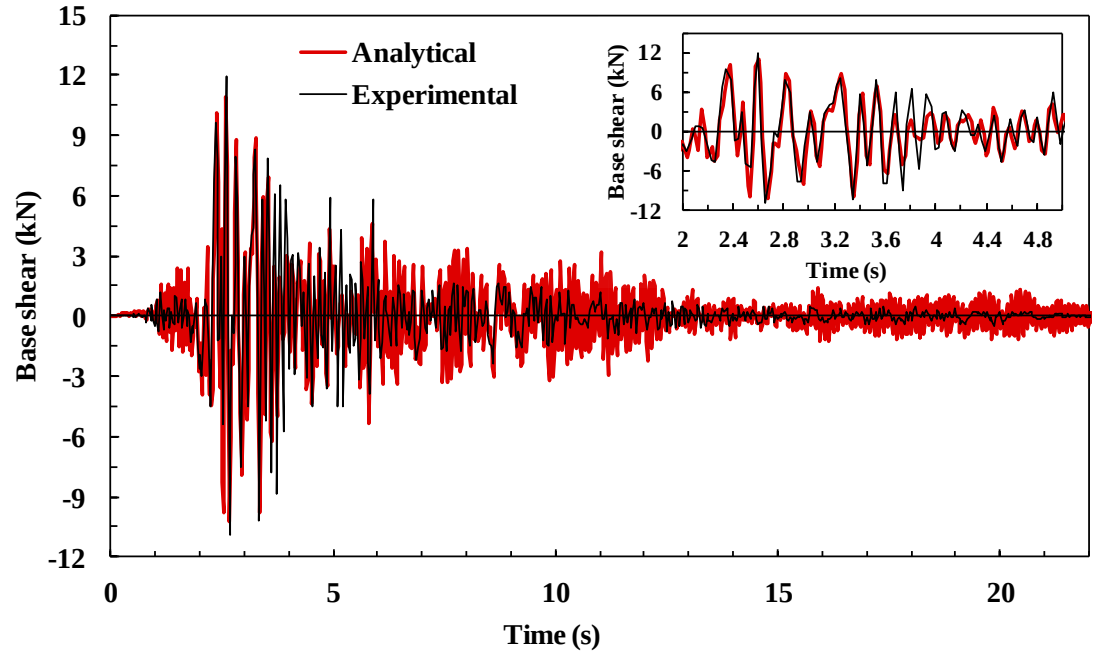

c)

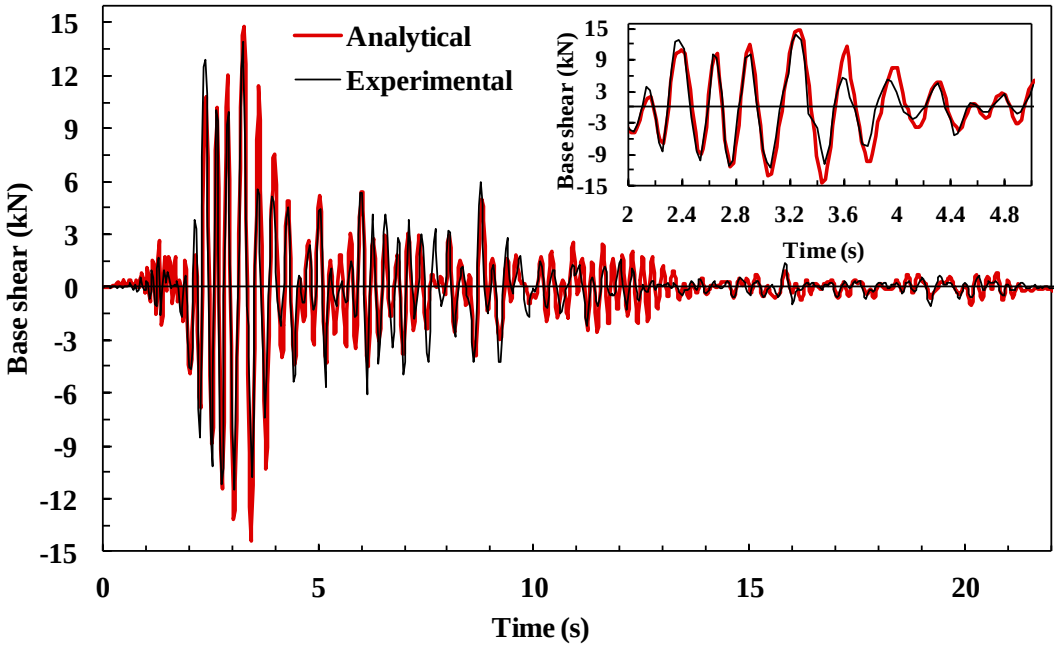

d)

Figure 5.6 (cntd): Experimental and analytical response histories of base shear of walls during L2 earthquake. **c)** Wall 3, **d)** Wall 4

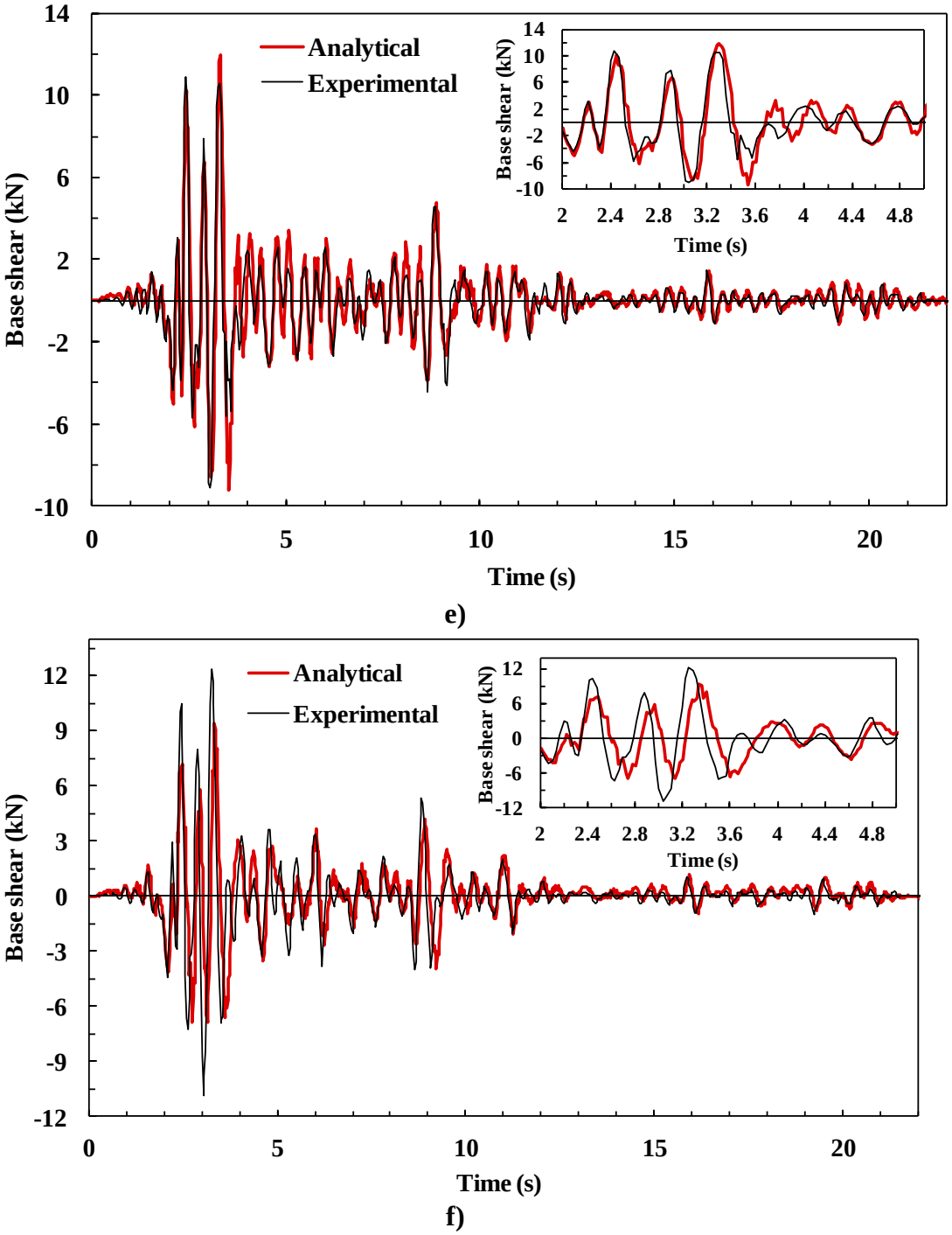

Figure 5.6 (cntd): Experimental and analytical response histories of base shear of walls during L2 earthquake. **e)** Wall 5, **f)** Wall 6

5.4.3 Peak Response Values

Peak experimental and analytical values for base shear, top floor acceleration, and top floor drift ratio of the walls at different record levels are presented in Table 5.4. The results are only presented up to the L3 earthquake, as most of the walls experienced extensive damage by this level. The analytical results of Walls 1 and 2 are not presented for L3 earthquake since these two walls failed during the L2 earthquake. Based on the values of the ratio of the analytical to experimental results presented in Table 5.4, the errors in the analytical evaluations are a maximum of 27%, 24%, and 37% for the base shear, top floor acceleration, and top floor drift ratio, respectively. It should be noted that the relatively small lateral deflections (maximum of 2.4 mm) experienced by Wall 3 at lower excitation levels introduced greater measurement error. The average error for evaluation of the peak values of the base shear, top floor displacement, and top floor acceleration (excluding the drift ratios of Wall 3 at L1 and L2 earthquakes) are 14%, 11%, and 9% respectively. The experimental and analytical values of top floor displacement ductility at maximum lateral load are shown in Fig. 5.7. The values of displacement ductility levels are conservatively computed as the ratio of the top floor lateral deflection at the maximum load to the top floor lateral deflection at the yield level. The latter is defined as the onset of the yielding of the wall end vertical bars. This figure shows that the analytical predictions are generally close to the experimental measurements with errors in the range of 4-

6% for Walls 2, 4, and 5 and 15-24% for Walls 1, 3, and 6, with an average of 12% for all walls.

Table 5.4: Experimental and analytical evaluations of peak values base shear, top floor acceleration, and top floor drift ratio of the walls at different record levels

Wall	1	2	3	4	5	6
L1						
$V_{max,E}(kN)$	8.40	7.11	3.70	8.51	10.05	7.94
$V_{max,A}/V_{max,E}$	0.89	0.96	1.14	0.75	0.81	0.86
$a_{max,E}\ (g)$	0.54	0.45	0.31	0.47	0.61	0.48
$a_{max,A}/a_{max,E}$	0.86	1.05	1.21	0.76	0.88	1.00
$D_{max,E}(\%)$	0.6	0.5	0.1	0.1	0.6	0.6
$D_{max,A}/D_{max,E}$	0.70	0.96	1.19	0.86	0.81	1.20
L2						
$V_{max,E}(kN)$	10.53	8.58	10.57	14.26	13.90	12.27
$V_{max,A}/V_{max,E}$	0.86	1.01	0.73	1.04	0.87	0.79
$a_{max,E}\ (g)$	0.62	0.52	0.89	0.84	0.77	0.74
$a_{max,A}/a_{max,E}$	1.07	1.15	0.79	1.04	1.08	0.91
$D_{max,E}(\%)$	2.2	2.1	0.2	1.2	1.9	2.1
$D_{max,A}/D_{max,E}$	0.93	1.01	0.63	0.95	1.14	1.02
L3						
$V_{max,E}(kN)$	F.R.	F.R.	14.17	13.09	13.33	9.82
$V_{max,A}/V_{max,E}$	F.R.	F.R.	0.78	1.22	0.94	1.06
$a_{max,E}\ (g)$	F.R.	F.R.	1.20	0.76	0.82	0.69
$a_{max,A}/a_{max,E}$	F.R.	F.R.	0.84	1.13	1.01	1.07
$D_{max,E}(\%)$	F.R.	F.R.	0.3	1.5	3.1	2.9
$D_{max,A}/D_{max,E}$	F.R.	F.R.	1.09	1.07	0.97	1.01

F.R. : Failure Reached

The variations between the analytical predictions and experimental evaluations are attributed to a number of factors, the most important of which are the simplifications employed in the developed model pertaining to the hysteretic

behaviour of the plastic hinge region. However, the average error in all cases is less than 14%, which is acceptable considering the inherently complex behaviour of RM structures and the simplifications employed in the model development.

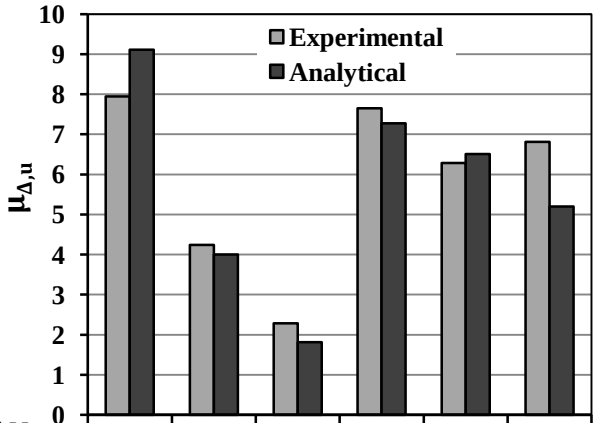

Wall No.	1	2	3	4	5	6
Experimental	7.9	4.2	2.3	7.7	6.3	6.8
Analytical	9.1	4.0	1.8	7.3	6.5	5.2

Figure 5.7: Experimental and analytical values of top floor displacement ductility of walls at maximum lateral load

5.5 Fragility Assessment

Fragility curves show the conditional probability that the seismic demand (D) of a specific Engineering Demand Parameter (EDP) exceeds its capacity (C), corresponding to a specified limit state, when an earthquake with an Intensity Measure (IM) occurs. Assuming that both the demand and capacity follow a lognormal probability distribution (Wen et al. 2003), the above statement can be written in the form of the following equation (Melchers 2001):

$$P[D > C|IM] = \Phi\left[\frac{\ln(S_d/S_c)}{\sqrt{\beta_{d|IM}^2+\beta_c^2}}\right] \quad (5.3)$$

where S_c and β_c are the median and dispersion of the capacity, S_d is the median of the demand which is a function of IM, and $\beta_{d|IM}$ is the dispersion of the demand for a given intensity level defined by IM. In Eq. 5.3, Φ is the standard normal Cumulative Distribution Function (CDF). Fragility analysis requires identifying limit states and quantifying each parameter appearing in Eq. 5.3.

5.5.1 Identifying Limit States

The limit states chosen for fragility analysis can be defined by specifying different levels of a key quantitative EDP. The limit states also need to be associated with certain damage levels with a qualitative and functional interpretation. In the current study, three limit states are considered, namely: LS1, LS2, and LS3. These limit states are quantitatively identified by the level of the moment at the base of the walls and are defined through the top floor lateral deformation of the wall. The limit states are also qualitatively associated with different levels of damages based on the experimental observations from the shake table tests. LS1 is identified by the model cracking moment (M_{cr}) defined in the current study as one-third of the model yield moment and associated with a minor level of damage to the walls mainly in the form of minimal horizontal cracking along the mortar lines affecting surface finishes. LS2 is identified by the

yield moment (M_y) and is associated with a moderate level of damage to the walls mainly in the form of a limited number of cracks in the face shells and horizontal cracks along the mortar lines and at the base of the walls, and hence can be essentially considered a serviceability limit state. LS3 is identified by the ultimate moment capacity (M_u) and is associated with a high level of damage to the walls in the form of severe cracks in the face shells, wide horizontal cracks along the mortar lines and at the base of the walls, and extensive yielding of the reinforcement bars causing permanent deformations of the walls.

5.5.2 Estimation of Wall Capacities

With the limit states are defined, the capacity of the walls, in terms of the means and dispersions assuming lognormal distributions (Wen et al. 2003), should now be evaluated. The capacity can be determined based on expert opinion, from experimental tests, or analytical models as discussed earlier (Nielson 2005). Following the experimental approach, the parameters for a specific class of SFRS can be identified by conducting experiments on different structural components in the same class of the SFRS. In this study, the limit states described above are defined by the top floor lateral deformation of the walls. The capacity of the walls are obtained based on the shake table test results by measuring the top floor drift ratio of each wall when it reached a particular limit state identified by the level of base moment as described above. The results are presented in Table 5.5. The value of mean (S_c) and dispersion (β_{c1}) of the top drift ratio capacity of the walls

computed based on the same experimental measurements are also presented in this table. The result for Wall 6 were not considered as a result of the slight damage that occurred in this wall prior to testing (Mojiri et al. 2013-a), making the results unreliable for wall capacity assessment.

Table 5.5: Computation of the mean and dispersion of the top drift ratio capacity of the walls for different limit states

Limit State	Top Drift Ratio (%)				S_c	β_{c1}	β_c
	Wall 1	Wall 2	Wall 4	Wall 5			
LS1	0.07	0.07	0.03	0.07	0.07	0.44	0.51
LS2	0.23	0.32	0.12	0.29	0.26	0.42	0.49
LS3	1.84	1.48	1.00	0.92	1.24	0.33	0.41

Based on the recommendations of the Applied Technology Council (ATC) for seismic performance assessment of buildings (ATC 2011), since the test data are available for less than five specimens and the specimens were not tested under all configurations possible in an actual two-story lightly-reinforced masonry building, a minimum value of $\beta_u = 0.25$ was added to the dispersion based on the following equation:

$$\beta_c = \sqrt{\beta_{c1}^2 + \beta_u^2} \tag{5.4}$$

where β_{c1} is the dispersion obtained from the test data and β_c is the final dispersion of the limit state capacity used for fragility analysis. The values of β_c computed based on equation 5.4 and computed values of β_{c1} are also presented in

Table 5.5. Based on the values presented in this table, the dispersion of the capacity of the walls takes the maximum value of 0.51 at the LS1 limit state.

5.5.3 Estimation of Seismic Demands

5.5.3.1 Probabilistic Seismic Demand Analysis (PSDA)

The seismic demands was estimated based on a PSDA following the approach suggested by Cornell et al. (2002) to estimate the median and dispersion of the demand corresponding to each IM value (S_d and $\beta_{d|IM}$). Based on this approach, S_d can be estimated from the following equation:

$$S_d = A(IM)^B \tag{5.5}$$

where A and B are regression parameters. In order to obtain the necessary data for performing the regression, the models are tested under a sufficient number of earthquake records covering a range of IM and the maximum demand (D) during each of the simulations is recorded. The regression is then performed on the $D - IM$ data points. For N number of $D - IM$ data points, the dispersion of the demand conditioned to intensity measure ($\beta_{d|IM}$) can be calculated using the square root of the mean squared error (MSE) of the regression following**:**

$$\beta_{d|IM} = \sqrt{\frac{\sum_{i=1}^{N}\left[\ln \mathrm{D_i} - \ln a{IM_i}^b\right]^2}{N-2}} \tag{5.6}$$

$N-2$ in the denominator of this equation is the number of statistical degrees of freedom for computation of the dispersion which is considered as the number of data points (N) minus the number of estimated parameters (Steel and Torrie 1961).

5.5.3.2 Seismic Intensity Measure (IM)

Different parameters can be considered as measures for intensity of ground motion records, with the Peak Ground Acceleration (PGA) and the spectral acceleration at a specific period ($S_a(T)$) being the most commonly used. Using PGA as an IM can result in higher dispersion values due to dependency of the structural response on the frequency content of the ground motions, thus, requiring careful selection of the ground motions compatible with seismotectonics of the region being studied. On the other hand, using $S_a(T)$) as an IM, reduces the dependency of the structural response on the ground motion and hence reduces the dispersion in the seismic demand making it possible to perform PSDA even with a moderate number of ground motion records (Kwon 2007). As such, for this study, the spectral acceleration evaluated at the elastic fundamental period of the walls is chosen as the IM.

5.5.3.3 Ground Motion Record Selection

For this study, a suit of 30 synthetic ground motions produced by Atkinson (2009) is used for PSDA. The ground motions are compatible with the 2010 version of the NBCC (NRCC 2010) uniform hazard spectra having 2% chance of

exceedence in 50 years. As the models for Walls 1, 2, 4, and 5 had different design parameters, varying fundamental periods were used for PSDA, the average 5% damped $S_a(T)$ values over the range of elastic fundamental periods of the models were used as the records IM. The records are grouped in five spectral acceleration bins with increasing intensity.

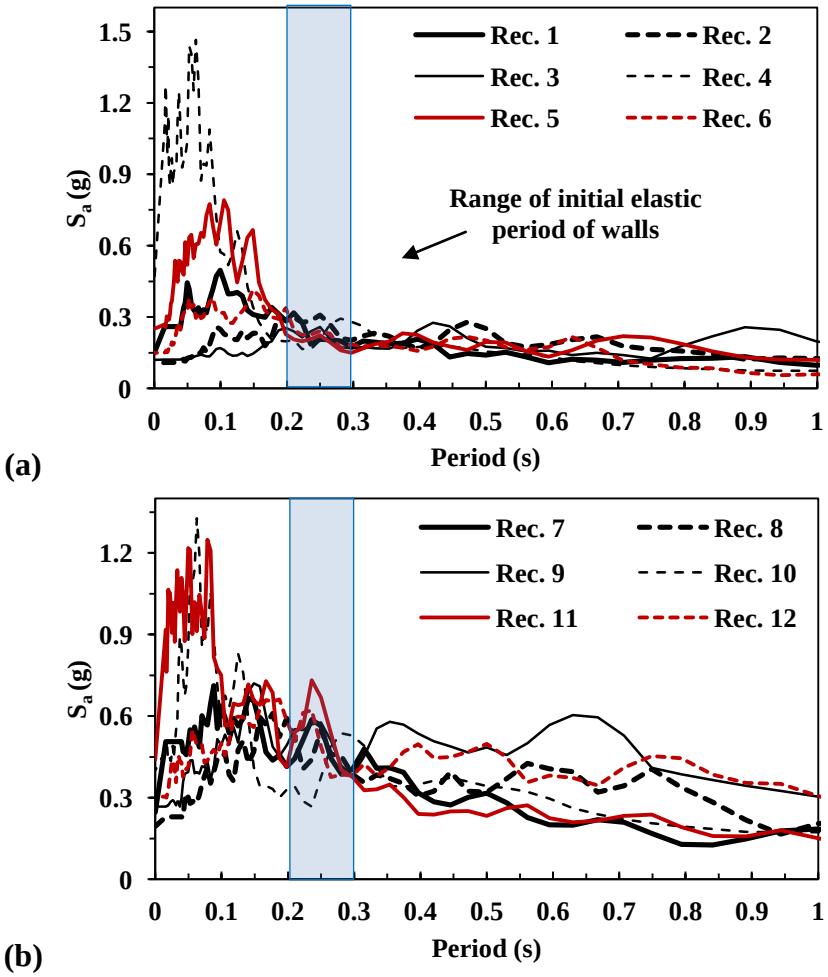

Figure 5.8: The acceleration response spectra of selected simulated ground motions for different ranges of $S_a(T)$: **a)** 0-0.3g, **b)** 0.3-0.6g.

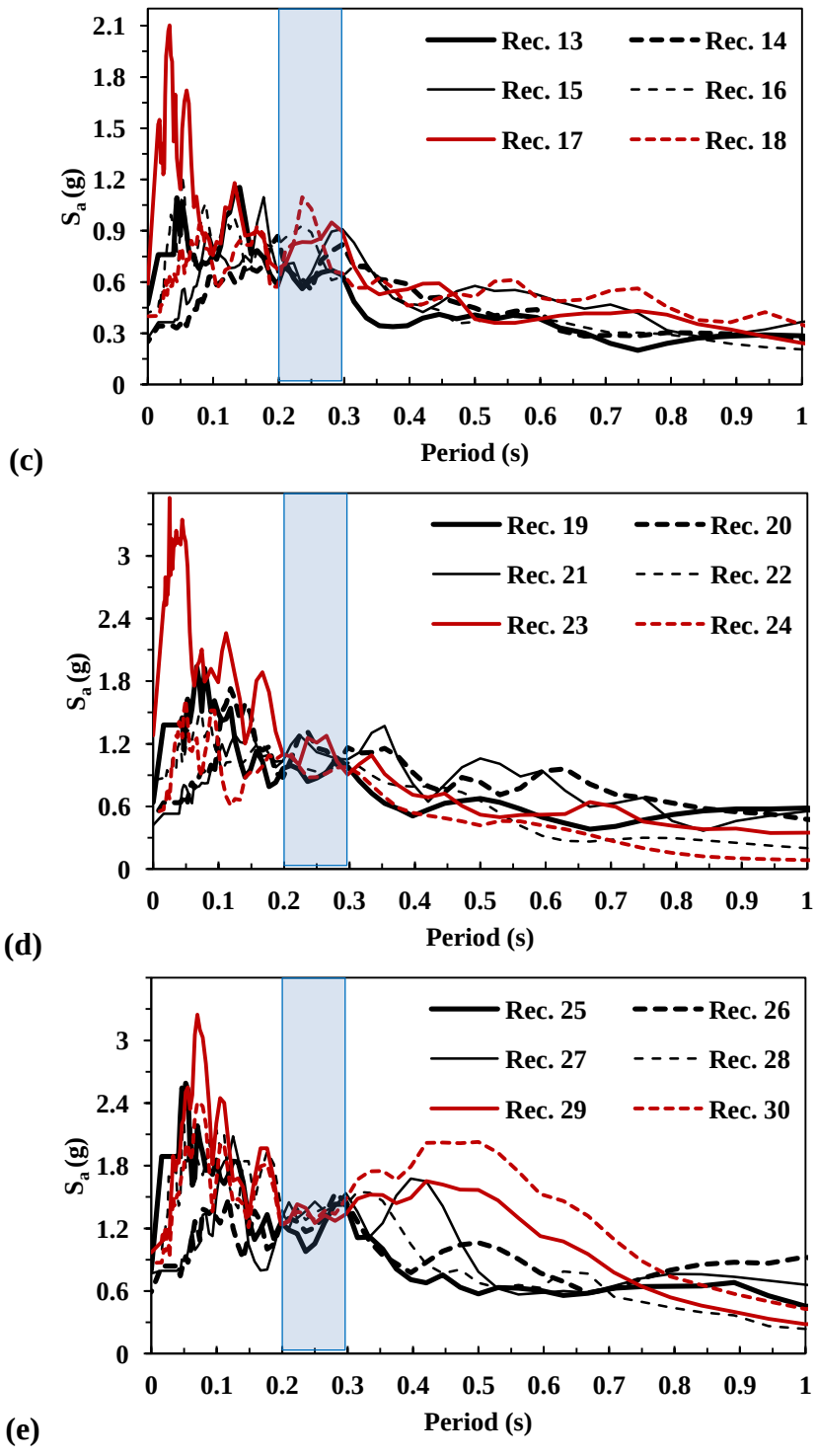

Figure 5.8 (cntd): The acceleration response spectra of selected simulated ground motions for different ranges of $S_a(T)$: **c)** 0.6-0.9g **d)** 0.9-1.2g, **e)** 1.2-1.5g

The records were selected such that representative records from the East and West with varying fault distance, magnitude, and soil conditions were represented in each bin. The characteristics of the ground motions selected for PSDA are presented in Table 5.6. Figure 5.8 shows the acceleration response spectra of the selected ground motions for different ranges of $S_a(T)$. The $S_a(T)$ values of were limited so that the maximum base curvature ductility (see Fig. 5.2-b) would not be exceeded during the simulations.

5.5.3.4 Simulations

In order to generate the PSDA data for the walls in this study, the reduced-scale analytical models of Walls 1, 2, 4, and 5 were subjected to scaled versions of each of the selected ground motions. Each wall model was represented a specific design parameter such as the wall length, the vertical reinforcement ratio, and the vertical reinforcement spacing for the class of two-story lightly-reinforced concrete block masonry shear wall SFRS. The seismic demands on the walls in terms of top drift ratio were obtained by performing NRHA on the developed wall models. It should be noted that the drift ratios are dimensionless and the records were scaled following dynamic similitude requirements (Harris and Sabnis 1999) such that the acceleration values of the full-scale and reduced-scale records were identical. Therefore, the fragility assessment results obtained for reduced-scale wall models are also valid for their full-scale counterparts.

Table 5.6: The ground motion records used for PSDA

S_a (g) Range	Record No.	Record Designation [1]	East/ West	Magnitude	Soil Class	Fault Dist. (km)	PGA (g)	S_a (g)
0-0.3	1	west6a2	West	6.0	A	25.8	0.15	0.23
	2	west7c2	West	7.0	C	50.7	0.10	0.25
	3	west7d2	West	7.0	D	100.4	0.12	0.21
	4	east6a1	East	6.0	A	17.0	0.45	0.25
	5	east6d2	East	6.0	D	26.3	0.25	0.19
	6	east7c2	East	7.0	C	50.3	0.15	0.24
0.3-0.6	7	west6a1	West	6.0	A	14.5	0.25	0.41
	8	west7c1	West	7.0	C	26.3	0.19	0.49
	9	west6d2	West	6.0	D	21.6	0.27	0.46
	10	east6d1	East	6.0	D	17.0	0.40	0.46
	11	east7a1	East	7.0	A	25.6	0.44	0.44
	12	east7e1	East	7.0	E	25.7	0.30	0.45
0.6-0.9	13	west6a1	West	6.0	A	11.1	0.47	0.64
	14	west7c1	West	7.0	C	26.3	0.25	0.80
	15	west6d1	West	6.0	D	13.0	0.27	0.79
	16	east6d1	East	6.0	D	17.0	0.42	0.71
	17	east7a1	East	7.0	A	25.2	0.59	0.83
	18	east7e1	East	7.0	E	25.6	0.40	0.68
0.9-1.2	19	west711	West	7.0	A	12.9	0.64	0.99
	20	west7c1	West	7.0	C	18.1	0.48	1.03
	21	west6d1	West	6.0	D	12.3	0.42	1.06
	22	east6d1	East	6.0	D	16.6	0.85	1.00
	23	east7a1	East	7.0	A	14.0	1.28	1.09
	24	east6c1	East	6.0	C	14.4	0.53	1.00
1.2-1.5	25	west7a1	West	7.0	A	10.2	0.80	1.33
	26	west7c1	West	7.0	C	15.2	0.59	1.38
	27	west6d1	West	6.0	D	10.8	0.77	1.39
	28	east7c1	East	7.0	C	14.9	0.97	1.40
	29	east7c1	East	7.0	C	14.8	0.97	1.29
	30	east7e1	East	7.0	E	14.8	0.87	1.34

1: Refer to Atkinson (2009)

In addition, for typical modular RM buildings built with similar shear walls, the natural period and dynamic characteristics of such RM buildings can be

considered to be similar to each of its RM shear wall components with their tributary inertial mass (Shedid et. al 2010-a) when coupling is ignored. Therefore, the fragility assessment results developed for the RM walls in this study can be considered to be valid for such RM buildings (NIST 2010).

The parameters required for Fukada hysteresis model used in the models of the walls were calibrated based on the experimental evaluations from L0 level earthquakes presented in Table 5.2 representing the walls with no pre-damage state. A total of 120 NRHA runs were performed on the wall models. The resulting $D - IM$ data points are plotted in Fig. 5.9-a. Figure 5.9-b shows the plot of the natural logarithm of the data together with the linear least squares regression results. Based on the regression results shown in Fig. 5.9, the values for parameters A and B in Eq. 5.5 are 0.80 and 1.33, respectively and the corresponding value for $\beta_{d|IM}$ is 0.40.

5.5.3.5 Validation of failure modes

To check for possible non-simulated shear failures of the walls during the simulations, the maximum base shear of the walls were compared to their nominal diagonal and sliding shear strengths computed based on the equations proposed by the Canadian masonry design code CSA-S304.1 (2004) for RM shear walls using the material properties obtained from the laboratory tests ($i.e. \emptyset_m$=$\emptyset_s = 1.0$). The results indicated no shear failure for the walls except for Wall 5 for which the simulations predicted base shear of up to 13% and 33% in excess of the computed

nominal diagonal and sliding shear strengths, respectively, for the records in the last spectral acceleration bin.

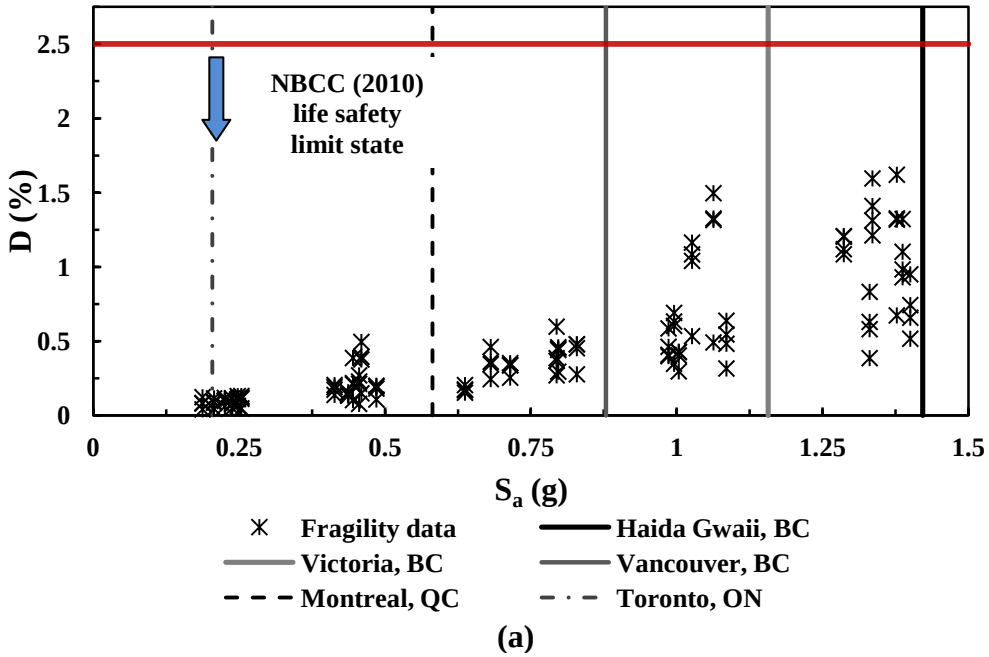

(a)

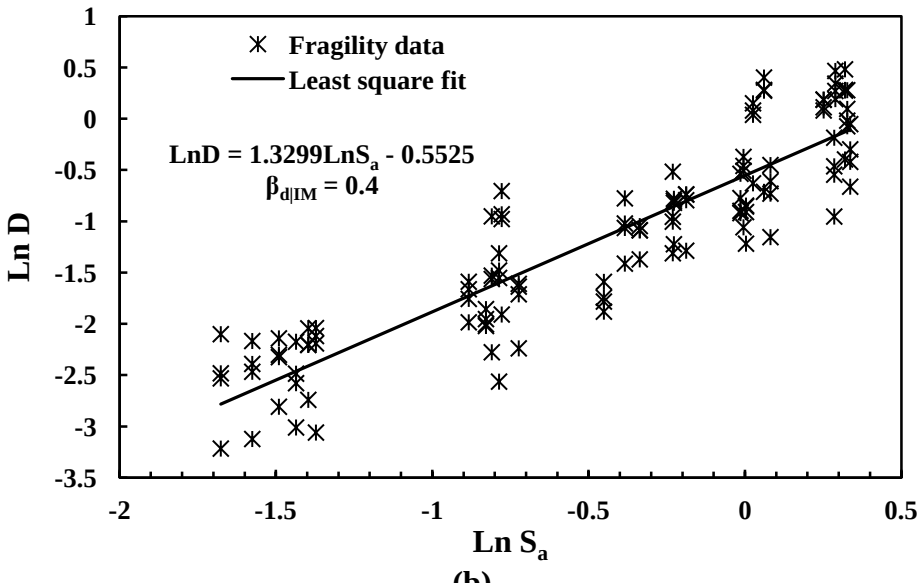

(b)

Figure 5.9: Top floor drift ratio of walls vs. spectral acceleration: **a)** Raw data, **b)** Regression results

However, as discussed earlier, the shake table experimental results did not show any sign of shear failure prior to flexural failure for any of the tested walls including Wall 5. Moreover, the nominal sliding shear strengths of the walls were computed conservatively as the contribution of the end vertical reinforcement bar were not considered following the CSA-S304.1 (2004) specifications. Considering even a minor contribution of the end vertical reinforcement bar for Wall 5 results in sliding shear strength that is significantly higher than the predicted demands. The large degree of conservatism inherent in the current CSA-S304.1 (2004) shear design expression was also observed and confirmed in a recent study (Banting and El-Dakhakhni 2013). Based on this and considering the experimental findings, it can be assumed that no shear failure occurred in Wall 5 prior to flexural failure and therefore, the simulation results can be utilized for PSDA.

5.5.3.6 Derivation of the Fragility Curves

The $D - IM$ data points shown in Fig. 5.9-a show an increase in scatter between the responses of the walls for higher spectral acceleration values. This is attributed to the fact that under higher S_a values, the walls enter their nonlinear behaviour zone resulting in more variations in the dynamic response between walls with different design properties. Another contributing factor is the period

shift in the walls at higher $S_a$values due to damage development, which in turn causes variations in the absorption of ground motion energy amongst walls.

The average design spectral acceleration over the wall periods for some of the cities of Canada with different levels of seismicity as specified by the NBCC (NRCC 2010) are shown in Fig. 5.9. The maximum inter-story drift ratio proposed by the same code for the life safety limit state for buildings with normal application is also indicated on Fig 5.9-a. The results of the PSDA for the tested walls presented in Fig. 5.9-a indicate that for all cases the maximum top floor drift ratios are well below the specified limit defined by the NBCC (NRCC 2010) for life safety indicating the conformance of this RM SFRS category to this critical limit state even for high seismic zones in Canada.

Once all the required parameters of Eq. 5.3 are generated following the above steps, the analytical form of the fragility curve for each limit state can be obtained based on Eq. 5.3. Figure 5.10 shows the fragility curves for different limit states considered in this study. The fragility curves in Fig. 5.10 show that for the city of Toronto, which is considered to be a location of low seismicity in Canada, there is 48% chance that the walls exceed the LS1 limit state causing minor damage, which would affect surface finishes. Furthermore, there is negligible chance of exceeding the LS3 limit state, which would indicate wall reaching their maximum flexural capacity resulting in major wall damage. The fragility curves also indicate that even for the cities of Vancouver and Victoria and for the islands of Haida Gwaii, which are high seismicity regions in Canada,

there is only 5%, 16%, and 30% chances, respectively, that the walls exceed LS3 limit state, resulting in a high level of damage that would require extensive wall repair. The above observations clearly indicate that the lightly reinforced masonry shear walls considered in this study show acceptable seismic performance in terms of their lateral deformation even at some of the highest seismic zones in Canada. This result should be considered along with the fact that the design of the walls studied qualifies them for only the *conventional construction* SFSR category, which is limited to low seismic zones, based on the current provisions of the CSA S304.1 (2004) and the NBCC (NRCC 2010).

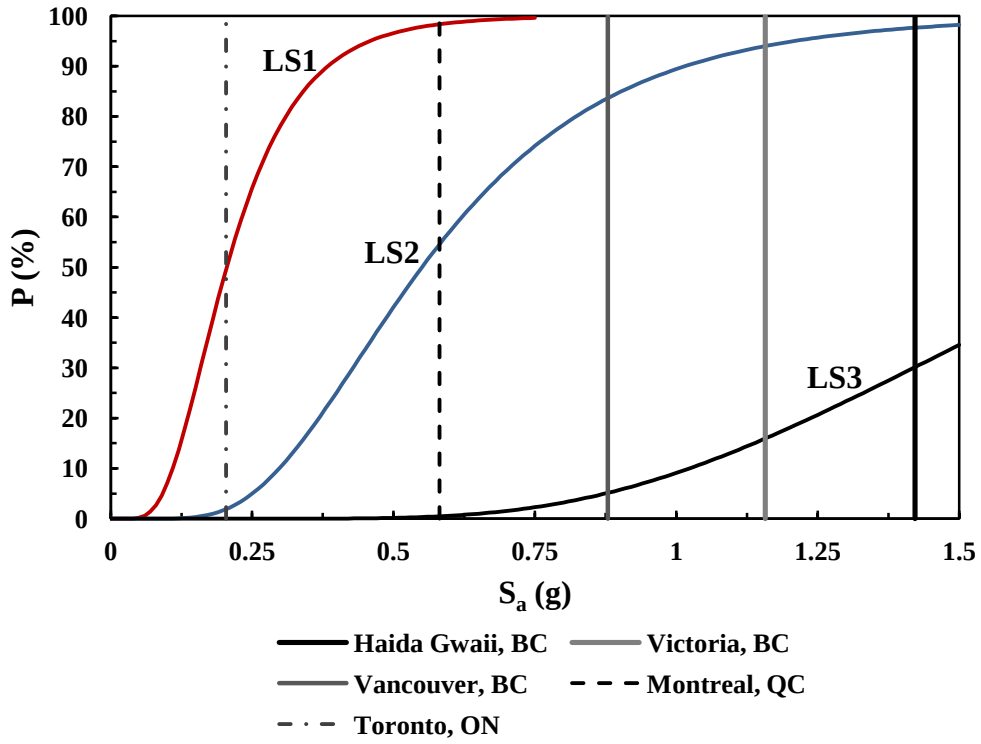

Figure 5.10: Fragility curves of walls for different limit states.

5.6 Conclusions

This study presented the analytical modeling and seismic fragility assessment of two-story lightly-reinforced masonry shear wall systems. The analytical model was capable of capturing the peak response values and times and the response variation trends for both the displacement and the base shear. For the majority of the walls, the average error in predicting the peak base shear, top floor displacement, and top floor acceleration at the L1 and L2 level earthquakes, were 14%, 11%, and 9%, respectively. For most of the walls the model was also capable of predicting, with reasonable accuracy, the earthquake level and time for wall yielding and failure. The analytical predictions of the values of top floor displacement ductility levels were also in agreement with the experimental results with errors in the range of 4-6% for Walls 2, 4, and 5 and 15-24% for Walls 1, 3, and 6 with an average error of 12% for all walls.

The variations between the analytical predictions and experimental evaluations observed in this study are mainly attributed to the simplifications employed in the analytical models especially for the hysteretic behaviour of the wall plastic hinge zone. Nevertheless, the average error in all cases did not exceed 14%, which is acceptable taking into consideration the inherently complex behaviour of the composite RM system and the statistical variation in masonry material properties. This behaviour is further complicated when dynamic testing is introduced and specific quantitative and qualitative seismic performance indicators are being monitored. On the other hand, the error values presented

above are obtained for an analytical model calibrated with realistic experimental results. In practice, such realistic experimental data may not be available for calibration of the models and hence increased discrepancies between the actual seismic response and analytical predictions are expected. However, the developed model generally provides a simple and practical tool for performance-based seismic evaluation of RM components, which is essential for the development of analytical fragility curves. Analytical fragility curves were derived based on the experimental capacity data and analytical demand results. The results of the PSDA conducted for the tested walls indicated that, for all cases, the walls satisfied the NBCC (NRCC 2010) life safety limit state in terms of maximum top floor drift ratio even for the highest seismic zones in Canada. The fragility curves also indicated that for walls with design parameters similar to the ones considered in this study, there is only a maximum of 30% chance that two-story lightly reinforced masonry shear walls would reach their maximum flexural capacity and undergo extensive damage requiring significant repairs.

Considering the fact that the studied walls fall under the *conventional construction category* (CSA S304.1 2004, and NRCC 2010), which are not permitted even in regions of moderate seismicity, indicate that the currently perceived seismic performance capabilities of such RM SFRS may be underestimated.

5.7 Notations for Chapter 5

A = Regression parameter for PSDA
B = Regression parameter for PSDA
A_g = Gross cross-sectional area of the wall
A_{se} = Effective shear area of the wall
C = Limit state capacity
D = Seismic demand/Top drift ratio
$\mathrm{E_s}$ = Young's modulus
G = Shear modulus
I = Moment of inertia of the section
IM = Ground motion intensity
K_0 = Cracking flexural stiffness
M = Moment
P = Probability/Lateral force
S_a = Spectral acceleration
$S_a(T)$ = Spectral acceleration at specific period
S_c = Median of the limit state capacity
S_d = Median of the seismic demand
S_v = Longitudinal reinforcement spacing
T_i = Initial elastic period
V = Shear force
a = Acceleration
f_s = Sampling frequency
f'_m = Compressive strength of masonry
h = Height of the wall/story
l_p = Equivalent plastic hinge length
r = The ratio of the post yield flexural stiffness to cracking flexural stiffness used in Fukada hysteresis model
ρ = Material density
ρ_v = Longitudinal reinforcement ratio
ν = Poisson's ratio
Δ = Top lateral elastic deformation
Δ_s = Lateral shear deformation at the top of the wall
β = Fukada hysteresis parameter
$\mu_{\varphi,u}$ = Curvature ductility

μ_{Δ} = Displacement ductility level based on displacement at top of the wall

ξ_{el} = Equivalent viscous damping ratio in the elastic range (elastic viscous damping ratio)

β_c = Dispersion of the limit state capacity

β_{c1} = Dispersion of the limit state capacity obtained from experiments

β_{cu} = Added dispersion of the limit state capacity

$\beta_{d|IM}$ = Dispersion of the seismic demand conditioned on the seismic intensity

Φ = Standard normal cumulative distribution function

$\emptyset_s$ = Resistance factor for reinforcing bars

$\emptyset_m$ = Resistance factor for masonry

φ = Curvature

α = The ratio of the yield flexural stiffness to cracking flexural stiffness used in Fukada hysteresis model

SUBSCRIPTS

A = Analytically evaluated

E = Experimentally evaluated

b = Evaluated at the base of the walls

u = Obtained at maximum load

y = Obtained at the yield level

cr = Cracking value

max = Maximum value

5.8 References for Chapter 5

ATC. (2011). "Seismic Performance Assessment of Buildings Volume 1- Methodology (ATC-58-1 75% Draft)." Applied Technology Council. Federal Emergency Management Agency, Washington D.C., USA.

Atkinson, Gail M. (2009). "Earthquake Time Histories Compatible with the 2005 National Building Code of Canada Uniform Hazard Spectrum." *Canadian Journal of Civil Engineering*, 36(6), 991-1000.

Banting, B. and El-Dakhakhni, W. W. (2013). "Normal Strain-Adjusted Shear Strength Expression for Fully-Grouted Reinforced Masonry Structural Walls." *Journal of structural Engineering*, 10.1061/(ASCE)ST.1943-541X.0000842 (Apr. 1).

Canadian Standard Association, (CSA S304.1). "Design of Masonry Structures." S304.1. Mississuaga, ON: CSA, 2004.

Carr, A.J. (2004). "Ruaumoko, Volume 1: Theory manual." Christchurch, New Zealand.

Chopra, Anil K. (2001). "Dynamics of Structures: Theory and Applications to Earthquake Engineering." Vol. 2. Upper Saddle River, NJ: Prentice Hall.

Cornell, C. A., Jalayer, F., Hamburger, R. O., Foutch, D. A. (2002). "Probabilistic Basis for 2000 SAC Federal Emergency Management Agency Steel Moment Frame Guidelines." *Journal of Structural Engineering*, 128 (4), 526-533.

Drysdale, R., and Hamid, A. (2005). "Masonry Structures- Behavior and Design." 3rd Ed., Canada Masonry Design Centre, Mississauga, Canada.

Fukada, Y. (1969). "Study on the Restoring Force Characteristics of Reinforced Concrete Buildings." *In Proceedings of Kanto District Symposium*, Architectural Institute of Japan, Tokyo.

Giberson, Melbourne F. (1969). "Two Nonlinear Beams with Definitions of Ductility." *Journal of the Structural Division*, 95(2), 137-157.

Harris, H., Sabnis, G. (1999). "Structural Modeling and Experimental Techniques". (Second ed.), CRC Press.

Kwon, O.S. (2007). "Probabilistic Seismic Assessment of Structure, Foundation and Soil Interacting Systems." PhD Thesis, Civil Engineering Department, University of Illinois at Urbana-Champaign, Urbana, Illinois, USA.

Melchers, R. E. (2001). "Structural Reliability Analysis and Prediction." John Wiley & Sons Ltd., West Sussex, England, second edition.

Mojiri, S., El-Dakhakhni, W. W., Tait, M. J. (2013-a). "Shake Table Seismic Performance Assessment of Fully Grouted Lightly Reinforced Concrete Block Shear Walls". *Journal of Structural Engineering*, Under Review.

Mojiri, S., Tait, M. J., El-Dakhakhni, W. W. (2013-b). "Seismic Response Analysis of Fully Grouted Lightly Reinforced Concrete Block Masonry Shear Walls Based on Shake Table Tests." *Journal of Structural Engineering*, Under Review.

National Institute of Standards and Technology (NIST). (2010). "Evaluation of the P-695 methodology for quantification of building seismic performance factors." NIST GCR 10-917-8., NIST, Gaithersburg, MD, USA.

National Research Council of Canada (NRCC) (2010). "National Building Code of Canada (NBCC)." Institute for Research in Construction, Ottawa, Canada.

Nielson, Bryant G. (2005). "Analytical Fragility Curves for Highway Bridges in Moderate Seismic Zones." PhD Thesis, School of Civil and Environmental Engineering, Georgia Institute of Technology, Atlanta, Georgia, USA.

Otani, S. (1974). "SAKE: A Computer Program for Inelastic Response of R/C Frames to Earthquakes." Report UILU-ENG-74-2029, Civil Engineering Studies, University of Illinois at Urbana-Champaign, Illinois, USA.

Pacific Earthquake Engineering Research Center: NGA Database. (Accessed September, 2011). http://peer.berkeley.edu/nga/

Paulay, T., Priestley, M., J., N. (1992). "Seismic Design of Reinforced Concrete and Masonry Buildings." John Wiley & Sons, Inc., New York and Toronto.

Priestley, M.J.N., Calivi, G.M., Kowalsky, M.J. (2007). "Displacement-Based Seismic Design of Structures." Pavia: IUSS Press.

Shedid, M. T., El-Dakhakhni, W. W., and Drysdale, R. G. (2010-a). "Seismic Performance Parameters for Reinforced Concrete-Block Shear Wall Construction." *Journal of Performance of Constructed Facilities*, 24(1), 4-18.

Shedid, M. T., El-Dakhakhni, W. W., and Drysdale, R. G. (2010-b). "Alternate Strategies to Enhance the Seismic Performance of Reinforced Concrete-Block Shear Wall Systems." *Journal of Structural Engineering*, 136(6), 676-689.

Steel, Robert GD, Torrie, T. R. (1961). "Principles and procedures of statistics with special reference to biological sciences." McGraw-Hill, Inc. NY.

Takeda, T., Sozen, M. A., Nielsen, N. N. (1970). "Reinforced Concrete Response to Simulated Earthquakes." *Journal of the Structural Division*, 96(12), 2557-2573.

Wen, Y. K., Ellingwood, B. R., Veneziano, D., Bracci, J. (2003). "Uncertainty Modeling in Earthquake Engineering." MAE centre project FD-2 report 12.

CHAPTER 6: CONCLUSIONS AND FUTURE WORK

6.1 Summary and Conclusions

A research study has been carried out at McMaster University's Applied Dynamics Laboratory aiming at a realistic quantification of the seismic performance parameters of lightly-reinforced fully-grouted masonry shear walls. The research work focused on providing experimental evidence and further developing analytical tools within the context of performance-based seismic design philosophies. A key component of this research project comprised of shake table tests on single- and two-story RM shear walls components. The design of the walls did not meet the maximum vertical reinforcement spacing limitations of the Canadian masonry design code for either the *limited ductility* or the *moderately ductile* shear wall categories. As such, based on the reinforcement spacing, the wall qualified only for the *conventional construction* category that is restricted to low seismic zones. The results were used for seismic performance quantification and development of analytical tools for seismic performance prediction for this class of RM shear walls. This thesis presented the details of the experimental program undertaken for this research project. General observations in terms of cracking patterns and failure modes of the tested walls and the results on the lateral strength, hysteretic response, dynamic properties, and the contribution of different displacement components to the response of the walls were presented. The results of a detailed analysis on seismic performance quantification of the walls in terms of inelastic behaviour characteristics, various

energy components, and the effective dynamic properties of the tested walls were later outlined. Finally, the development of analytical models and analytical fragility assessment tools of the tested walls was presented. Based on the study, the several conclusions can be made based on their applications in and implications on PBSD of RM construction.

Reinforcing the masonry walls with horizontal and vertical steel bars successfully controlled the response and failure mode of the walls. Most of the walls reached their flexural strength prior to any brittle sliding and diagonal failure and hence the capacity design was successfully implemented by even using minor amounts of reinforcement. The flexural capacity of the walls was also shown to be well-predicted by simple beam theory formulations. The test observations and lateral deflection response analysis of the walls revealed that the walls' main response and mode of failure was flexural thus allowing a controlled and favourable energy dissipation mechanism at the base of the walls.

The investigations on the curvature and displacement ductility of the walls showed that RM shear walls even with minimal reinforcement, such as the tested walls, can develop considerable nonlinear deformation capacity that can be relied on for seismic design. Considerably higher values of ductility related response modification factors (R_d) were obtained for the tested walls compared to the recommendations by the National Building Code of Canada for the same category of the walls. This can potentially facilitate the application of this category of walls in regions with moderate seismicity.

Detailed analysis on the mechanism and distribution of energy dissipation throughout the walls confirmed that considerable amount of energy was dissipated by the flexural response of the walls. Most of the energy was dissipated at the base of the walls in the plastic hinge region. This was consistent with the observations during the tests that showed concentration of flexural damage at the base of the walls. These observations confirmed that lightly-reinforced masonry shear walls can develop plastic hinging mechanisms and reliably dissipate energy in the plastic hinge zone. This also reaffirms that, as prescribed by masonry design codes, special seismic design provisions should be employed in this region to facilitate reliable energy dissipation without extensive loss of wall strength.

The results showed a considerable variation in the wall seismic responses, like displacement ductility, for shear walls belonging to the same category of SFRS depending on their geometry, design, and seismic demands. When compared to the provisions of current seismic codes, including the NBCC 2010, which prescribe a single ductility related response modification factor (R_d) for each type of SFRS, this draws attentions to the fact that force-based approaches may lead to SFRS designed with a non-uniform risk of failure. The findings, however, support the notion that displacement ductility demands considered for computation of design seismic forces for the walls and generally any SFRS, should be obtained based on the actual level of seismic demand and realistic estimations of response of structures during earthquakes. This issue was further confirmed by the investigations on the effective dynamic properties of the walls at

different response levels that revealed significant variations of such properties at different response levels. The investigation on the input seismic energy also revealed considerable variations in the amount of absorbed energy by an SFRS during an earthquake based on the variations of its dynamic properties. In addition, the experimentally obtained base shear of the walls was successfully estimated based on the effective dynamic parameters while the estimations based on the initial elastic dynamic properties considerably underestimated the actual base shear values.

A simple analytical model was used to predict the seismic response of the walls. The results indicated that the model was capable of predicting the seismic response of the tested walls with reasonable accuracy. The model can be used as simple and practical yet an accurate tool for performance-based seismic design and evaluation of RM components. In this study the model facilitated analytical fragility assessment of the two-story RM walls and provided further insight into the seismic performance of the walls under an extensive range of seismic demands.

The results of the fragility assessment of the two-storey lightly reinforced masonry shear walls indicated that there is a low chance that such walls would reach their maximum flexural capacity and undergo extensive damage requiring significant repairs even in high seismic areas in Canada. The results can be further extended to modular RM buildings built with similar shear walls, if the coupling between the walls can be neglected. However, following seismic design

provisions of National Building Code of Canada (NBCC 2010) and Canadian masonry design code, design parameters of the studied walls, do not qualify them for more than the *conventional construction category* which are not permitted even in regions of moderate seismicity. This indicates that the seismic performance capabilities of such RM SFRS may be underestimated.

Generally, the experimental and analytical investigations reported by this thesis report confirmed the adequate seismic performance of lightly RM shear walls even for high levels of seismic demands. It can be inferred that widely-spaced reinforcement can be very cost-effective in RM wall construction in areas with low to moderate seismicity. In general, the test results contribute to the RM SPD and can facilitate further seismic performance analyses and calibration of numerical models towards better quantification of the seismic performance of RM SFRS.

6.2 Future work

A special test setup was designed and fabricated by the author for shake table testing of multi-story shear walls. The proposed mass carrying system built and used in the test setup was effective in increasing the performance of the uni-axial shake table at the ADL enabling the investigation of seismic performance of the reinforced masonry shear walls at real high amplitude earthquakes. Earthquakes with different amplitudes up to PGA of 0.84g were run for walls with different configurations by the table without significantly changing its performance. The test setup was also very effective in increasing the safety of the

tests after the complete failure of the walls and also in facilitating the installation of the specimens. The axial loading system was also found to be efficient for applying and controlling the desired axial loads on the specimens. Regarding the effect of the added coulomb friction damping on the real response of the specimens, as reported in chapter 4, findings revealed that for the tested walls the added friction damping decreased the spectral response acceleration by less than 12%, confirming that the external mass supporting system does not alter the seismic response of the walls significantly. On the other hand, the setup is flexible for further extensions in future enabling testing walls with more stories.

Based on the discussions above, the test setup can be considered as a reliable device for realistic seismic performance evaluation of different structures. Therefore, as next steps towards better seismic performance evaluation of RM shear walls and as extensions of this research project, it is proposed to test RM shear walls with other deign and geometric parameters, e.g. with higher reinforcement ratio, with special boundary elements, with openings, with higher number of stories, etc, or with other response and energy dissipation mechanisms, like post tensioned self -centring rocking walls, etc.

APPENDIX A: THE DISPLACEMENT, DRIFT RATIO, AND ACCELERATION RESPONSE HISTORIES OF THE WALLS

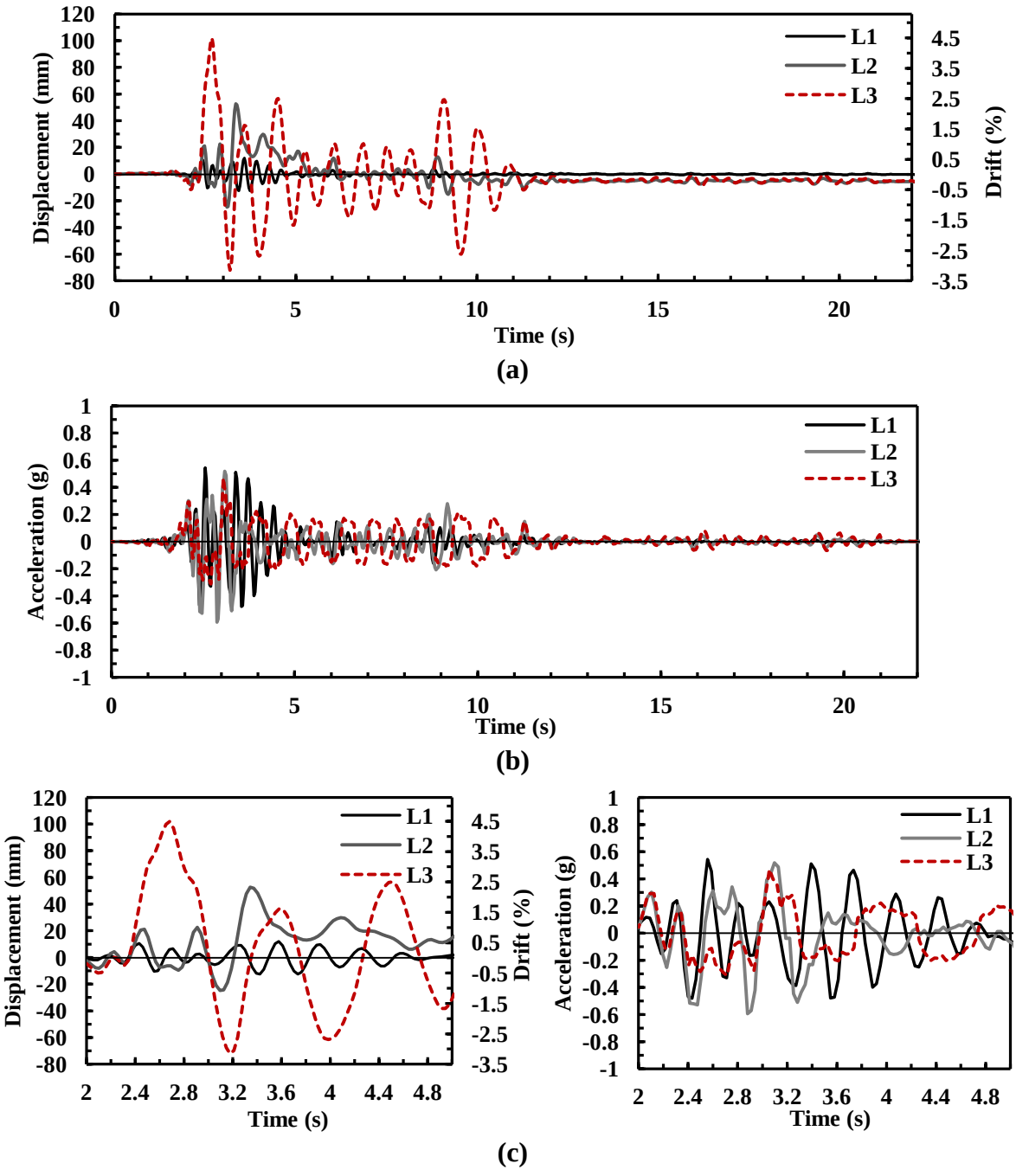

Figure A-1: Responses history of top story of Wall 1 under the L1, L2, and L3 level records: **a)** Relative lateral displacement and drift, **b)** Acceleration, **c)** Responses between 2-5 seconds

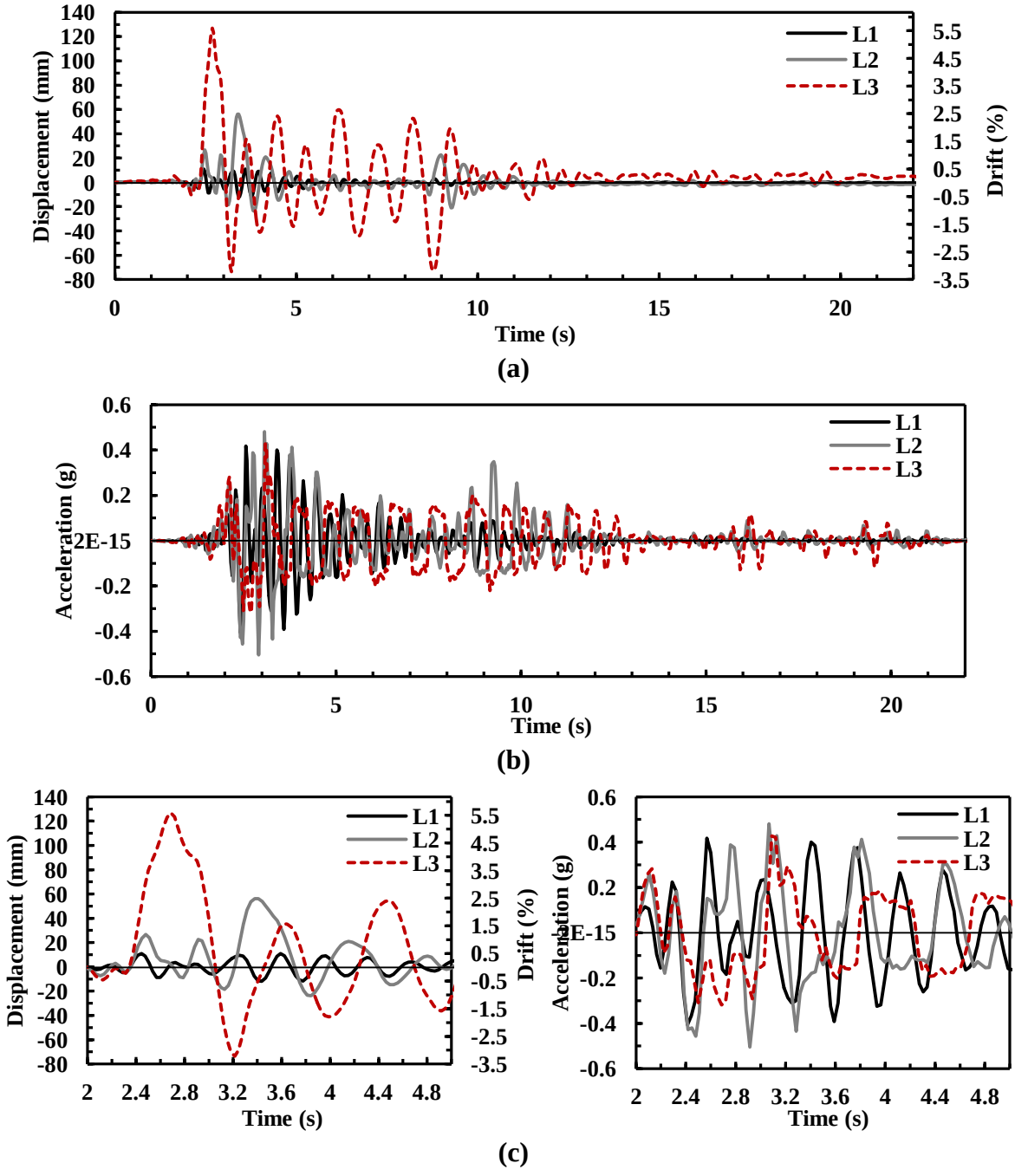

Figure A-2: Responses history of top story of Wall 2 under the L1, L2, and L3 level records: **a)** Relative lateral displacement and drift, **b)** Acceleration, **c)** Responses between 2-5 seconds

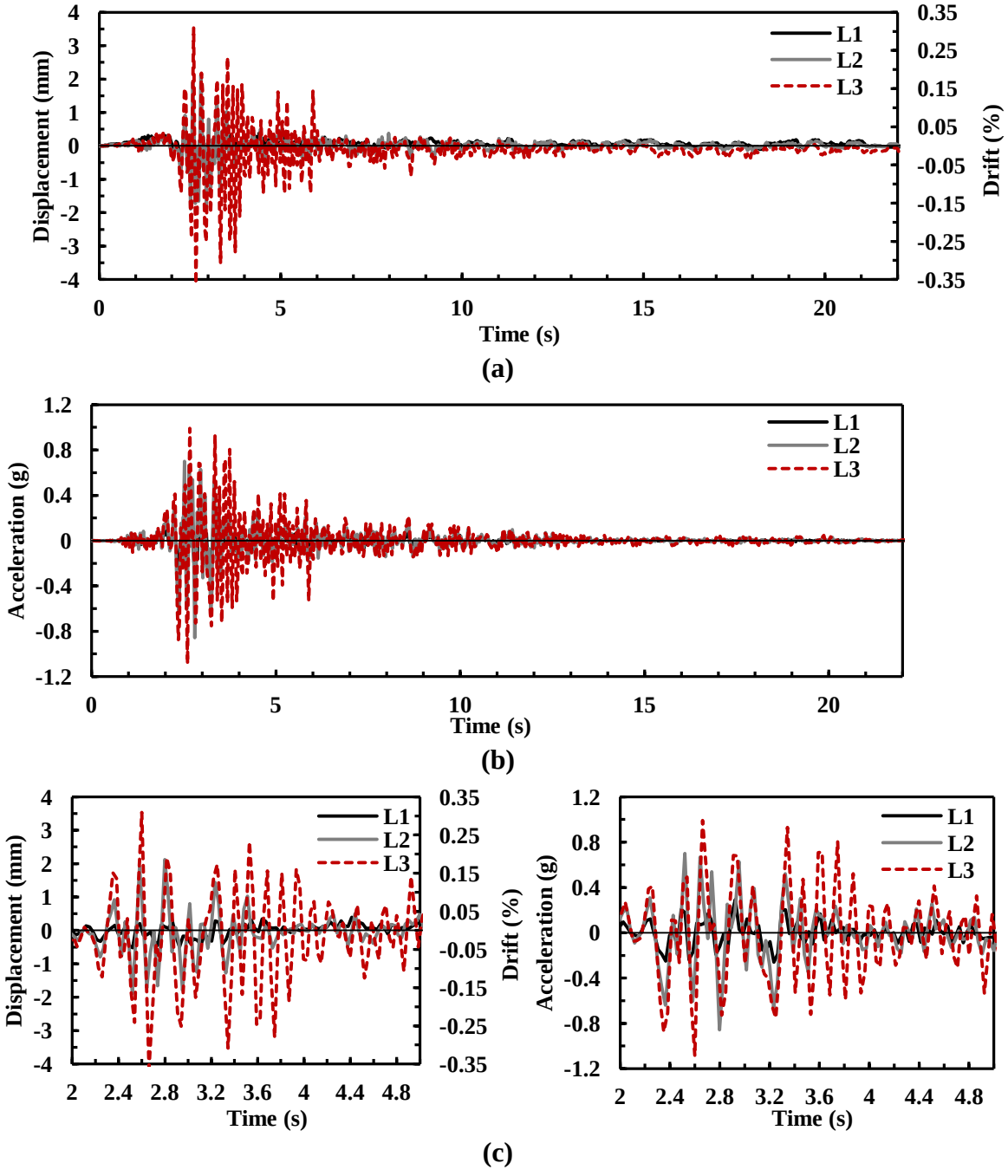

Figure A-3: Responses history of top story of Wall 3 under the L1, L2, and L3 level records: **a)** Relative lateral displacement and drift, **b)** Acceleration, **c)** Responses between 2-5 seconds

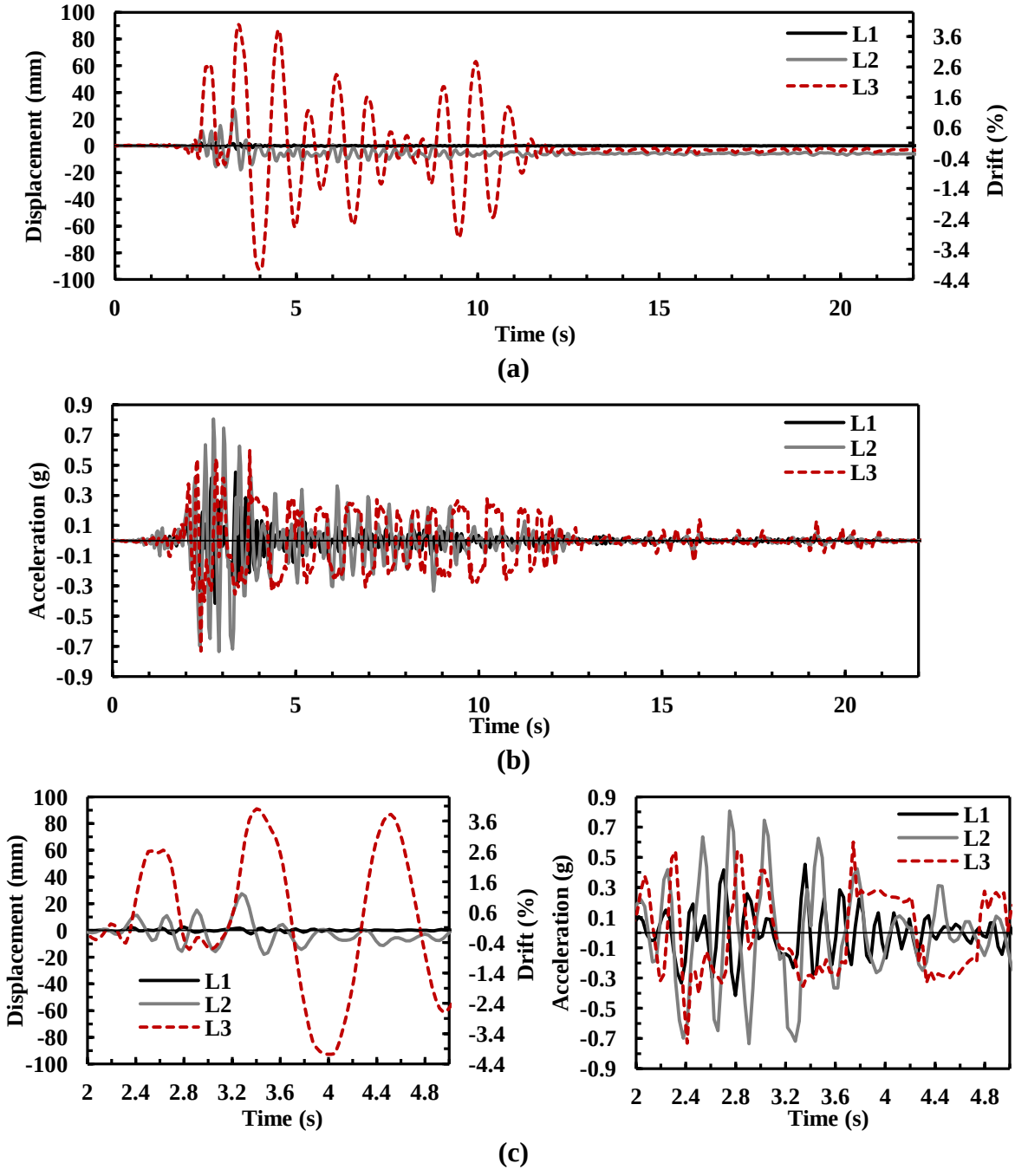

Figure A-4: Responses history of top story of Wall 4 under the L1, L2, and L3 level records: **a)** Relative lateral displacement and drift, **b)** Acceleration, **c**) Responses between 2-5 seconds

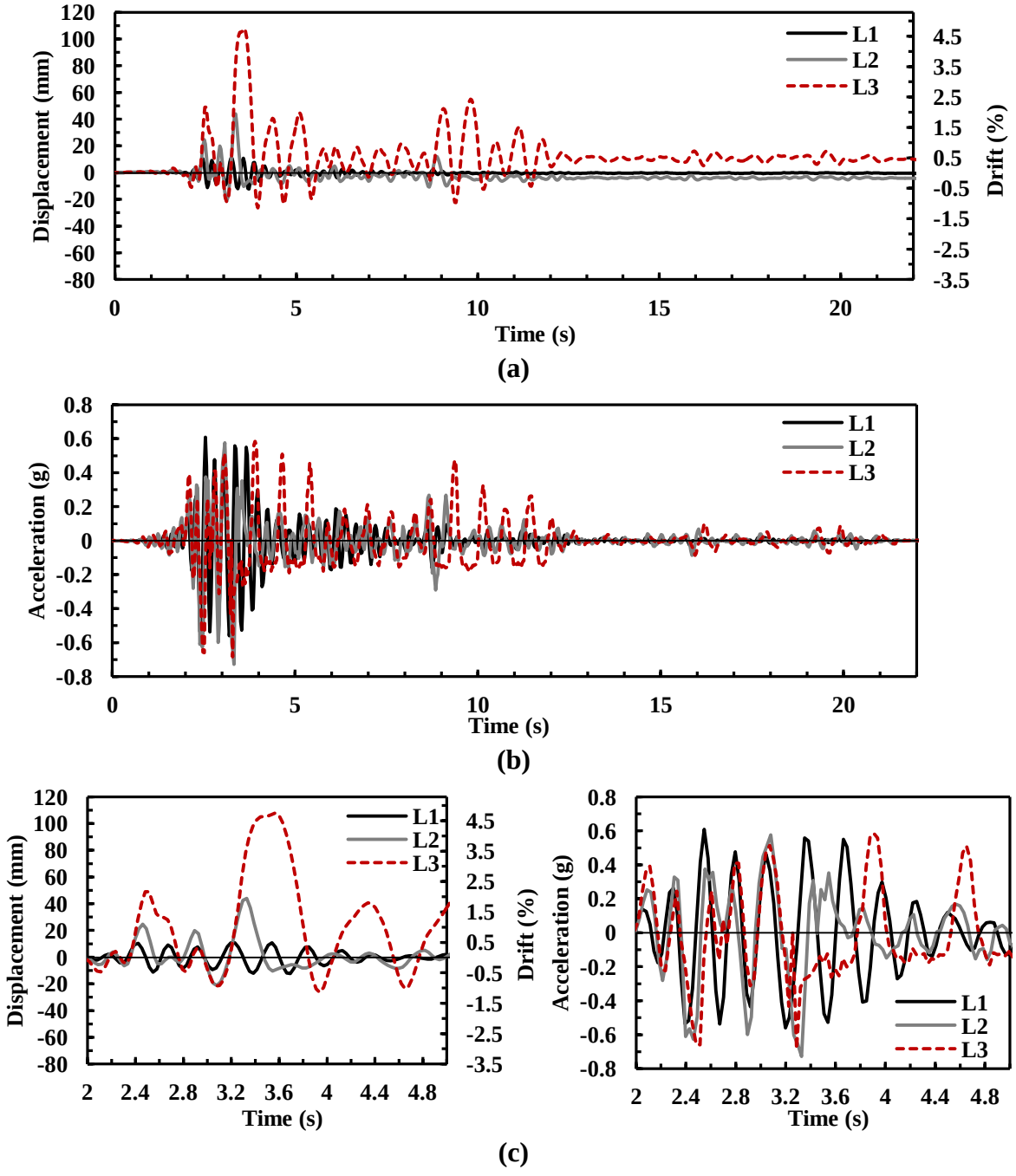

Figure A-5: Responses history of top story of Wall 5 under the L1, L2, and L3 level records: **a)** Relative lateral displacement and drift, **b)** Acceleration, **c)** Responses between 2-5 seconds

APPENDIX B: QUANTIFICATION OF FORCE AND ENERGY COMPONENTS

This section describes the equations for quantification of different force and energy components based on the shake table experimental data for the shake table-model wall system. Note that i and n indexes in the following equations refer to the values at time t_i and t_n(end of the record) respectively and j index refers to the j^{th} story. The positive direction of the forces, accelerations, and displacements is taken to be in the west direction as indicated in Fig. 4.2. The readings of the load cells mounted in the loading beams are also considered positive and negative respectively when they are in tension and compression.

Input energy: The cumulative absolute input energy at time t_n ($E^a_{in,n}$) can be obtained from:

$$E^a_{in,n} = \sum_{i=1}^{n} F_{st,i}\, \Delta u_{st,i} \tag{B-1}$$

where $\Delta u_{st,i}$ is the shake table displacement increment. $F_{st,i}$ is the total force exerted by the shake table into the shear wall-mass supporting system and can be computed by:

$$F_{st,i} = m_1 \ddot{u}_{st,i} - \sum_{j=1}^{m} F_{s,j,i} \tag{B-2}$$

In Eq. B-2, $\ddot{u}_{st,i}$ is the acceleration of the shake table,m_1 is the portion of the mass of the system that moves rigidly with the shake table which in this case is approximately the mass of lower half part of the model walls. Also, $F_{s,j,i}$ in Eq. B-2 is the total lateral story force acting on the wall at the corresponding story heights and considering the instrumentation scheme used in the test setup as shown in Fig 4.2 can be obtained from:

$$F_{s,j,i} = -m_{j1}\ddot{u}_{j,i,1} + F_{LC,j,i} \quad \text{(B-3)}$$

where m_{j1} is part of the inertial mass of the j^{th} floor supported by the walls, composed of the partial mass of the walls, total mass of the RC slabs, mass of the lateral support attached to the walls (ball-bearing supports, etc.), and the portion of the mass of the loading beams between the load cells and the walls. $\ddot{u}_{j,i,1}$ is the absolute acceleration of the j^{th} floor recorded by the accelerometers attached to the RC slabs (AC1 and AC2 in Fig. 4.3). $F_{LC,j,i}$ is the lateral load measured by the j^{th} floor load cells (LC1 and LC2 in Fig. 4.3). The cumulative absolute input energy ($E^a_{in,n}$) can then be computed by combining Eqs. B-1, B-2, and B-3 from the discrete experimental data.

Absolute kinetic energy: The instantaneous absolute kinetic energy ($E^a_{k,i}$) in the system is computed based on the following equation:

$$E^a_{k,i} = \frac{1}{2}m_1\dot{u}^2_{st,i} + \sum_{j=1}^{m}\frac{1}{2}m_j\dot{u}^2_{j,i} \quad \text{(B-4)}$$

where $\dot{u}_{st,i}$ and $\dot{u}_{j,i}$are the absolute velocity of the shake table and the j^{th}story, respectively, which can be computed by directly integrating their corresponding measured absolute displacements, and m_j is the total inertial mass corresponding to the j^{th} floor.

Viscously damped and absorbed energy: The sum of the viscously damped and absorbed energies by the walls ($E_{a,d,n}$) can be obtained by integrating these forces with their corresponding relative displacements at each story based on the following equation:

$$E_{a,d,n} = E_{d,n} + E_{a,n} = \sum_{j=1}^{m} \sum_{i=1}^{n} (F_{d,j,i} + F_{r,j,i})\, \Delta\, u_{j,i}^{r} \quad \text{(B-5)}$$

where $\Delta\, u_{j,i}^{r}$ is the relative lateral displacement increment of the j^{th} story. The equilibrium of forces at each story dictates that the sum of the resisting forces composed of the viscous damping forces (F_d) and restoring forces (F_r) in the walls is equal to the lateral story forces exerted on the walls:

$$F_{d,j,i} + F_{r,j,i} = F_{s,j,i} \quad \text{(B-6)}$$

Combining Eqs. B-3, B-5, and B-6, the sum of the viscously damped and absorbed energy in the system can be expressed as:

$$E_{a,d,n} = E_{d,n} + E_{a,n} = \sum_{j=1}^{m} \sum_{i=1}^{n} (-m_{j1} \ddot{u}_{j,i,1} + F_{LC,j,i}) \, \Delta u_{j,i} \quad \text{(B-7)}$$

The energy absorbed by the walls is composed of two energy components; namely the strain energy (E_s) and hysteretic energy (E_h):

$$E_{a,n} = E_{s,n} + E_{h,n} \quad \text{(B-8)}$$

The strain energy is the recoverable energy stored in the system through elastic deformations of the structural members, while hysteretic energy is the energy dissipated in the system through inelastic deformations in the structural members and is non-recoverable. The cumulative absorbed energy computed at the end of the earthquake when there is no motion only includes the total hysteretic energy dissipated during the earthquake. Dissipation of this energy occurs with the damage to the structural members. Unless a measure of the nonlinear restoring forces of the structural components is available, the absorbed energy cannot be obtained directly. Instead it can be obtained indirectly by subtracting the viscously damped energy from the total absorbed energies obtained from Eq. B-7. The viscous damping energy can in turn be obtained from the following equation:

$$E_{d,n} = \sum_{j=1}^{m} \sum_{i=1}^{n} F_{dj,i} \, \Delta u_{j,i} = C_j \dot{u}_{j,i}^{r} \, \Delta u_{j,i} \quad \text{(B-9)}$$

where $\dot{u}^{r}_{j,i}$ is the relative velocity. Determination of viscous damping energy based on the above equation requires determination or estimation of the story viscous damping coefficients (C_j).

APPENDIX C: RESPONSE HISTORIES OF DIFFERENT WALL ENERGY COMPONENTS

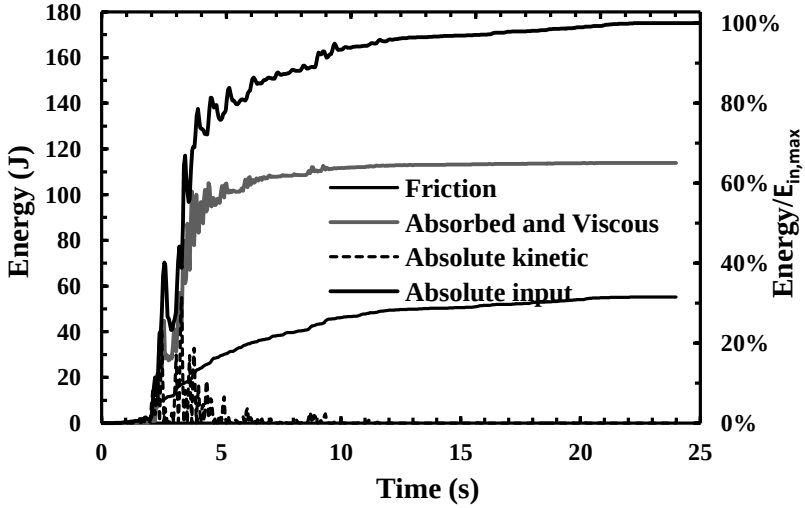

(a)

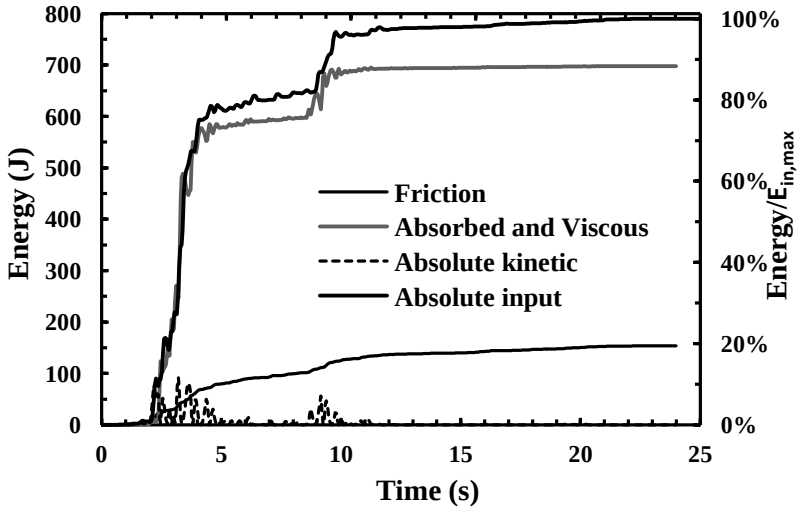

(b)

Figure C-1: Response history of different energy components for Wall 2: **a)** During the L1 level test, **b)** During the L2 level test

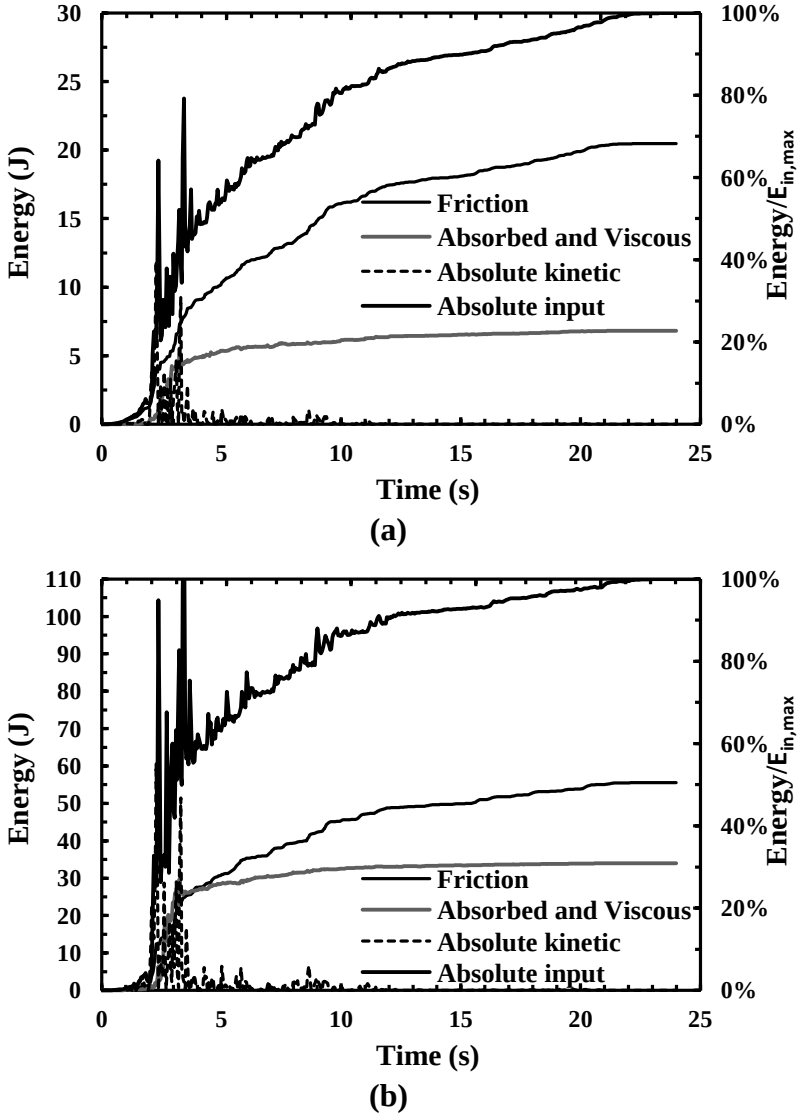

Figure C-2: Response history of different energy components for Wall 3: **a) During** the L1 level test, **b)** During the L2 level test

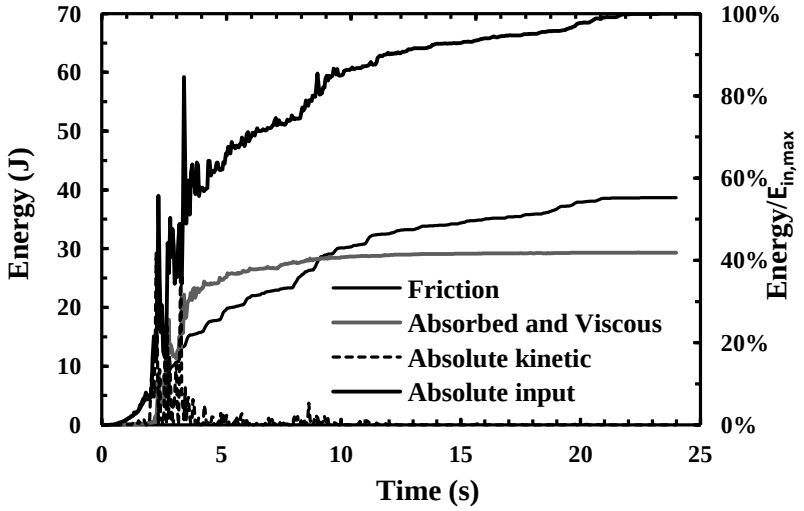

(a)

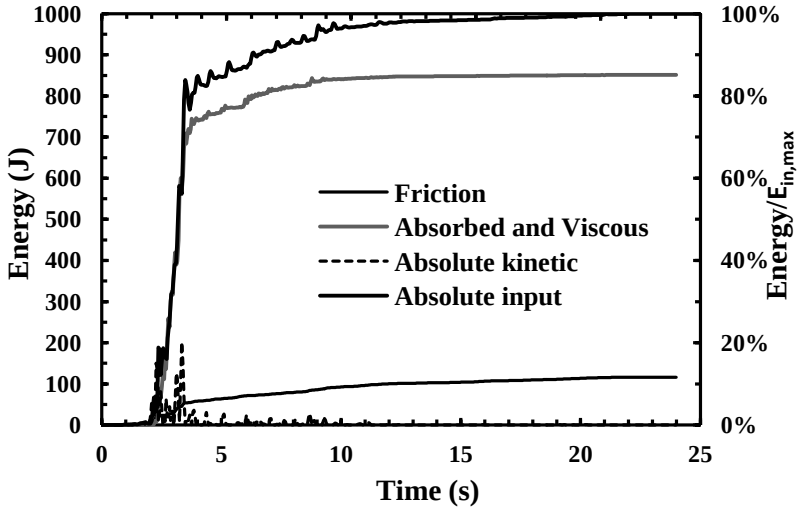

(b)

Figure C-3: Response history of different energy components for Wall 4: **a)** During the L1 level test, **b)** During the L2 level test

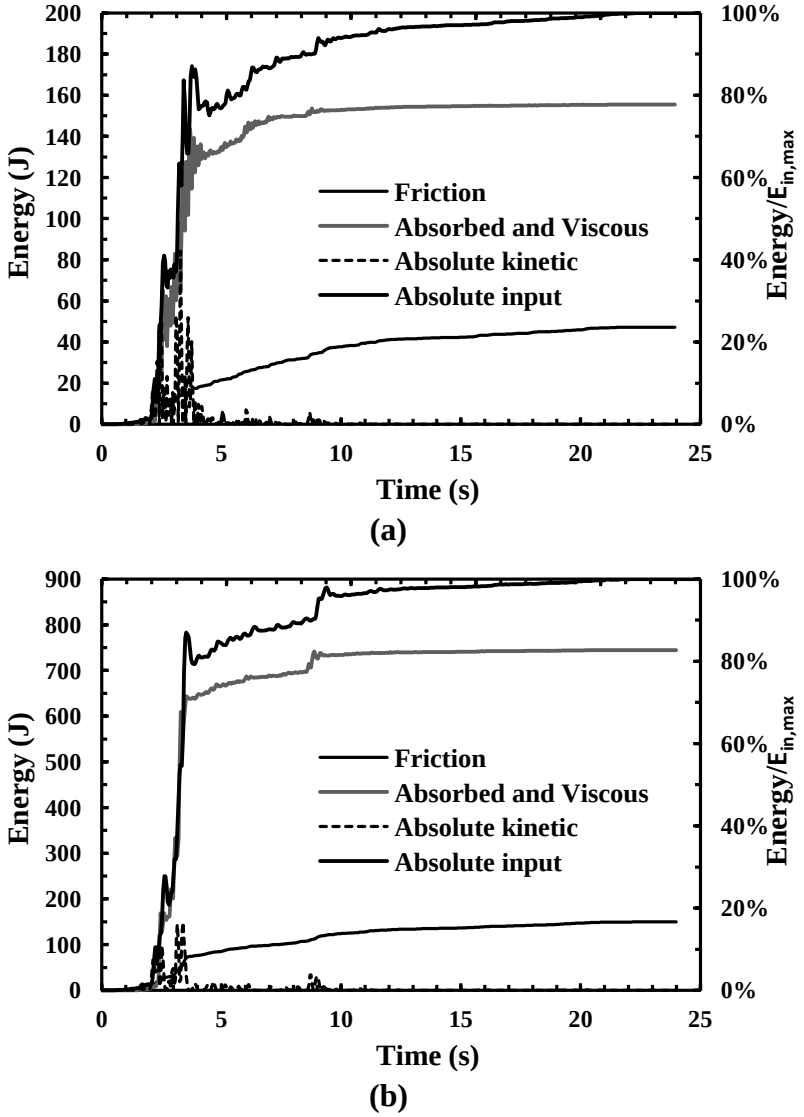

Figure C-4: Response history of different energy components for Wall 5: **a**) During the L1 level test, **b)** During the L2 level test

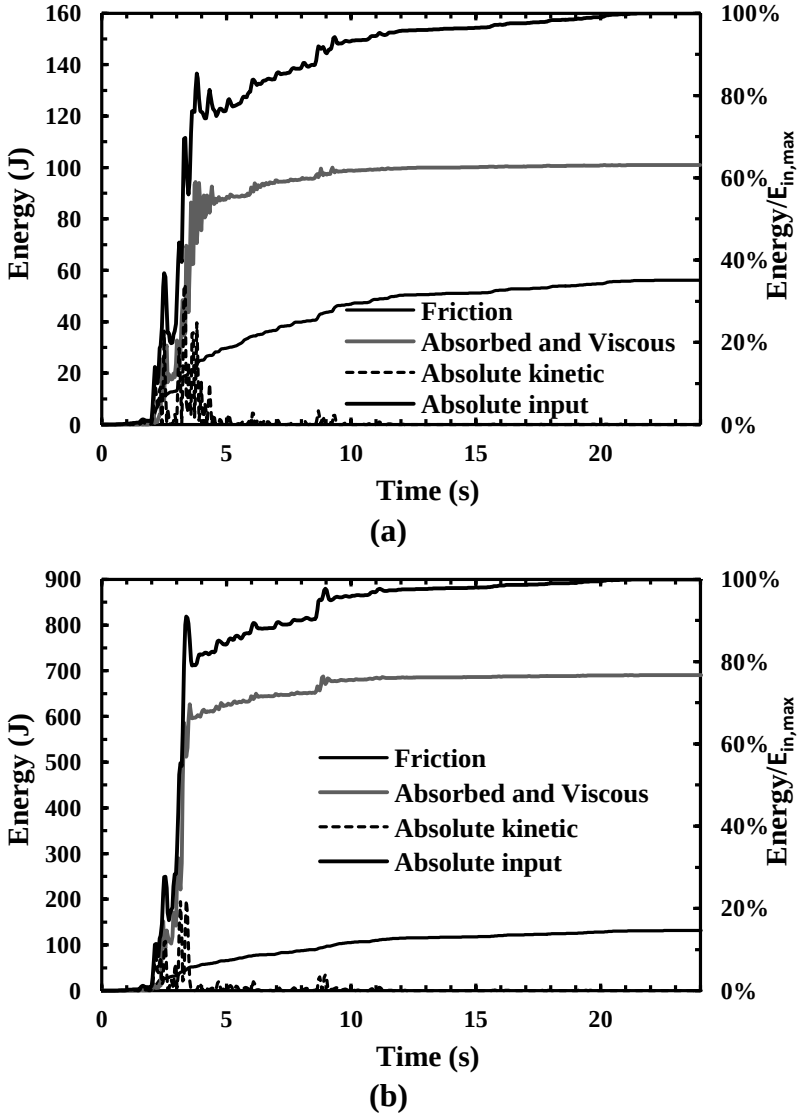

Figure C-5: Response history of different energy components for Wall 6: **a)** During the L1 level test, **b)** During the L2 level test